N74-10141

SEMI-ANNUAL STATUS REPORT III

on

The Influence of Polarization on Millimeter Wave Propagation through Rain

C. W. BOSTIAN, W. L. STUTZMAN,
PARIS H. WILEY and R. E. MARSHALL

Submitted To: National Aeronautics and Space Administration
Washington, D. C.

NASA GRANT NUMBER NGR-47-004-091

Covering the Period January 1 - June 30, 1973

July 1, 1973

Electrical Engineering Department
Virginia Polytechnic Institute and State University
Blacksburg, Virginia 24061

PROJECT PERSONNEL

Dr. Charles W. Bostian, Principal Investigator

Dr. Warren L. Stutzman, Co-Principal Investigator

Dr. Paris H. Wiley, Faculty Associate

Mr. Robert E. Marshall, Graduate Research Assistant

TABLE OF CONTENTS

1. Introduction

This report describes the third six months of a continuing program for the measurement and analysis of the depolarization and attenuation that occur when millimeter wave radio signals propagate through rain. Technical details covered in previous reports are repeated only as necessary for clarity.

During the reporting period, progress was made in three major areas: the processing of recorded 1972 data, acquisition and processing of a large amount of 1973 data, and the development of a new theoretical model to predict rain cross polarization and attenuation. Following a brief narrative summary of the report period, each of these topics will be described in more detail.

2. Narrative Summary of the Report Period

2.1 January

During January the primary concern was to develop an improved theoretical model for rain depolarization. An effort to represent rain scatter by Stevenson's 1953 low-frequency expansion for plane wave scattering by a lossy oblate spheroid was abandoned when it became apparent that Stevenson's approach would not converge for high permittivity scatterers like raindrops. Work continued on what was to become a new depolarization model based on Oguchi's 1973 single raindrop scattering functions.

2.2 February

The basic scattering model for depolarization prediction was completed this month.

An effort was made to achieve optimum antenna alignment prior to the 1973 thunderstorm season. Last year maximum cross polarization isolation had occurred simultaneously on both channels, but now when the isolation of one channel was maximized the isolation on the other was not. Apparently one antenna is slightly out of adjustment and its polarizations are not quite orthogonal (perhaps 89° apart instead of 90°). The manufacturer could offer no suggestions beyond a trial-and-error attempt at correction. As an interim solution the antennas were aligned so that the residual + to - and - to + cross polarization levels were about 25 dB and 50 dB respectively. Since our main interest is in high rain rate data, this was an acceptable interim solution.

2.3 March

The data processing computer programs were modified to calculate both the average cross polarization levels at each integer rain rate and the standard deviation of the cross polarization data contributing to each average value. Subroutines were written to draw error bars showing + and - one standard deviation on computer plots of average cross polarization level versus rainfall rate. Computer routines were developed to extract attenuation values from recorded data and to generate scatter plots of attenuation versus rain rates as well as plots of average attenuation with error bars. A subroutine was written to display average attenuation for each integer rain rate versus average cross polarization level for the same rain rate value. All of these programs were used to generate the data presented in later sections of this report.

Intense rainstorms were observed on March 16 and 17.

2.4 April

A new local oscillator (LO) for the receiver arrived and was installed. Although initially unstable in frequency, it stabilized after about a week's operation and remained stable for the rest of April and May.

A storm occured on April 4.

2.5 May

The receiver calibration was checked on May 17 and found to be unchanged.

An inspection of the raingauge network indicated that all gauges but one were in good repair and working properly. The outer housing of gauge #5 was replaced because of flaking paint.

Preparatory to setting up an on-line phase measuring system later this year, a vector voltmeter was connected between the IF output ports on the two receiver channels. With the instrument adjusted to read 0° phase difference between the incoming + channel and - channel co-polarized signals, phase differences of 120° were measured between the + channel direct signal and the - channel cross polarized signal and 160° between the - channel direct signal and the + channel cross polarized signal. In each case, the cross polarized signal was leading the copolarized signal. These phase differences remained constant over an observing period of about 10 minutes. While their absolute values are indicative only of slight component differences between the two channels, the stability of the clear weather phase differences indicates that measurements of rain-induced changes in differential phase shift can be made.

Storms occurred on May 23, 26, 27, and 28. The storm on May 28 produced a peak rainfall rate of 217.4 mm/hour on one gauge for one time interval between trips.

2.6 June

On June 3 a plexiglass roof was installed over the receiving antenna. This will reduce the amount of water collected on the reflecting surface and the feed. Sufficient data are not yet available to indicate whether or not the roof reduces the data scatter at low rain rates.

Frequency drift in the receiver LO again became a problem. An oven to keep the LO at a constant temperature was installed on June 14 in an effort to end the drift.

3. Theoretical Investigation

3.1 Introduction

During this report period a new method for calculating rain depolarization was developed. Called the scattering method, it was described in detail in Interim Report I of this project, and the information contained there will not be repeated. The scattering method provides a means for calculating rain depolarization and attenuation that is independent both of van de Hulst's equivalent refractive index (van de Hulst, 1957) and of the differential attenuation-differential phase shift method (Watson and Arbabi, 1973). Since the important rain parameters are explicit rather than implicit, it provides a rapid means for analyzing propagation through rain under arbitrary drop shape and size distribution.

3.2 Discussion of Theoretical Models

There are presently three models for predicting the cross polarization level at a given rainfall rate. The differential attenuation method developed by Thomas (1971) was used to generate theoretical curves for Semi-Annual Status Reports I and II of this project. Using Oguchi's 1964 differential attenuation coefficients for this and similar experiments, it usually predicts lower cross polarization levels (i.e. greater isolations) than are measured. Substitution of Oguchi's revised (1973) coefficients into the Thomas model leads to predicted cross polarization generally higher than those measured.

The values of Oguchi's 1973 coefficients have been confirmed independently by Watson (private communication); hence, the difference between measured cross polarization levels and Thomas's predictions seem to lie largely in Thomas's neglect of differential phase shifts and in the prevalent assumption that all raindrops are oblate spheroids. Watson and Arbabi (1973) have shown that differential attenuation and differential phase shift are equally important in determining the received cross polarization ratio, and if one takes phase shift into account, calculated cross polarization levels are significantly different from the Thomas model. This effect is illustrated in Figure 1.

If one assumes 100% oblate drops, the scattering model and Watson's differential attenuation-differential phase shift model predict essentially equivalent cross polarization levels. Figure 2 compares the two models for a 1 km path with +45° linear polarization and uncanted drops. However, there is meteorological evidence that the proportion of oblate drops in real rain is actually about 40% (see Interim Report I)

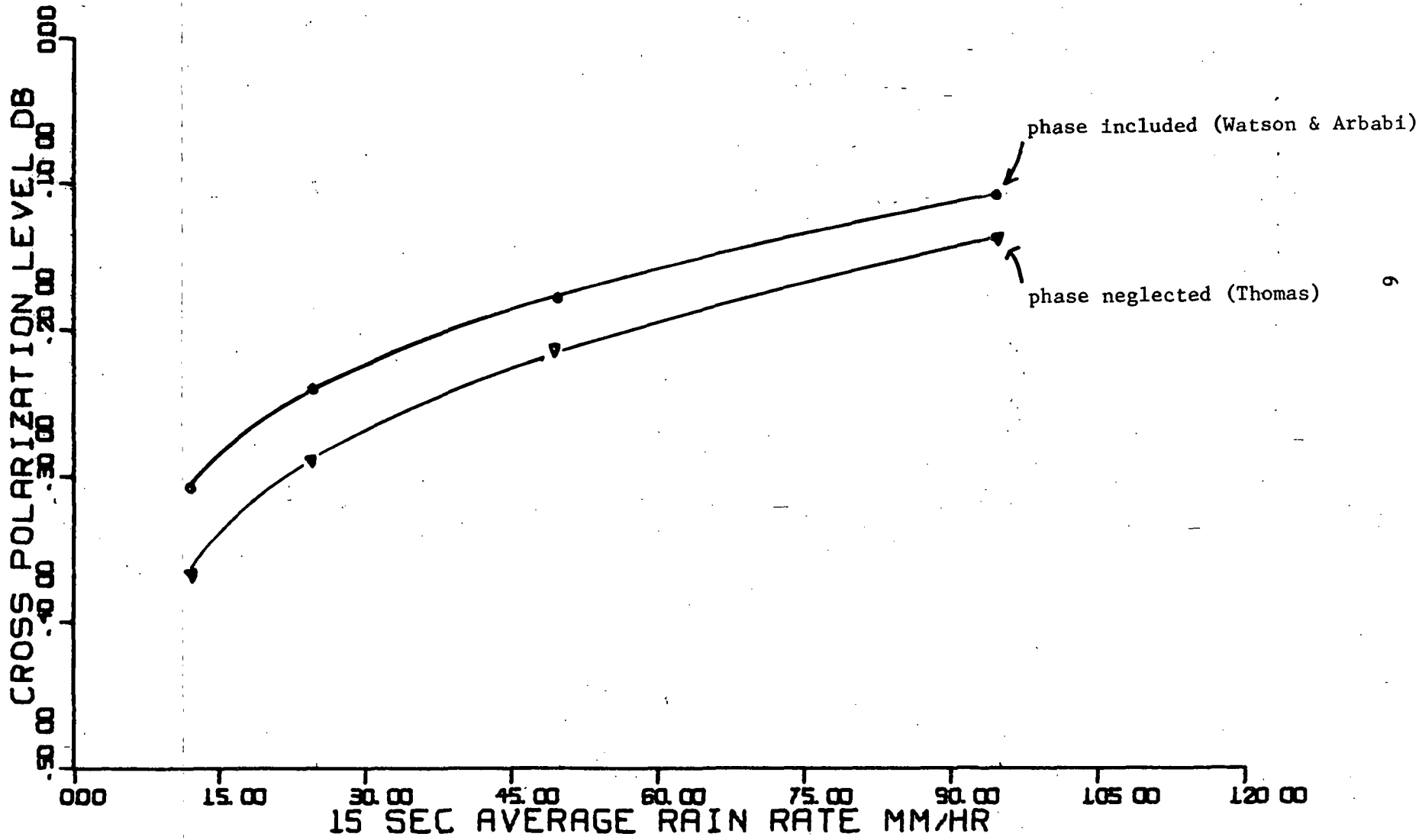

Figure 1. Comparison of Watson-Arbabi and Thomas Models for a 1.43 km Path at 19.3 GHz.

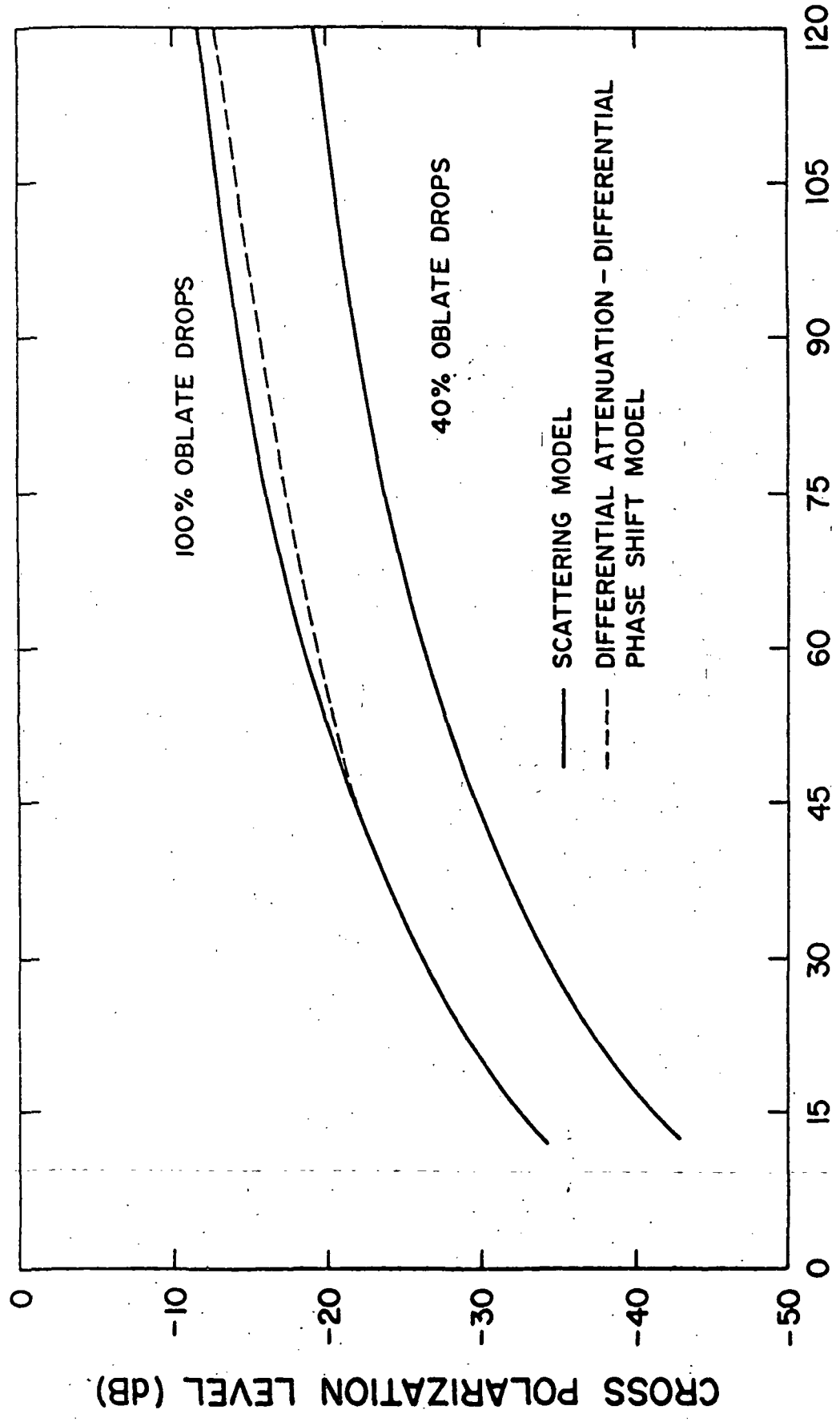

Figure 2. Theoretical predictions of cross polarization level versus rain rate for a 1 km path at 19.3 GHz.

and the data collected by this project support the 40% figure. The effect of a 40% proportion of oblate drops is shown in Figure 2. The theoretical curves which appear in the data presentations to follow have been drawn for a raindrop population which is 40% oblate.

3.3 The Question of Phase Shift

Although the scattering model and the differential attenuation-differential phase shift models predict essentially the same cross polarization level for a given raindrop population, the scattering model and the van de Hulst (1957) approach disagree as to the exact dependence of phase shift on polarization. For example, Figure 3 shows the differential phase shift at 19.3 GHz for a one kilometer path. In the figure, differential phase shift by which the phase of the received signal for a vertically polarized transmitted wave leads the phase of the received signal for a horizontally polarized transmitted wave. Shown for comparison are results of the scattering model, of Oguchi (1973), and of Morrison, et. al. (1973). Although there are no experimental data to support any of these curves, some differential phase measurements will be made during 1973.

4. Data Processing

4.1 Introduction

The principal data processing efforts during this report period were directed toward (1) the calculation of standard deviations for measured cross polarization data and the presentation of error bars on computer plots of average cross polarization level versus rainfall rate, (2) the development of programs to extract and display attenuation

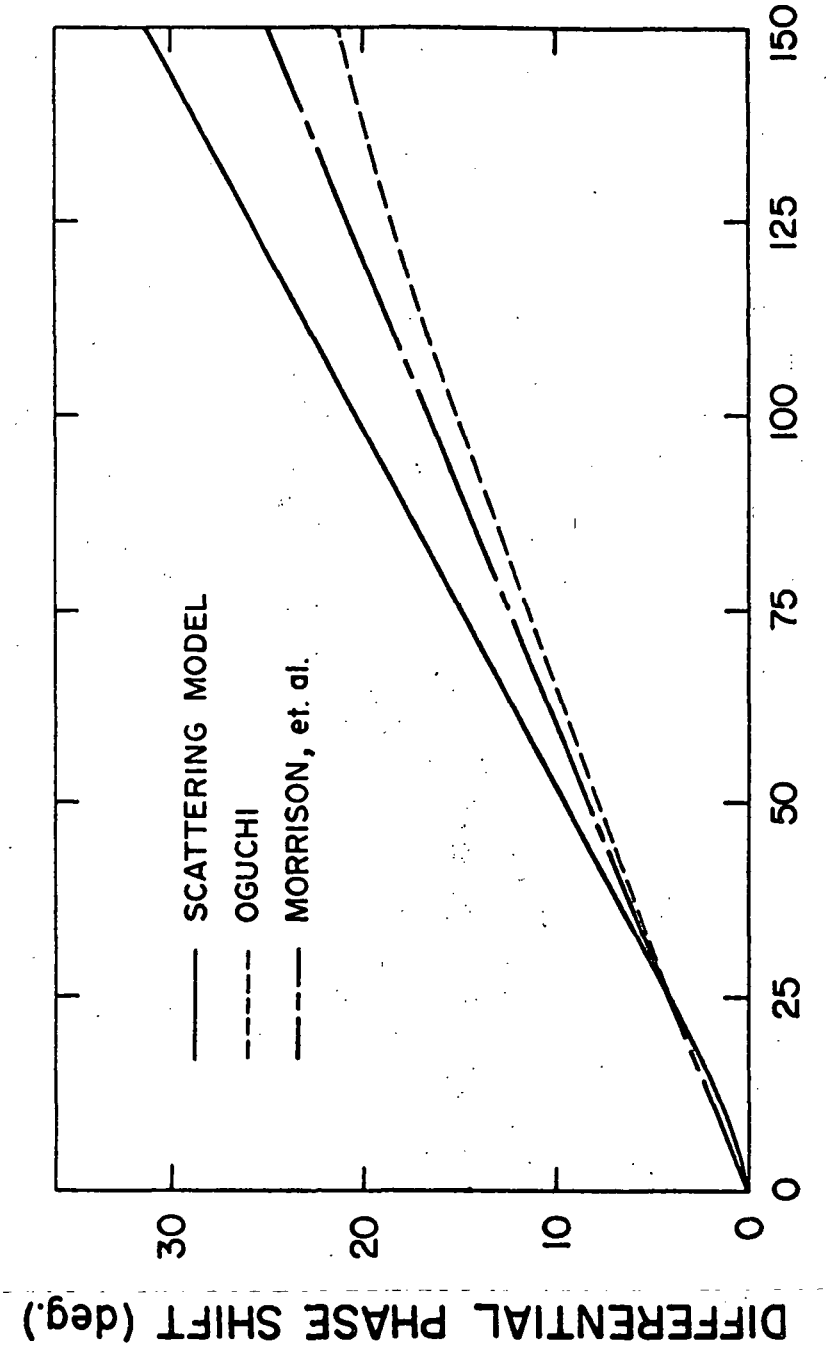

Figure 3. Theoretical predictions of differential phase shift for a 1 km path at 19.3 GHz.

data, and (3) streamlining the data reduction program.

4.2 Standard Deviations and Error Bars

The basic data reduction approach (see Semi-Annual Status Report II) has been to generate 15-second running averages of all data and to plot selected running averages at one-second intervals over the course of a storm. This leads to a scatter plot of cross polarization level (or some other signal parameter) versus rainfall rate. The average cross polarization level for each integer rainfall rate can then be determined by collecting all of the cross polarization values corresponding to rain rates greater than or equal to the integer value but less than the next highest integer rain rate and averaging them. Suppose we identify all of the cross polarization data points associated with rain rates R such that $I \leq R < I + 1$ where I is an integer. Let there be N(I) of these points. We can identify each point as X(I,J), J = 1, N(I). The average cross polarization level corresponding to an integer rain rate of I mm/hr is then

$$< X(I) > = \frac{1}{N(I)} \sum_{J=1}^{N(I)} X(I,J)$$

and the standard deviation of the X(I,J) population is

$$S(I) = \sqrt{\frac{\sum_{J=1}^{N(I)} [X(I,J)]^2 - \frac{1}{N(I)} \left[\sum_{J=1}^{N(I)} X(I,J) \right]^2}{N(I) - 1}} \quad .$$

This procedure was used to calculate standard deviations for the data in Section 5. To keep core requirements within reasonable bounds, N(I) was limited to a maximum value of 70. The plotting subroutines were modified to draw error bars extending from $< X(I) > - S(I)$ to

$< X(J) > + S(I)$ on plots of $< X(I) >$ versus rainfall rate.

4.3 Attenuation Calculation and Display

Rain attenuation is more difficult to measure than rain-induced cross polarization because attenuation measurement requires a clear weather reference signal that is precisely known and has the same value before and after a storm. So long as the cross-polarized signal stays above the receiver threshold, the measured cross polarization level is independent of transmitter power, antenna gains, path loss, and the receiver gain and hence unaffected by variations in these quantities. Because the reference signal depends strongly on all of these things, measured values of attenuation must be interpreted with this fact in mind.

A further difficulty peculiar to this project is that measured attenuation values tend to be small for the short path, i.e., about .124 dB per mm/hr. This means that a one dB error in estimating the clear weather reference signal can introduce a significant percentage error into attenuation computations.

For calculating attenuation it was decided to use as a reference a 30-second average of the received signal level centered 60 seconds after the beginning of a storm. For most storms this was satisfactory, but for the occasional storm that begins with a "step function" of rain, the rain rate was significant before the PB-440 computer began recording received signal levels. This meant that the reference signal was too low and that some calculated attenuations would come out negative. Since negative attenuation is non-physical (rain does not amplify) the IBM 370 data processing program was instructed to scan the attenuation

data array for each storm and, if it found negative values, to add the proper constant to make the minimum attenuation zero.

5. Data Presentation and Analysis

5.1 1972 Data

5.1.1 Introduction

Semi-annual Status Report II presented scatter plots and average plots of measured cross polarization level versus rainfall rate for six 1972 storms. At that time, scattering model predictions were not available for comparison with experiment and attenuation values had not been extracted from the measured data. For these reasons data from the important 1972 storms are included in this report. In all the figures which follow a * indicates an average of all data from both channels corresponding to an integer value of rain rate and a Δ indicates a value predicted by the scattering model. On cross polarization plot a | indicates + to - polarization conversion and - to + conversion is shown as a +. For attenuation plots + channel attenuation is shown as a + and - channel attenuation is shown as a |. In cases where separate averages from both channels appear on the same graph, points indicated by a | are displaced 0.03 inches to the right of their correct location to separate them from the + points.

Usually 5 figures are presented for each 1972 storm. These are (1) average cross polarization level versus rain rate for each channel, (2) average cross polarization level versus rain rate with both channels together, (3) average attenuation versus rain rate for each channel, (4) average attenuation versus rain rate with both channels together,

and (5) average attenuation versus average cross polarization level with rain rate as a parameter. The last eliminates measurement errors due to rain inhomogeneity and is perhaps the best experimental test of the scattering model.

5.1.2 August 4, 1972

During this storm only the + receiver channel was working. Figure 4 illustrates the average measured cross polarization level as a function of rainfall rate. The attenuation values measured are not displayed because they were essentially uncorrelated with rainfall rate and cross polarization level. This is illustrated by Figure 5 which plots average values of attenuation versus average cross polarization levels.

5.1.3 August 17, 1972

Figure 6 illustrates the average cross polarization level for each channel measured during this storm. In Figure 7 both channels are combined to yield a composite average. Figure 8 is a plot of average attenuation versus rain rate for each channel and Figure 9 indicates the average attenuation resulting when data from both channels are together. Figure 10 displays average attenuation versus average cross polarization level.

5.1.4 September 29, 1972

Figures 11 through 15 display data from this storm.

5.1.5 October 27, 1972

Data from this storm appear in Figures 16 through 20.

5.1.6 November 13, 1972

Data from this storm are shown in Figures 21 through 25.

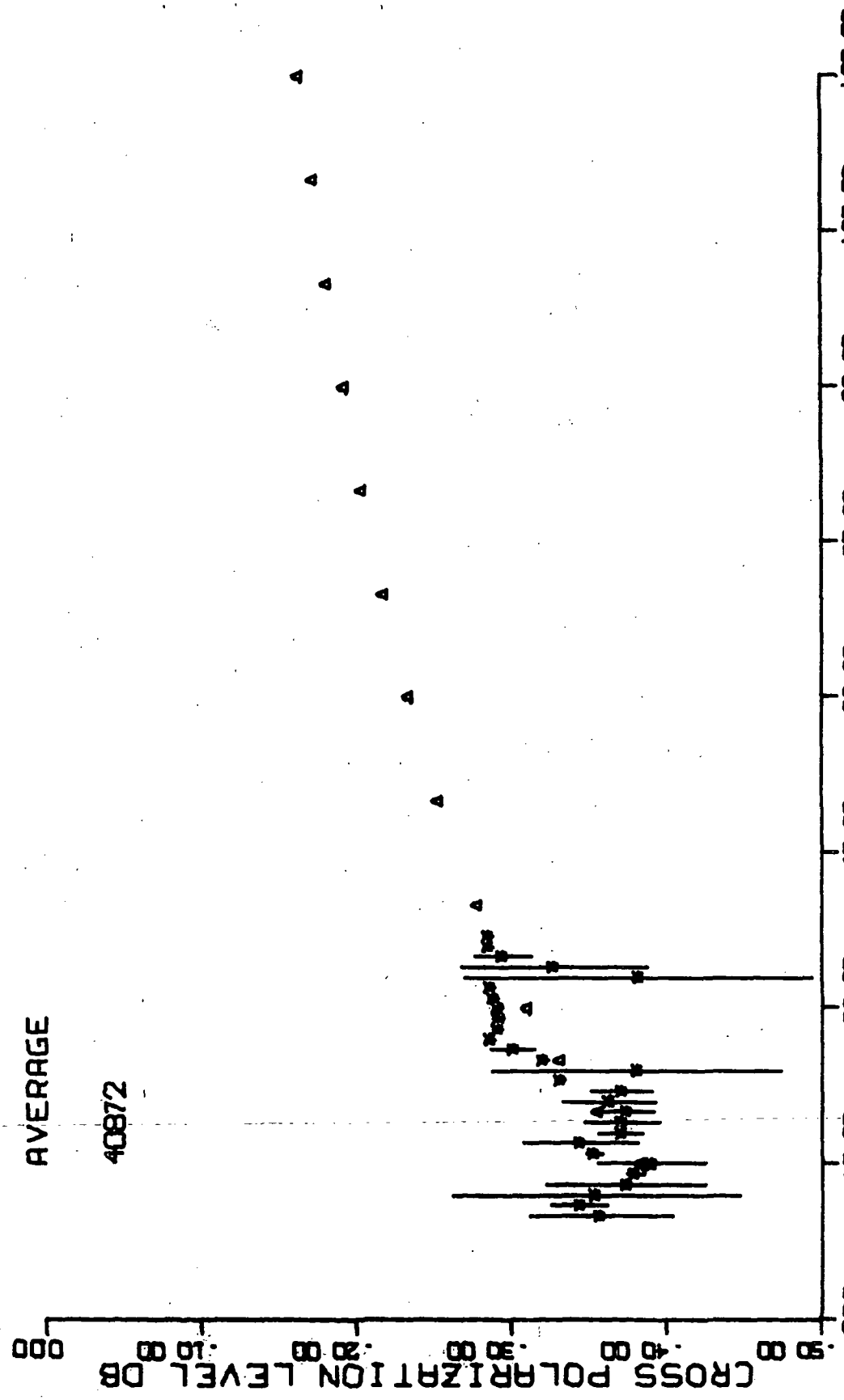

Figure 4. August 4, 1972, average cross polarization levels.

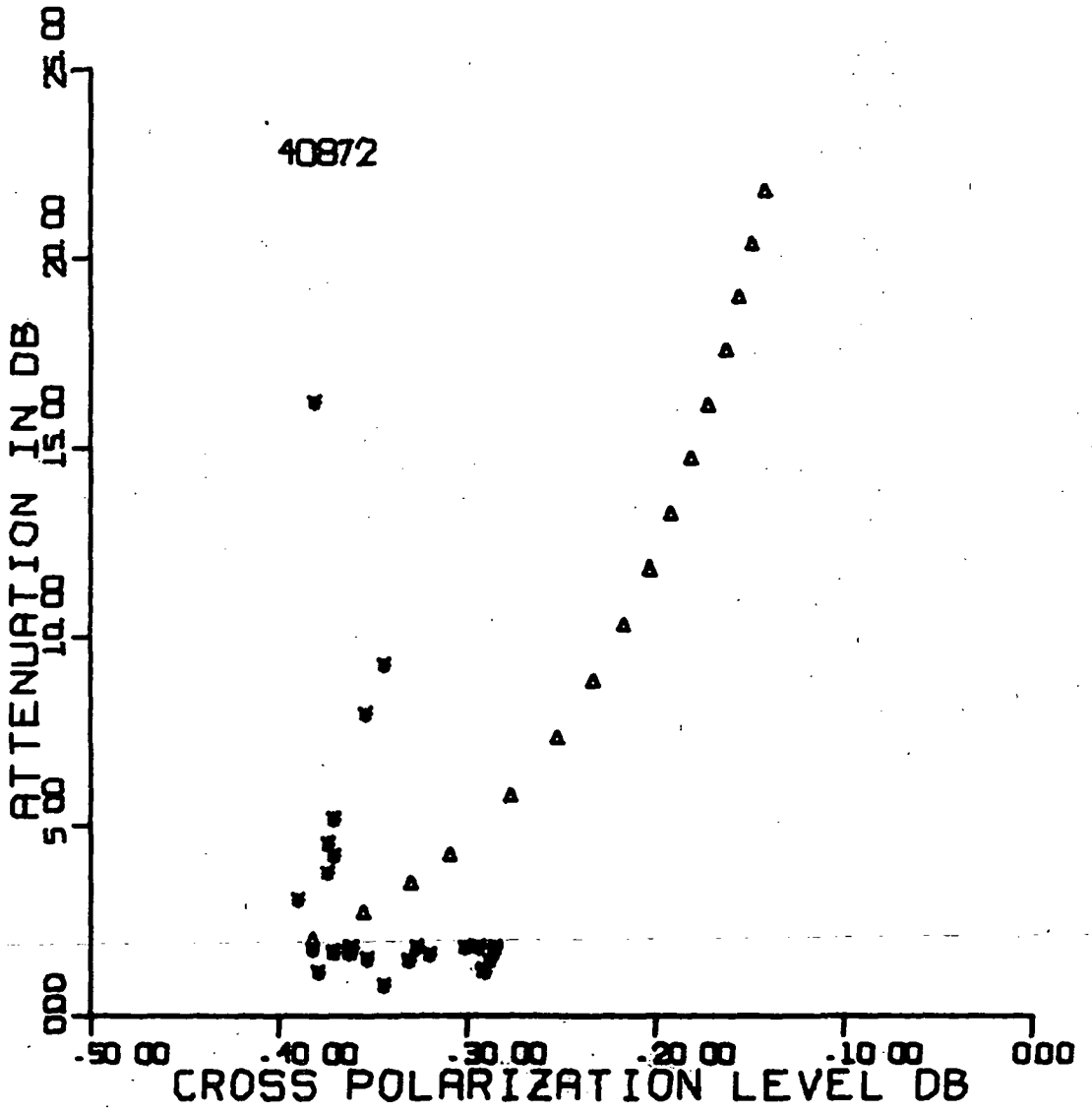

Figure 5. August 4, 1972,
average attenuation versus average cross polarization level.

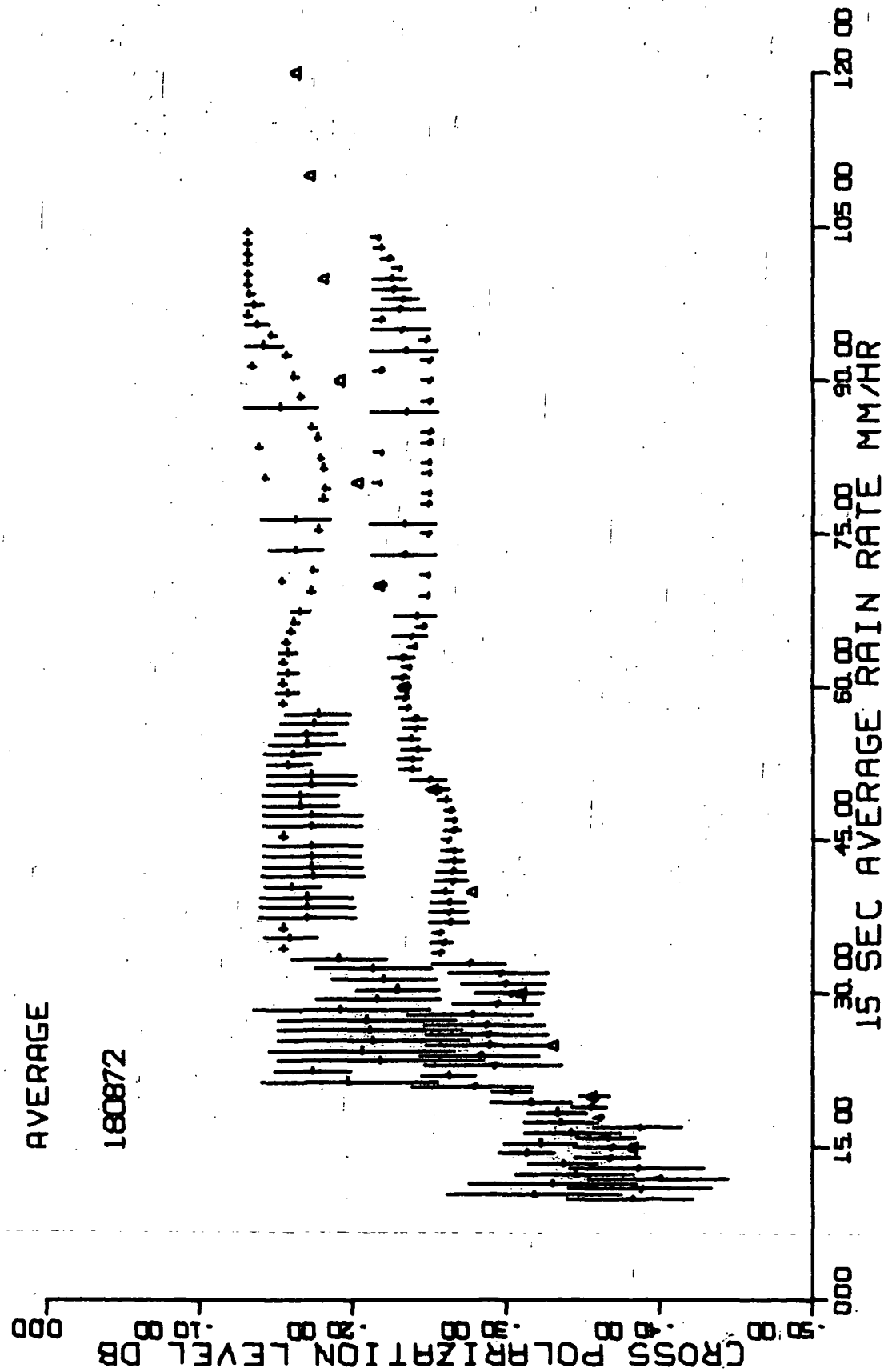

Figure 6. August 17, 1972, average cross polarization levels for each channel.

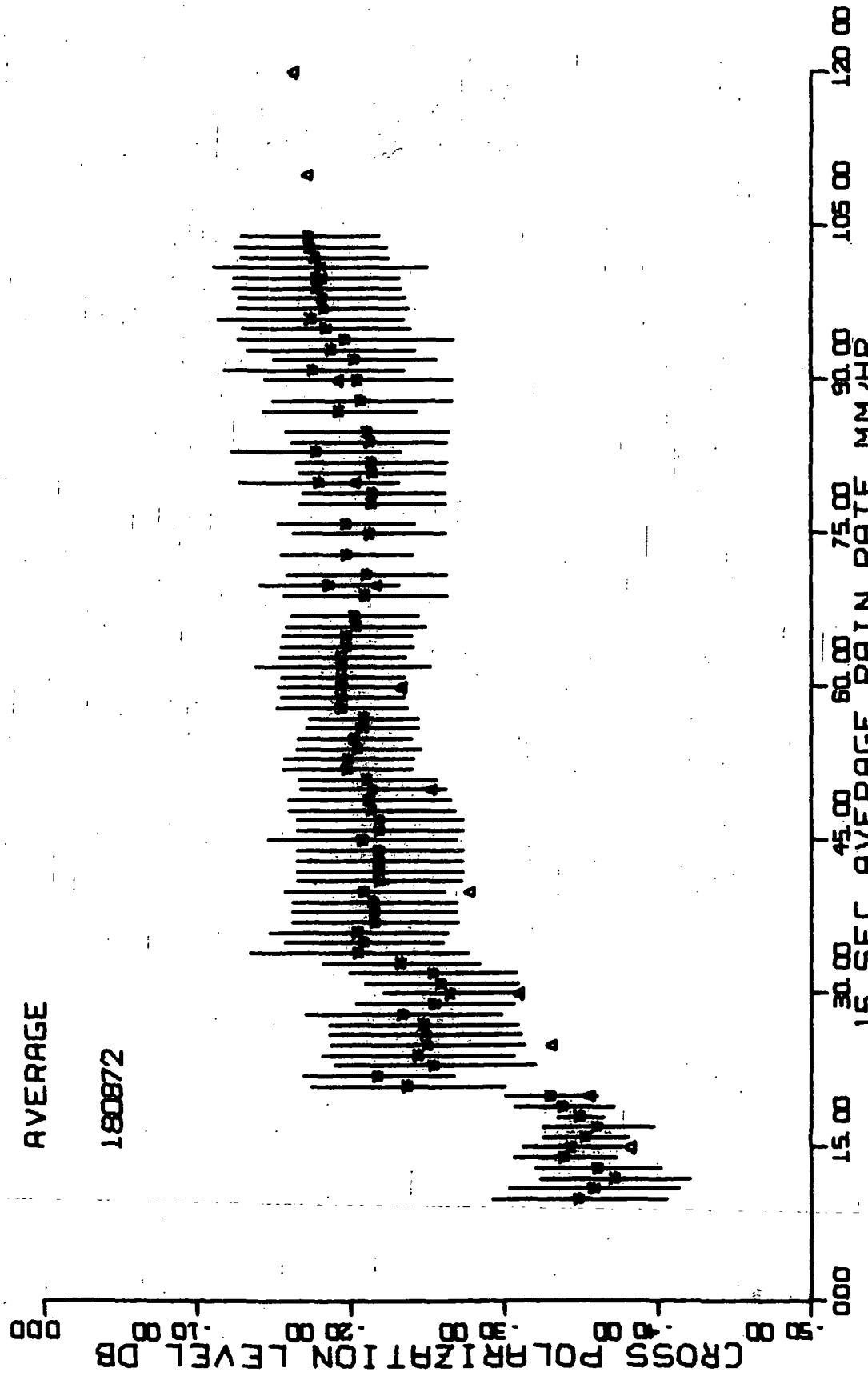

Figure 7. August 17, 1972, average cross polarization levels.

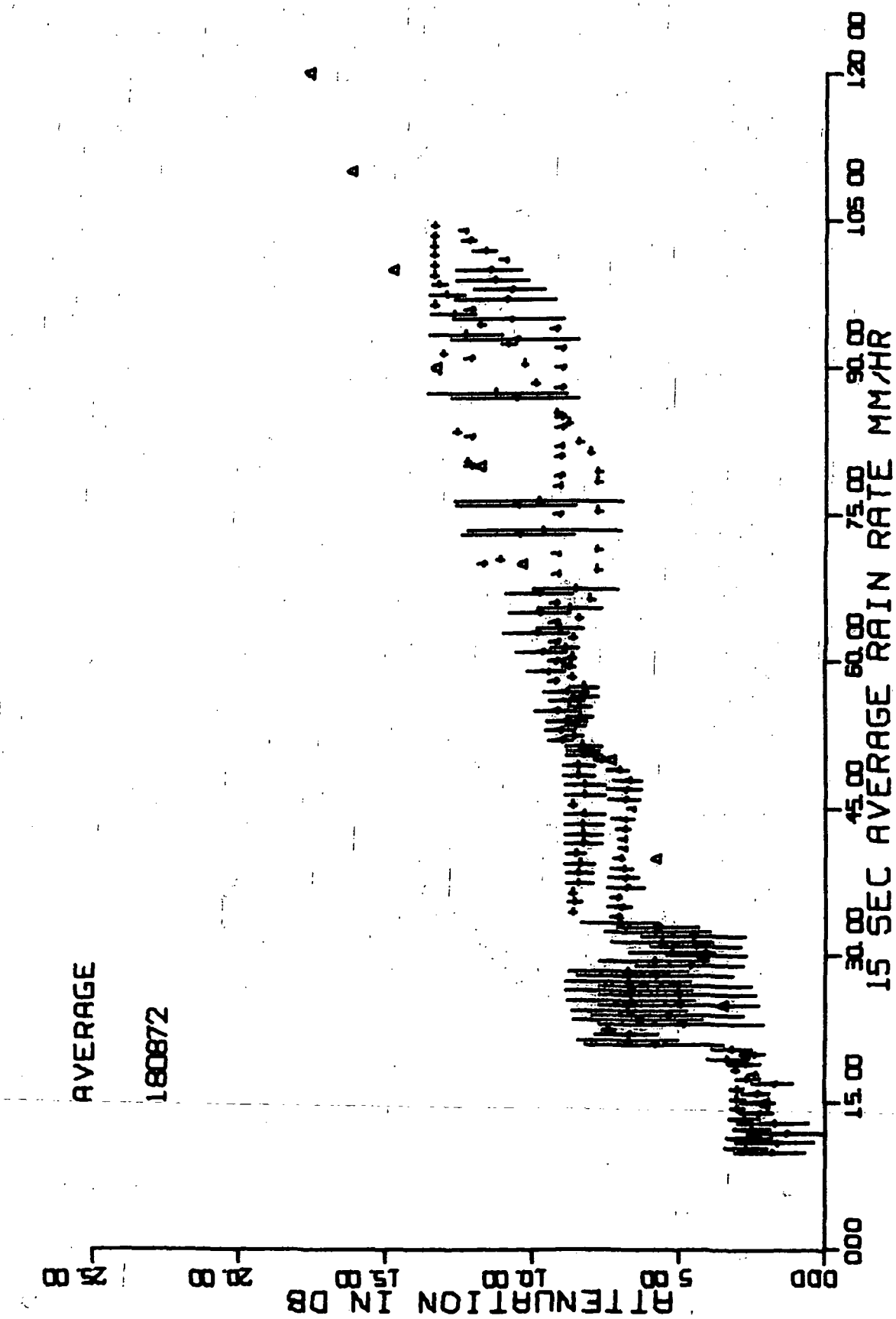

Figure 8. August 17, 1972, average attenuation values for each channel.

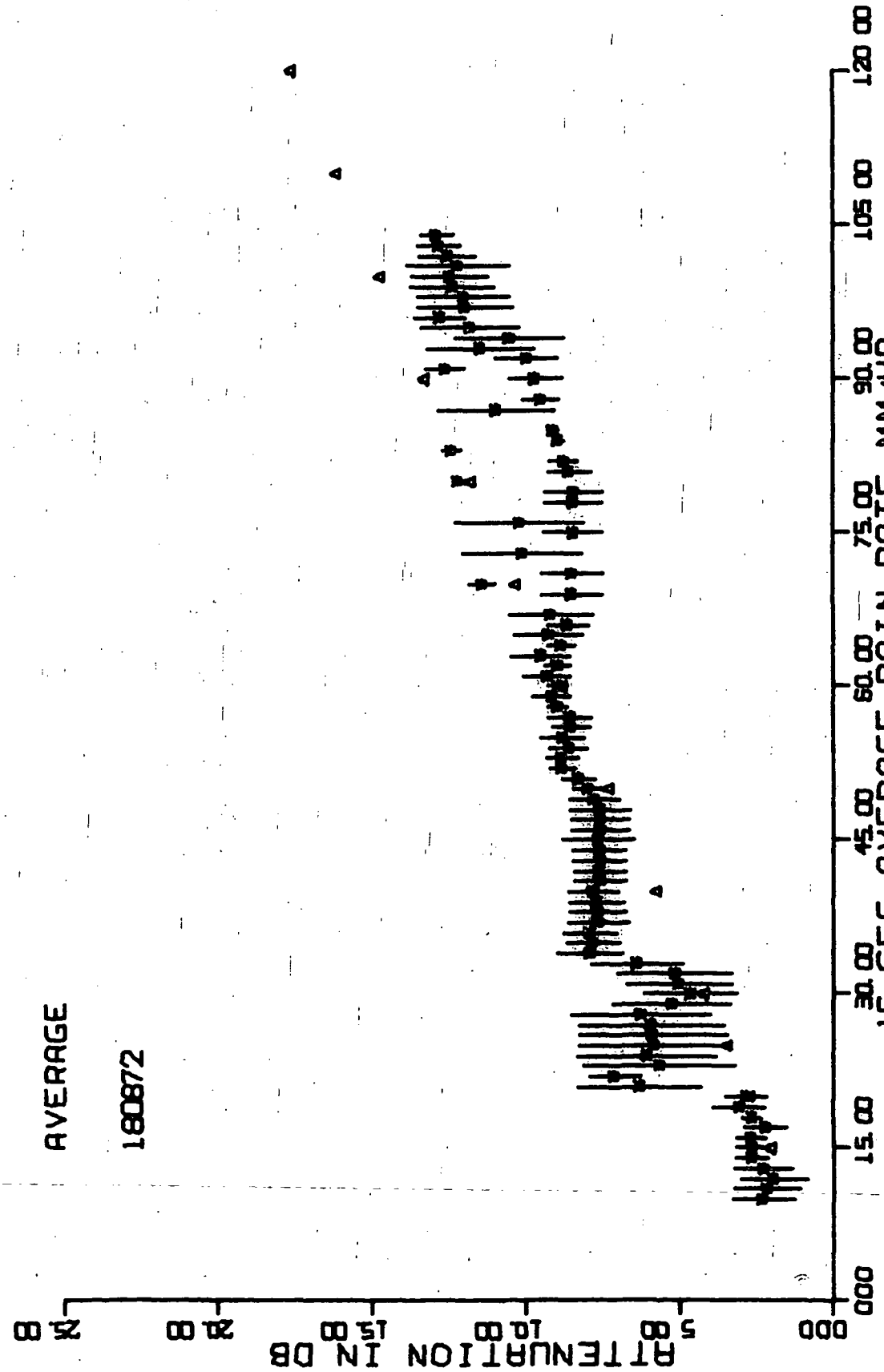

Figure 9. August 17, 1972, average attenuation values.

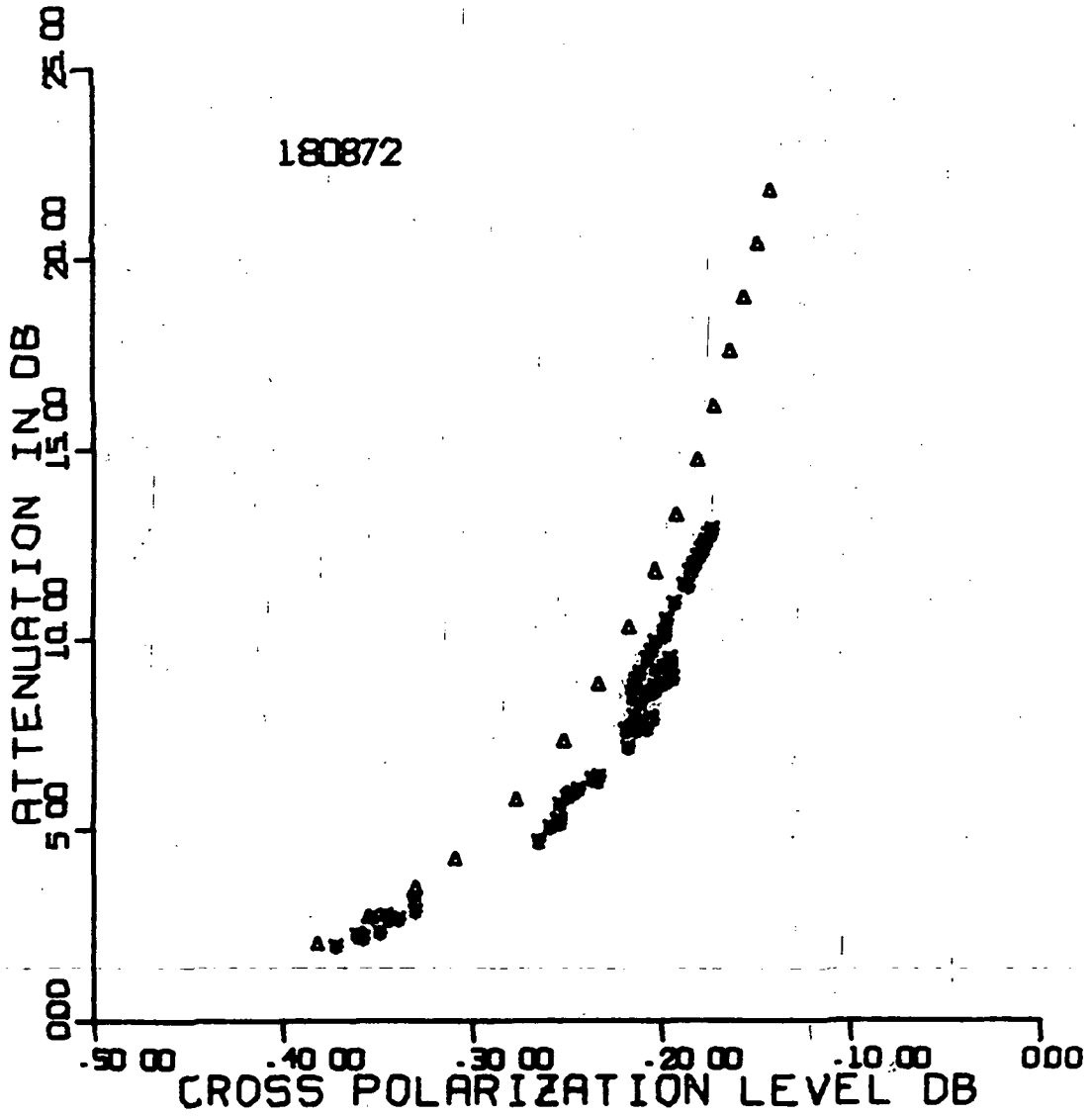

Figure 10. August 17, 1972,
average attenuation versus average cross polarization level.

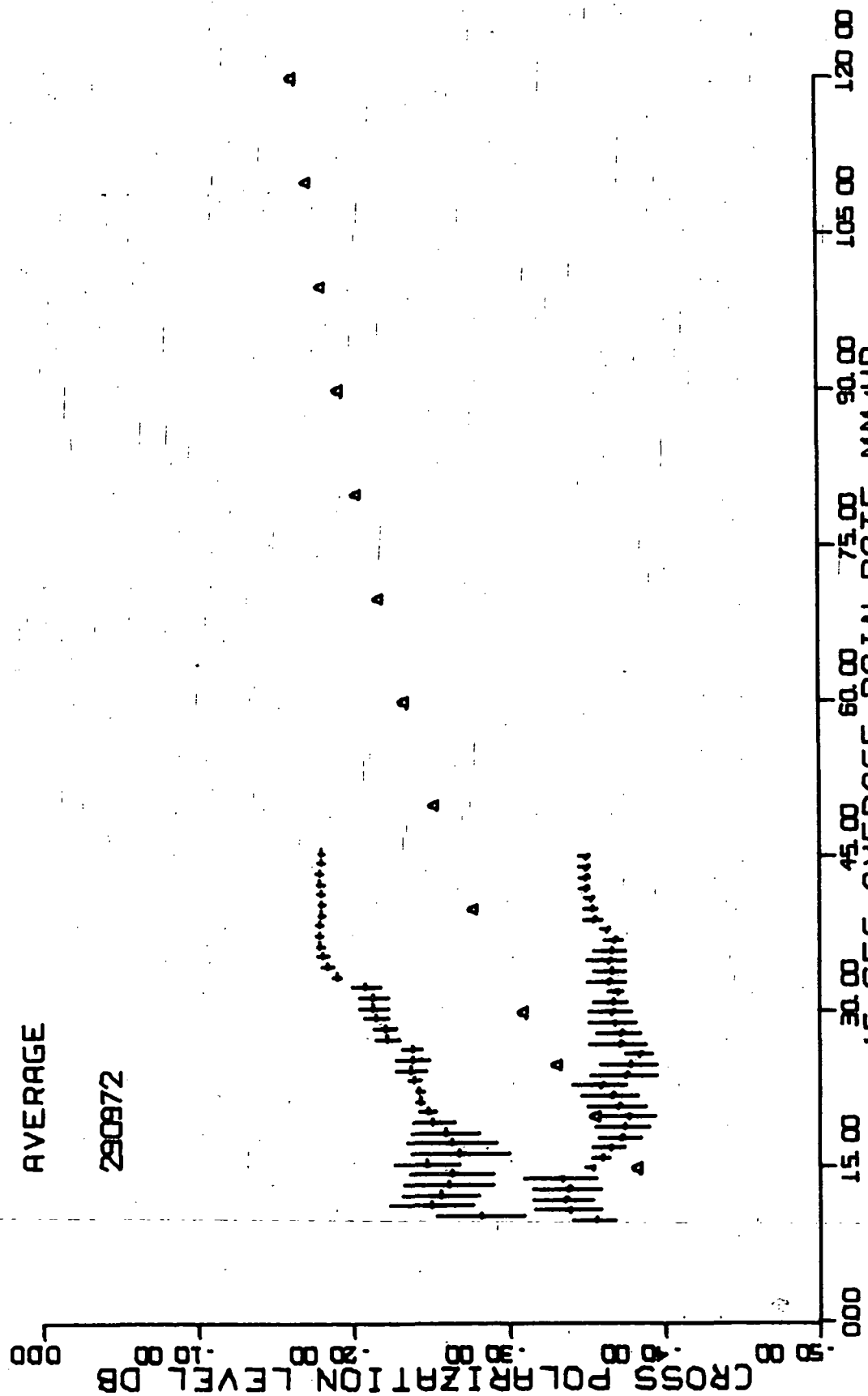

Figure 11. September 29, 1972, average cross polarization levels for each channel.

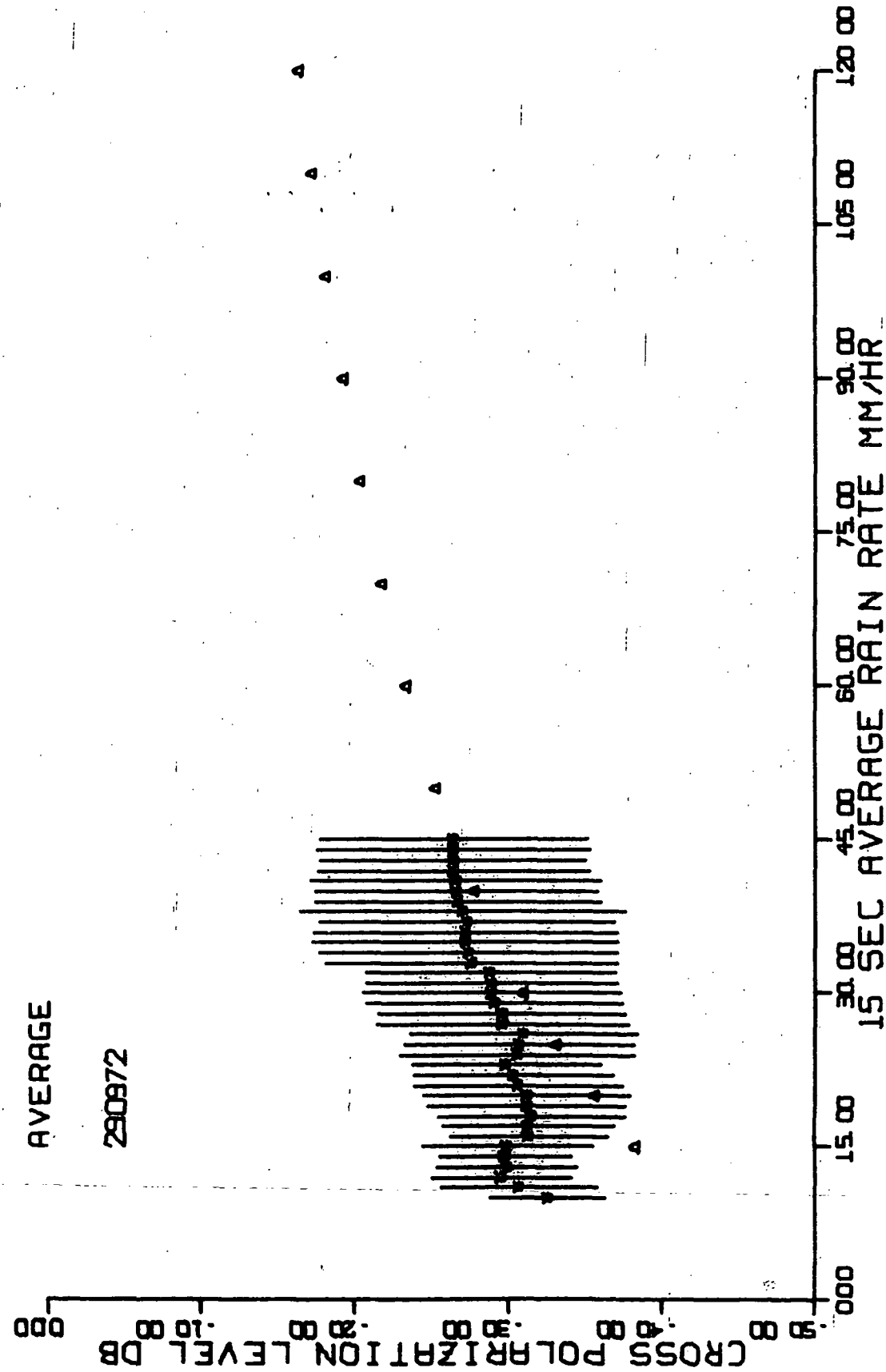

Figure 12. September 29, 1972, average cross polarization levels.

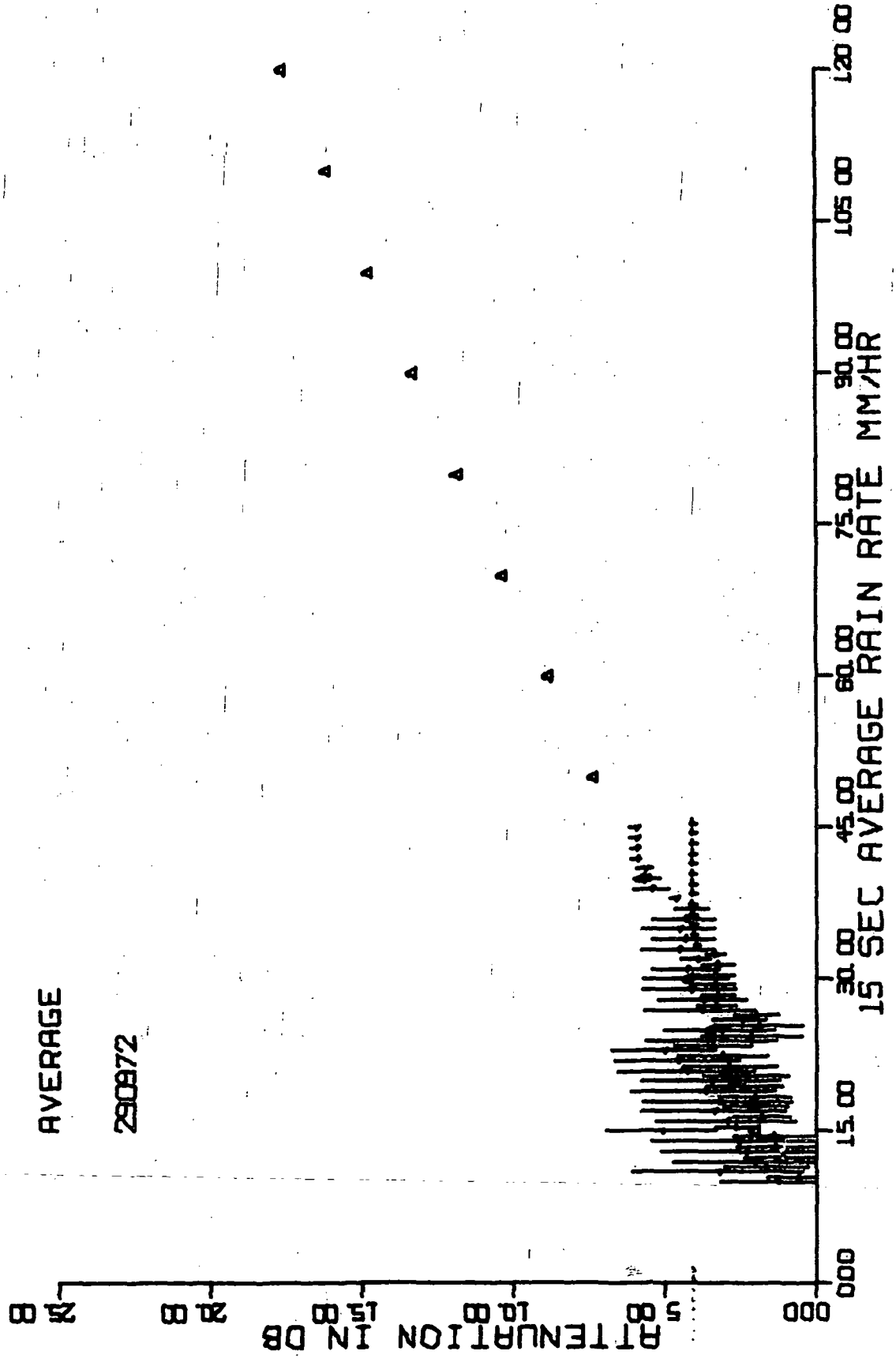

Figure 13. September 29, 1972, average attenuation values for each channel.

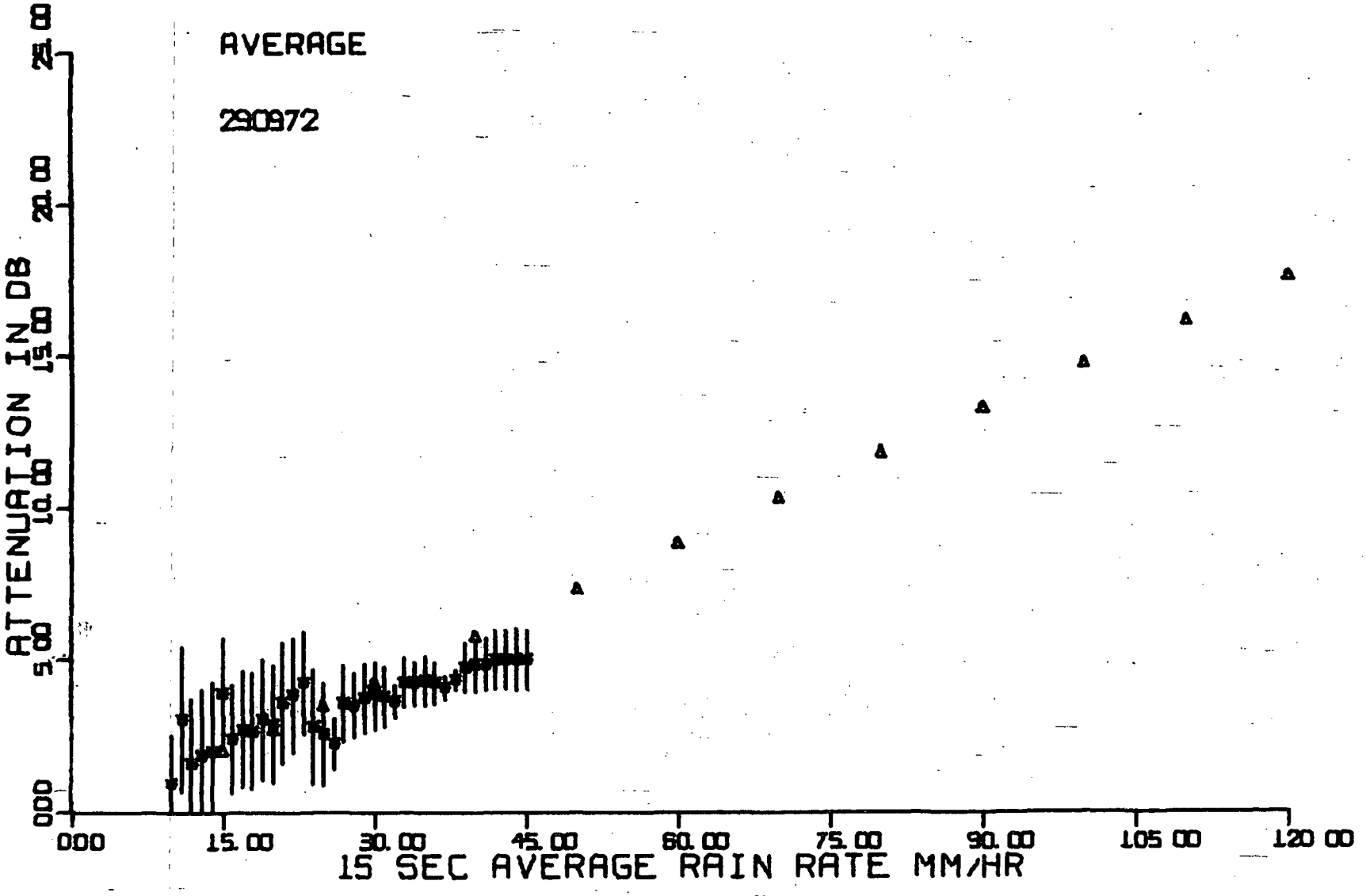

Figure 14. September 29, 1972, average attenuation values.

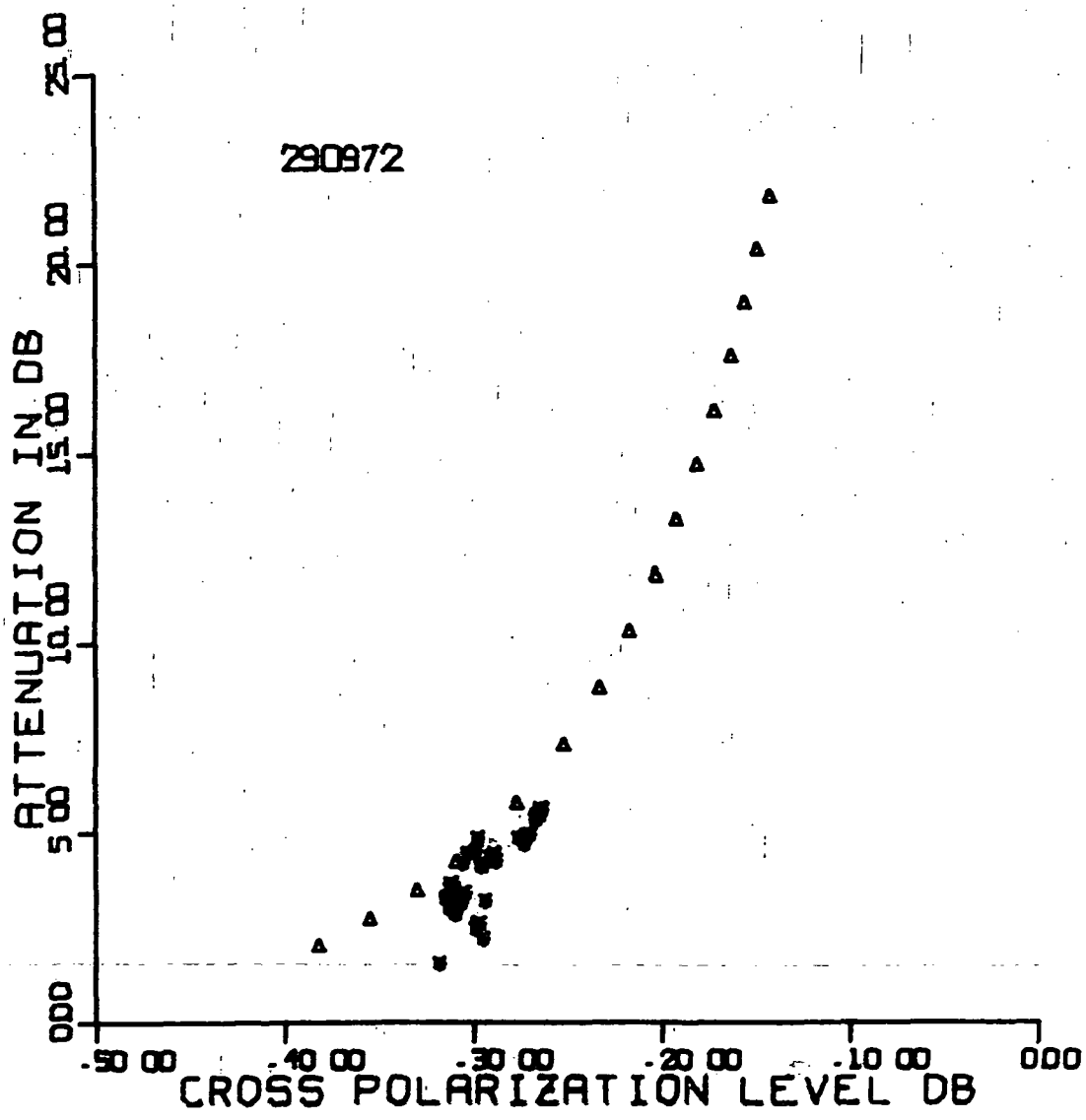

Figure 15. September 29, 1972, average attenuation versus average cross polarization level.

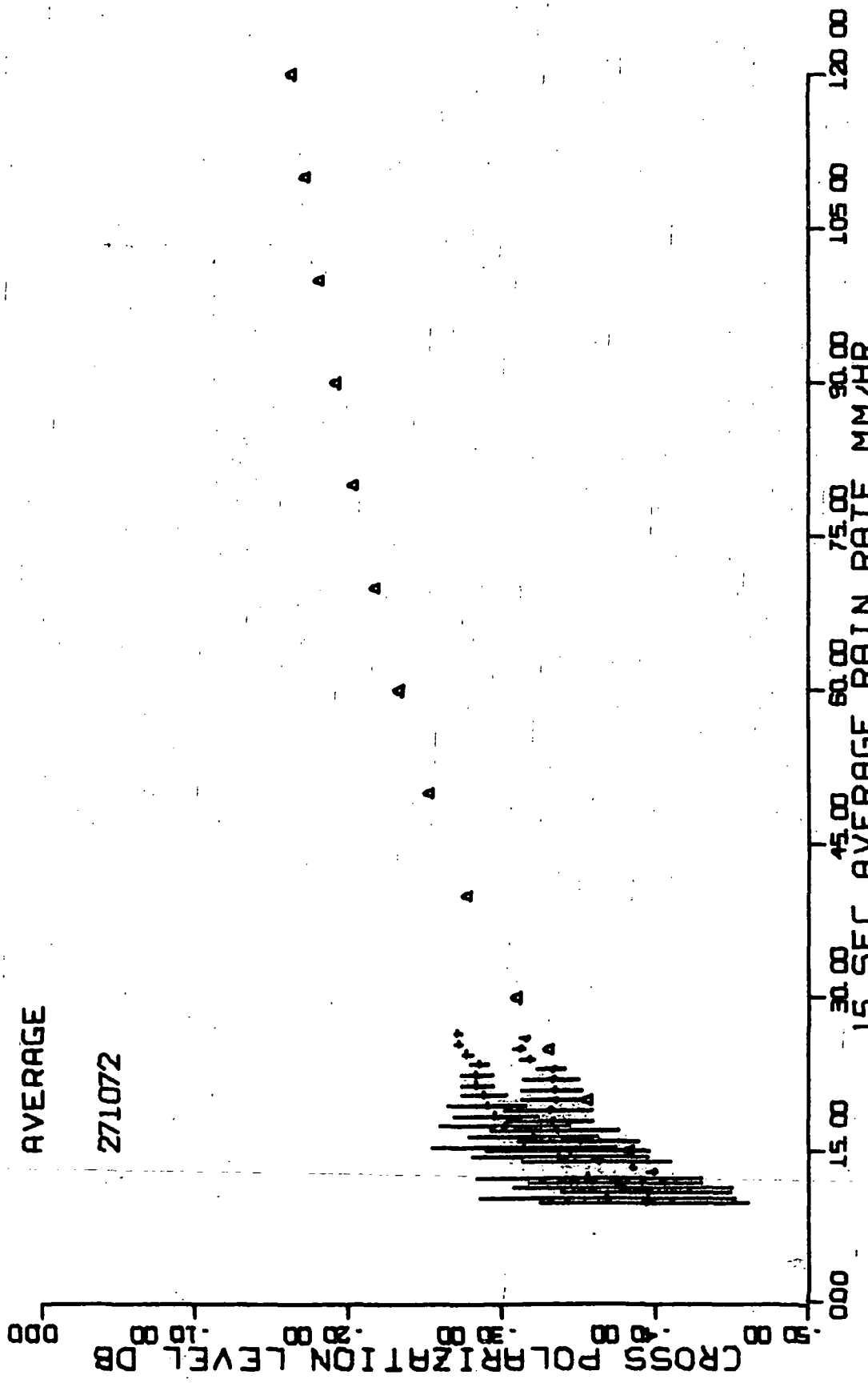

Figure 16. October 27, 1972, average cross polarization levels for each channel.

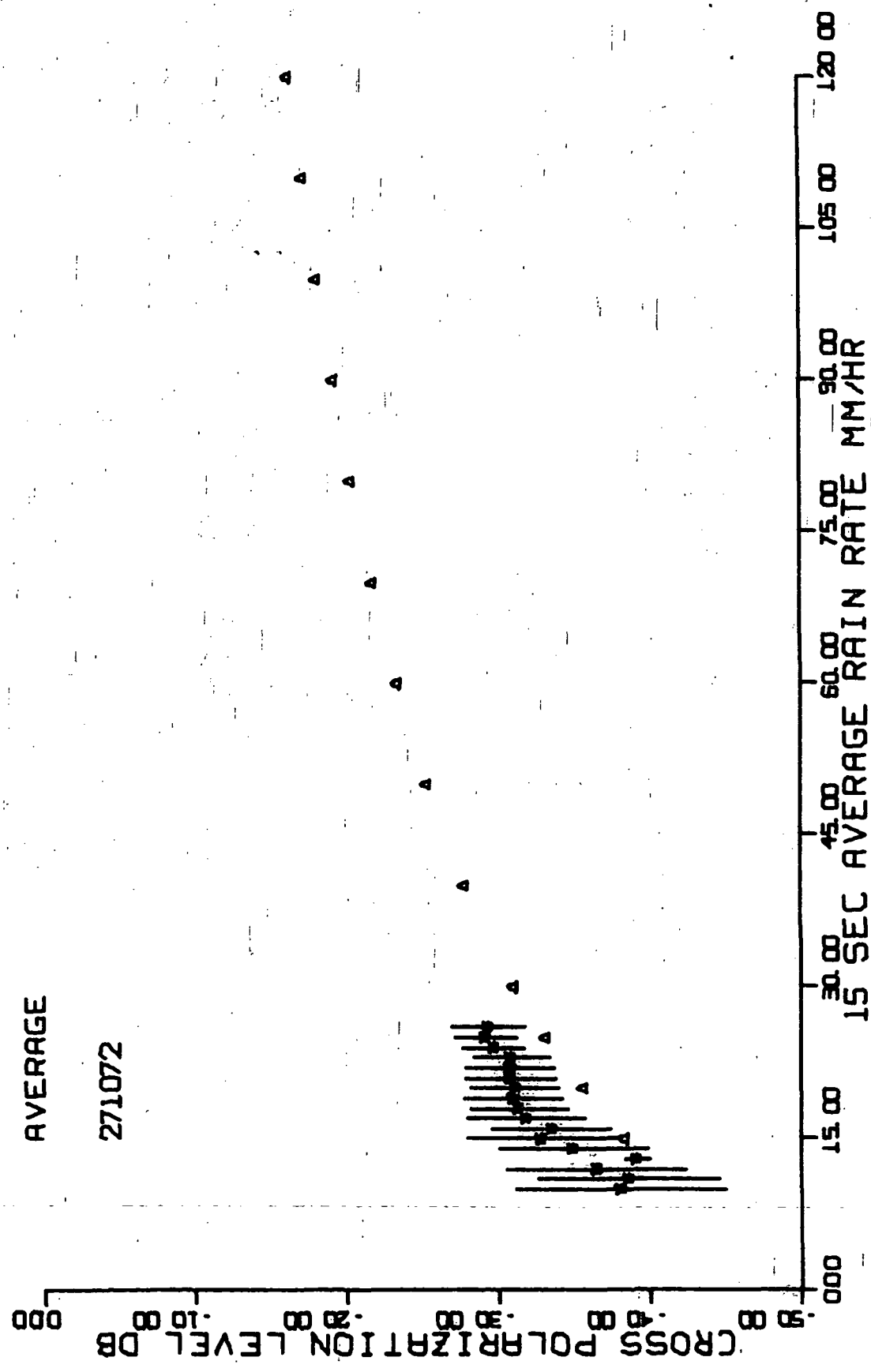

Figure 17. October 27, 1972, average cross polarization levels.

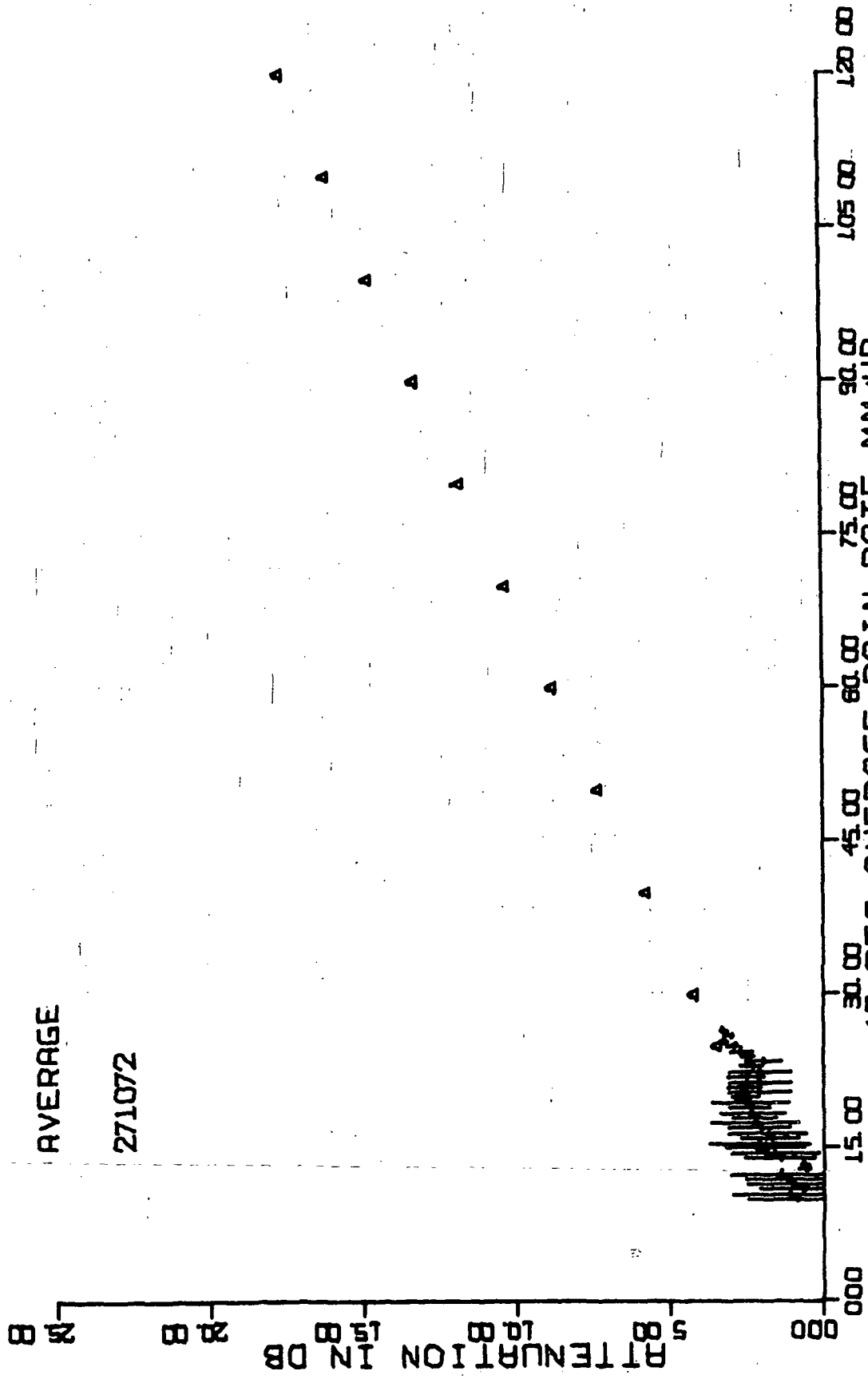

Figure 18. October 27, 1972, average attenuation values for each channel.

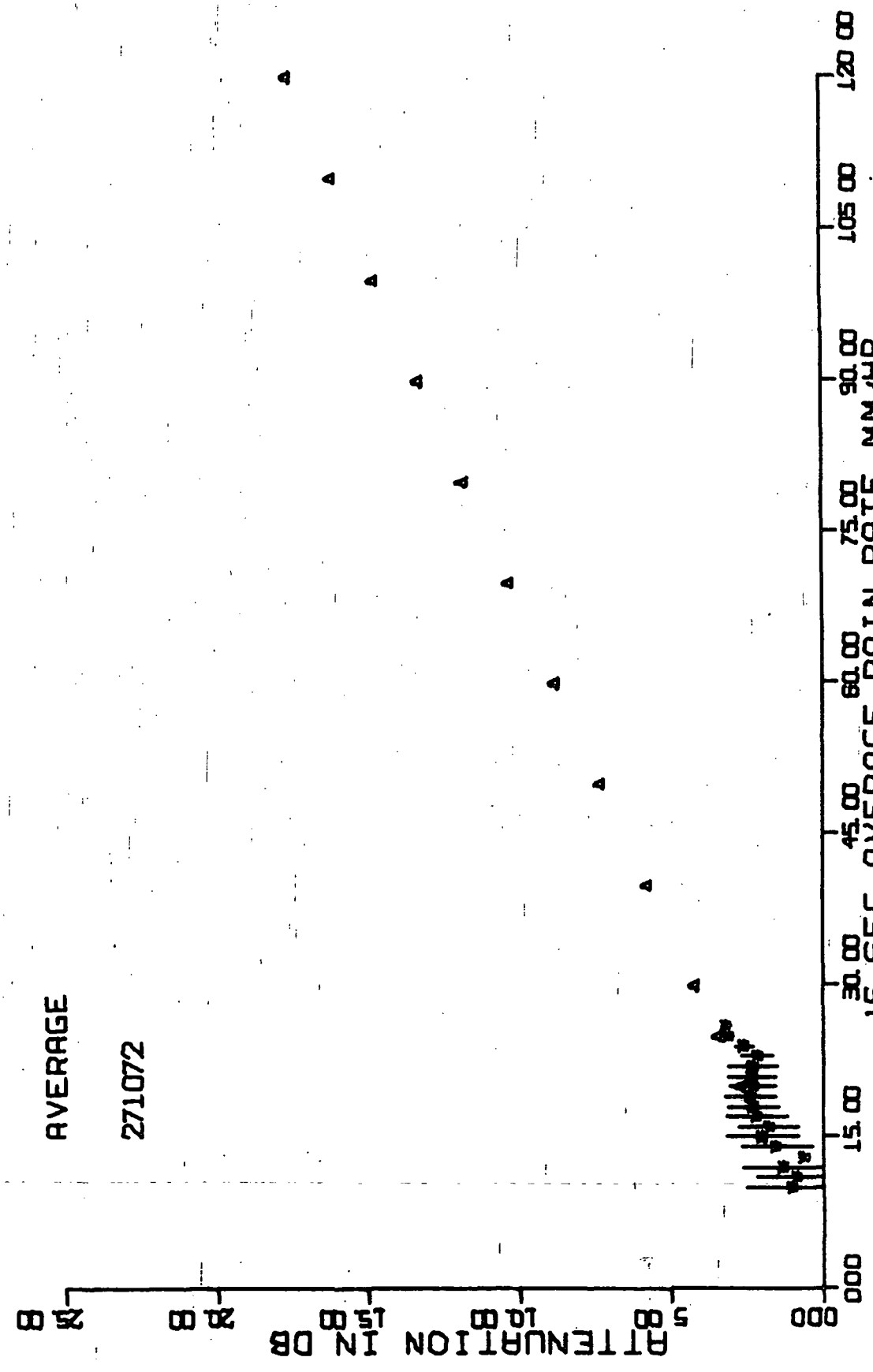

Figure 19. October 27, 1972, average attenuation values.

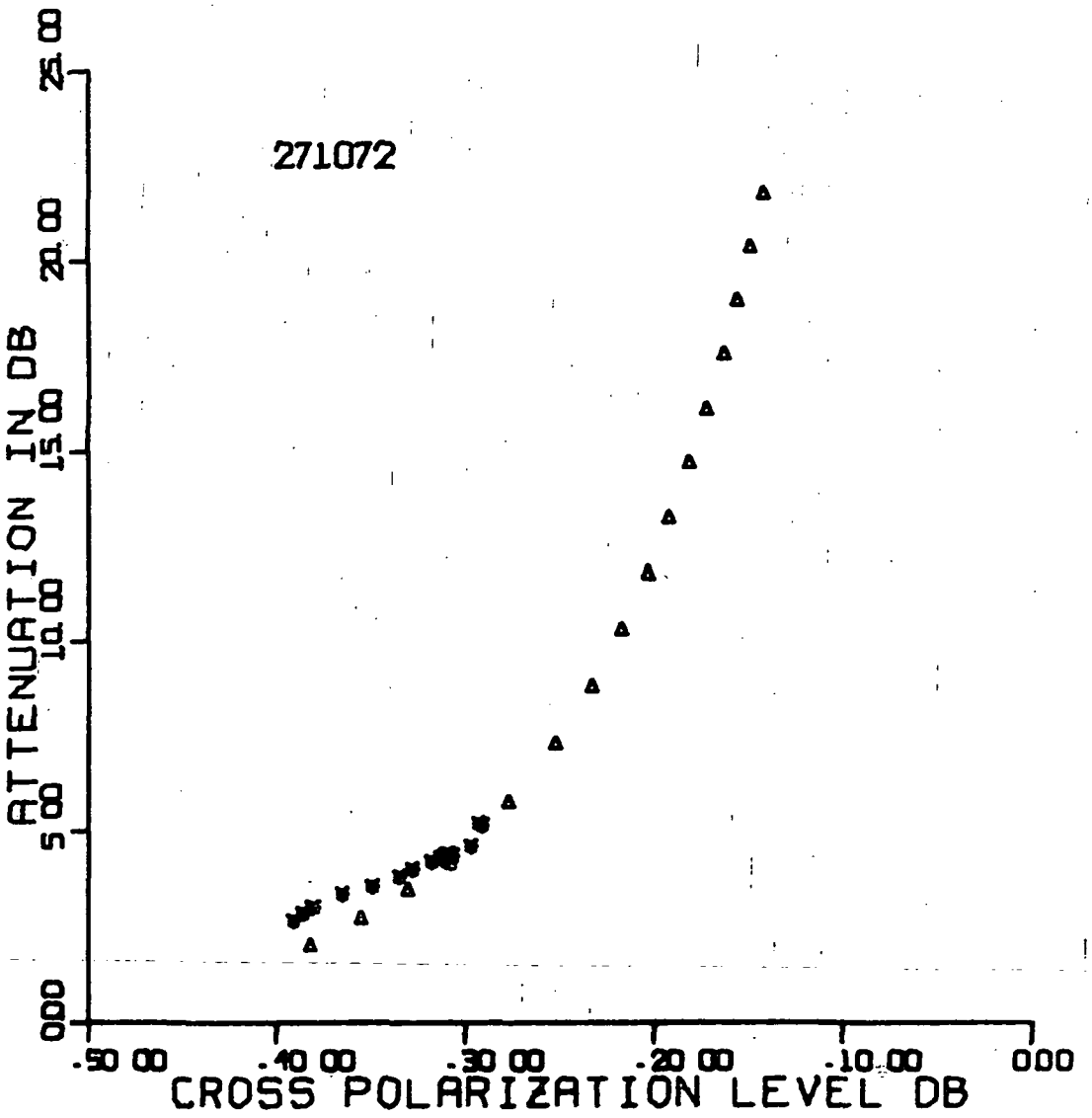

Figure 20. October 27, 1972,
average attenuation versus average cross polarization level.

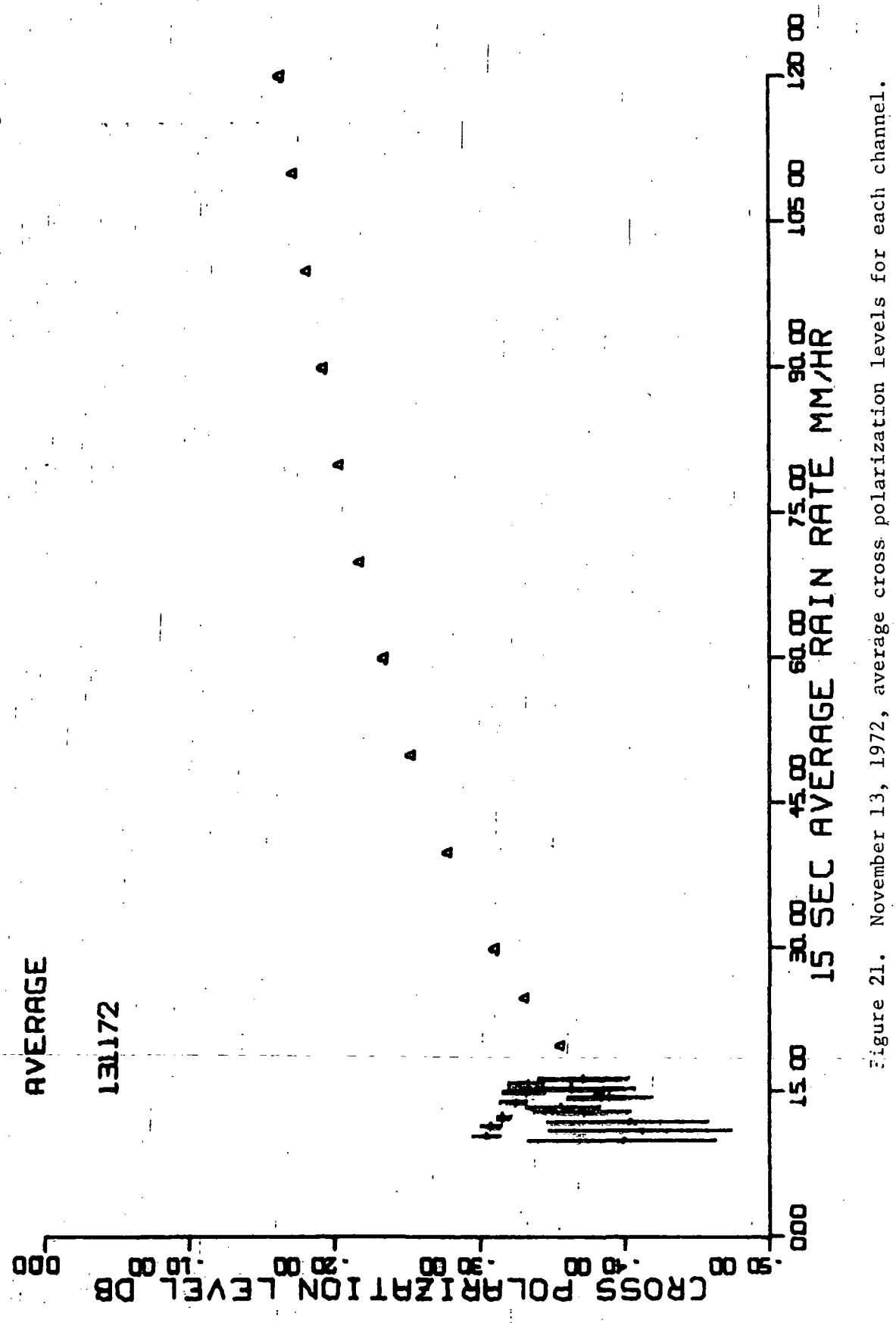

Figure 21. November 13, 1972, average cross polarization levels for each channel.

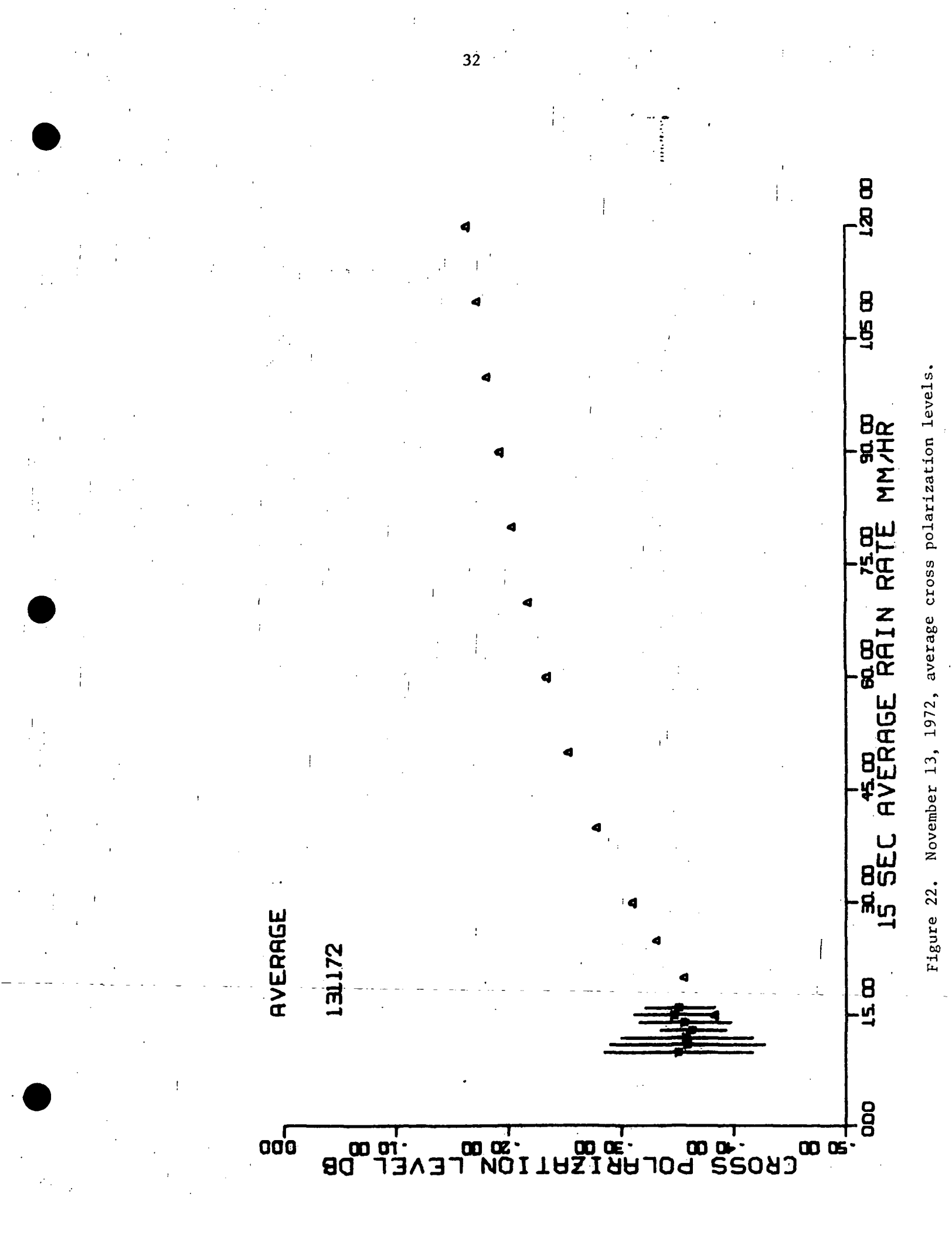

Figure 22. November 13, 1972, average cross polarization levels.

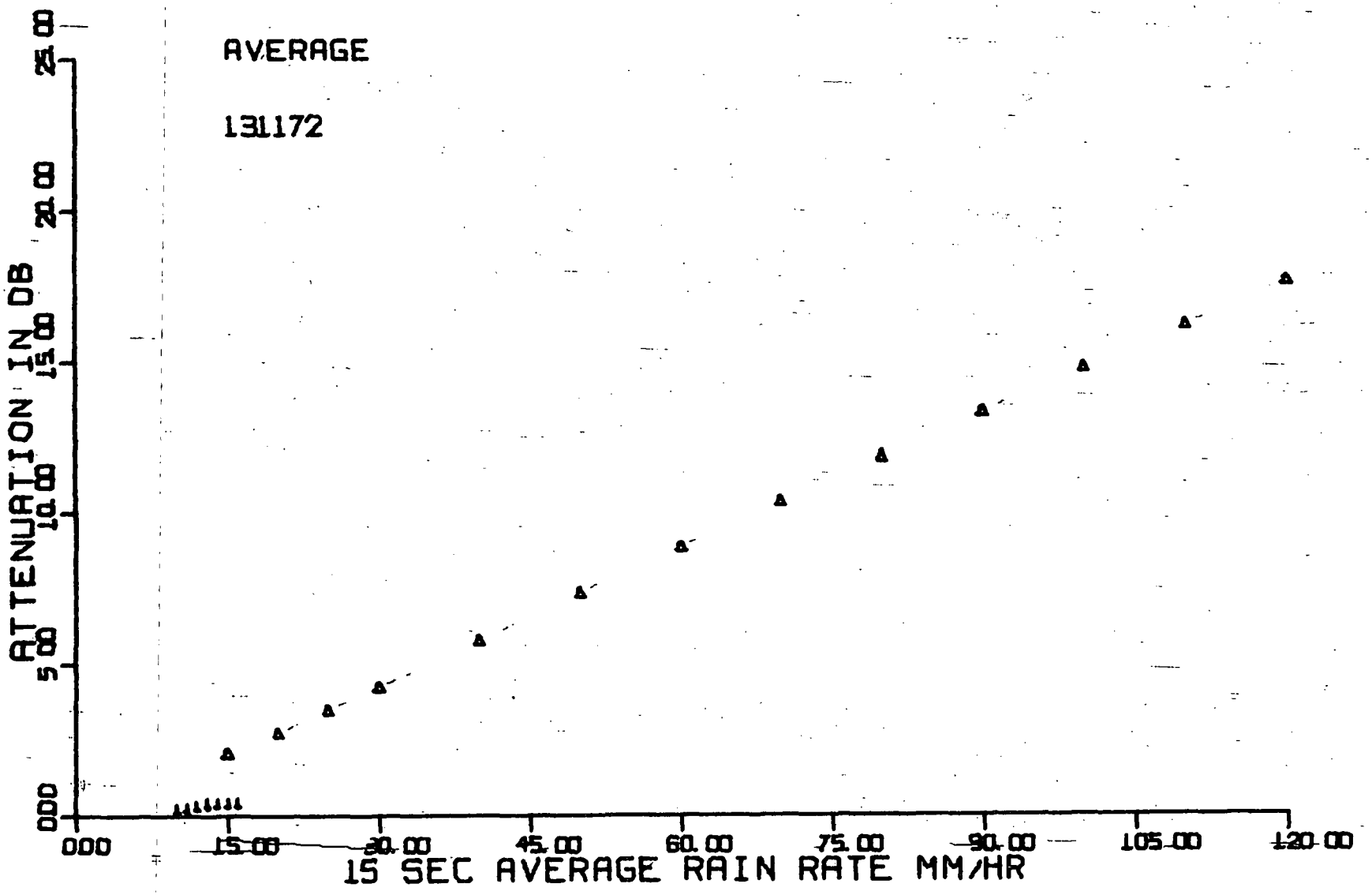

Figure 23. November 13, 1972, average attenuation values for each channel.
(+ channel values were zero.)

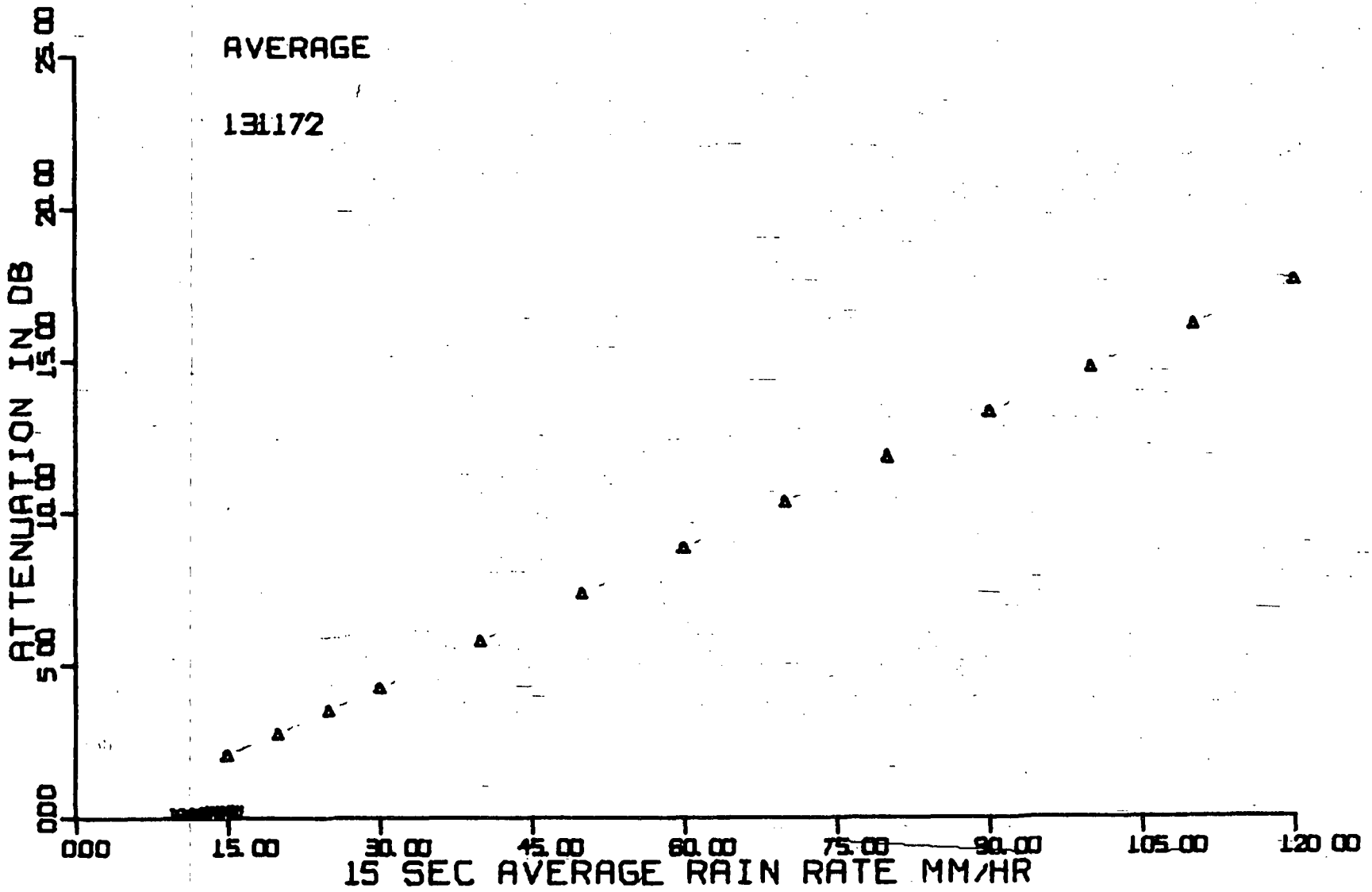

Figure 24. November 13, 1972, average attenuation values.

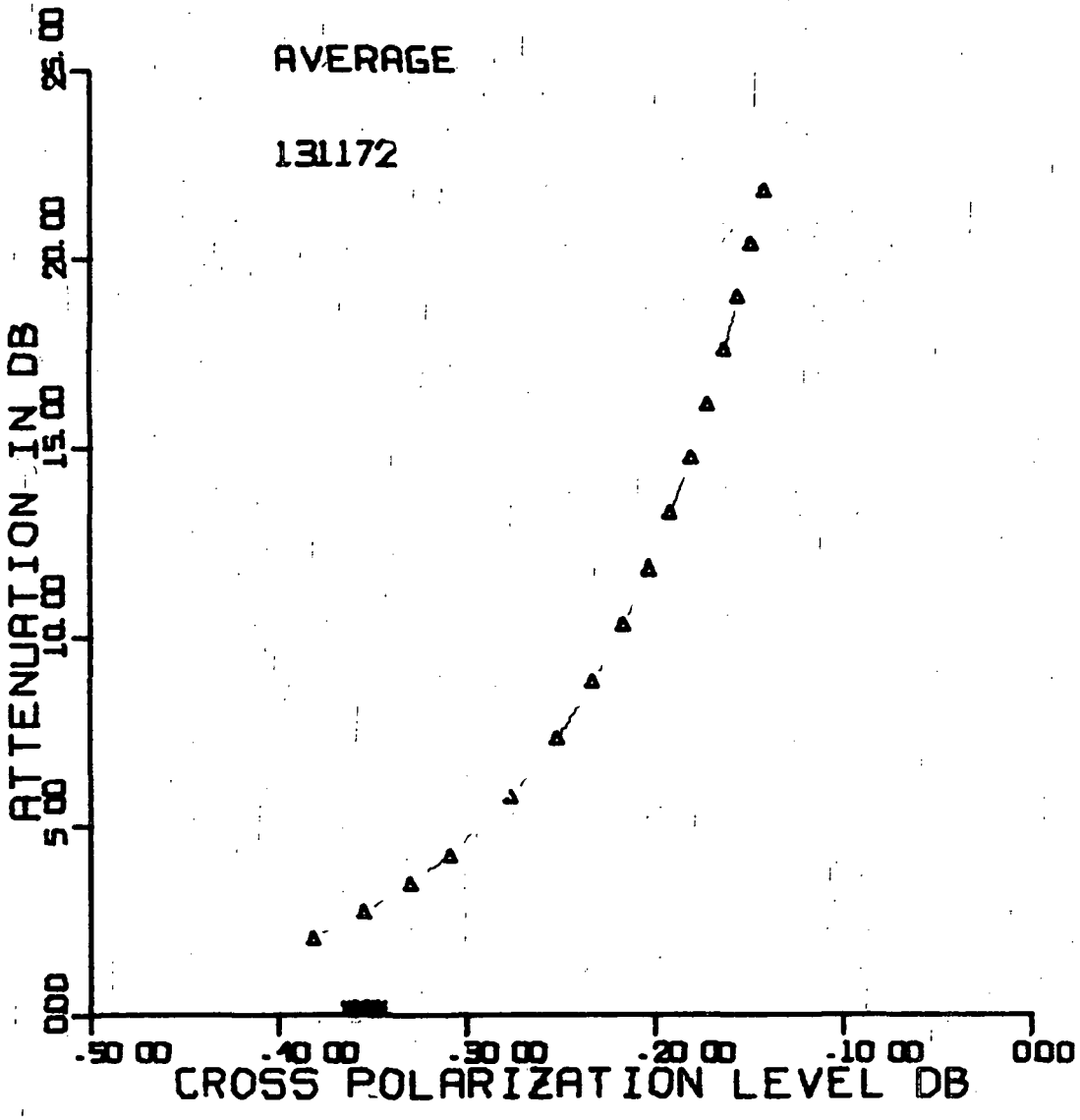

Figure 25. November 13, 1972,
average attenuation versus average cross polarization level.

5.1.7 November 14, 1972

Figures 26 through 30 present data from this storm.

5.2 1973 Data

5.2.1 Introduction

At the time of writing 7 storms have been observed in 1973 and two of these brought the highest rain rates recorded thus far in the project. Table 1 lists the important parameters of the 1973 storms; all are discussed in the following paragraphs except that of April 4. Data reduction difficulties with that storm necessitate postponing it until the next report. Because of the time delay involved in processing the data, storms which occurred after June 1, 1973, will appear in the next report.

5.2.2 March 16, 1973

Data from this storm appear in Figures 31 through 36. Figure 31 is a scatter plot displaying 15 second running average cross polarization levels taken at successive one second intervals. Data for rain rates less than 10 mm/hr have been suppressed.

5.2.3 March 17, 1973

Figures 37 through 42 display data for this storm.

5.2.4 April 4, 1973

Plots from this storm were not available at the time of publication because of computer problems.

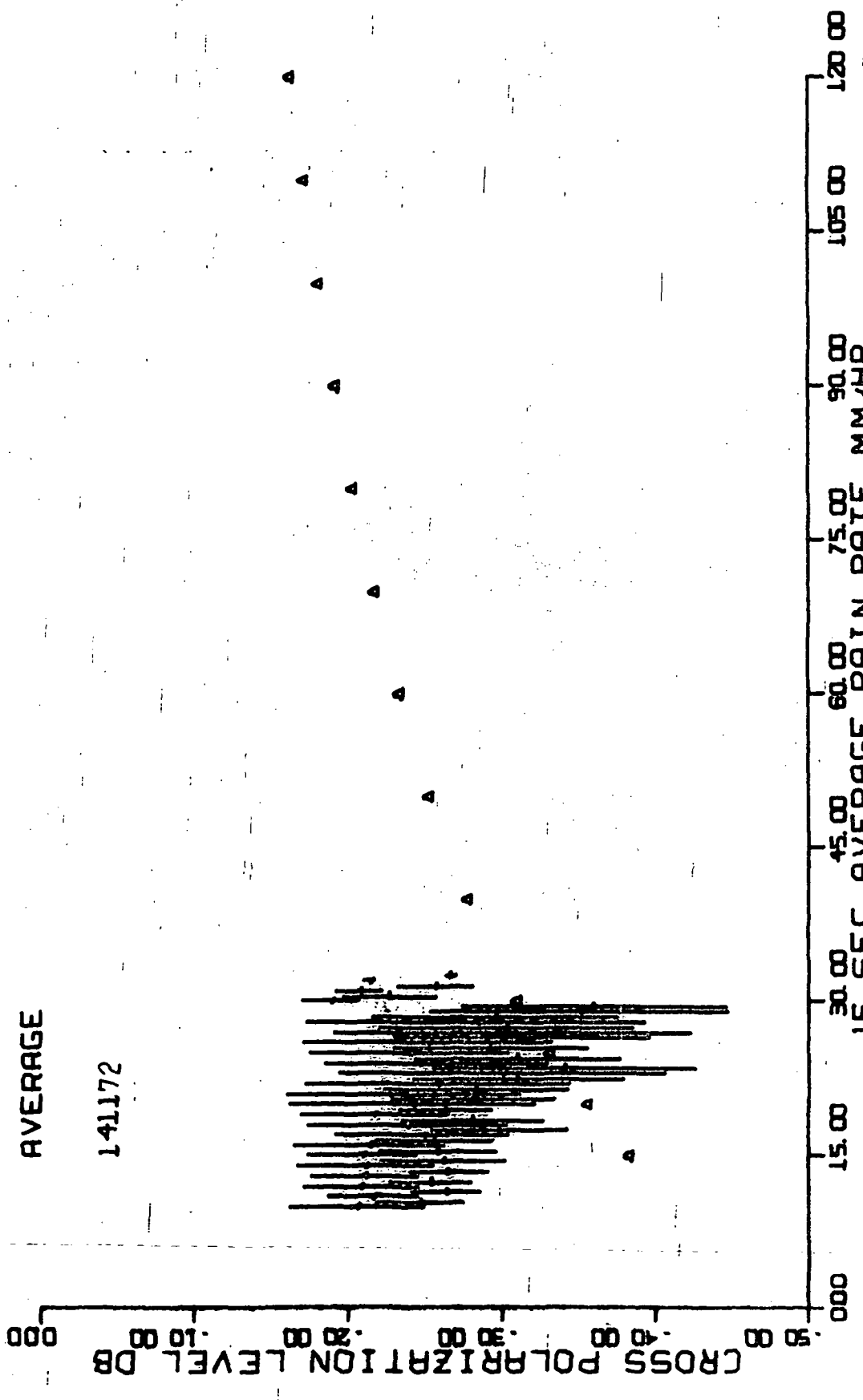

Figure 26. November 14, 1972, average cross polarization levels for each channel.

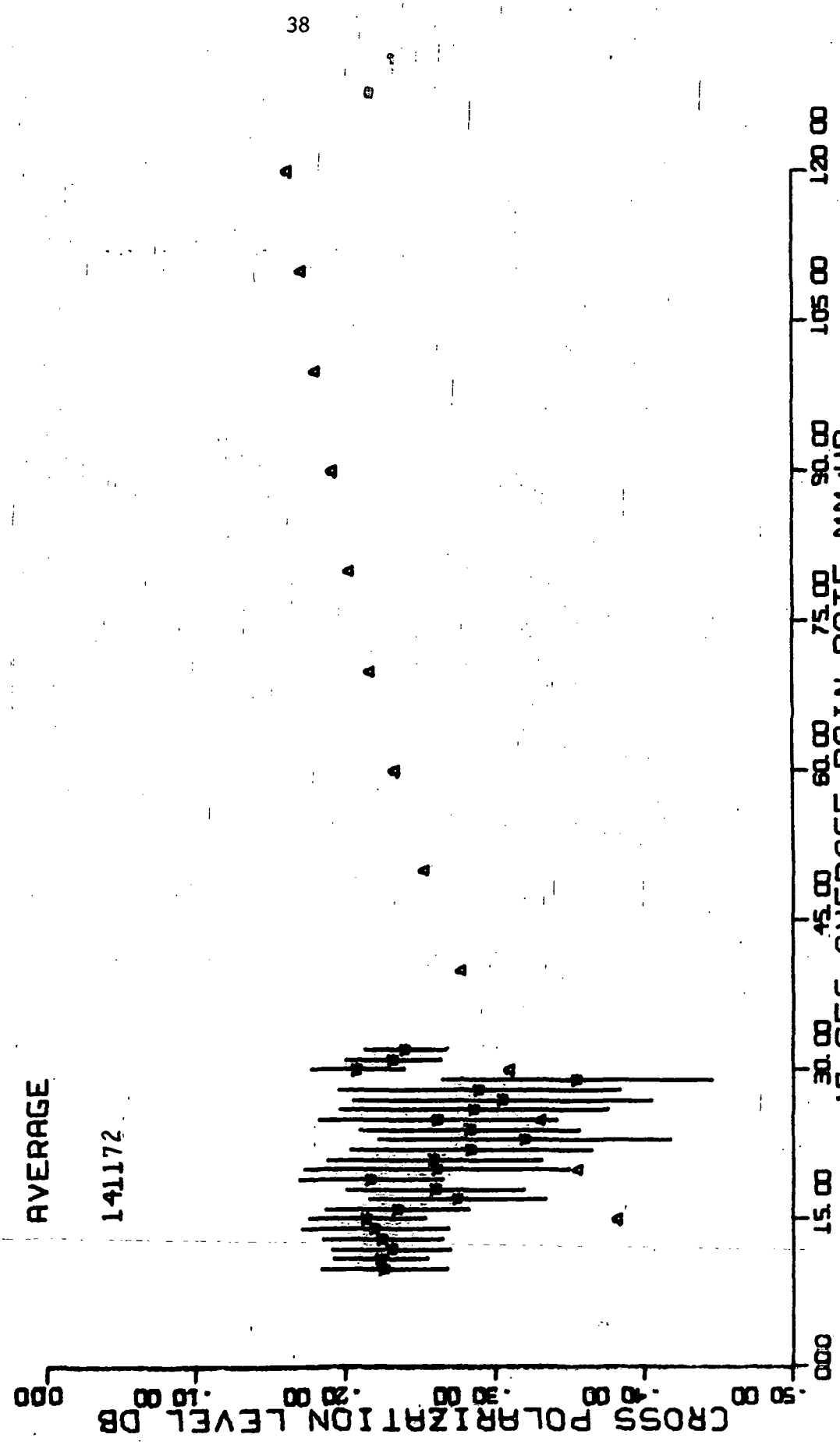

Figure 27. November 14, 1972, average cross polarization levels.

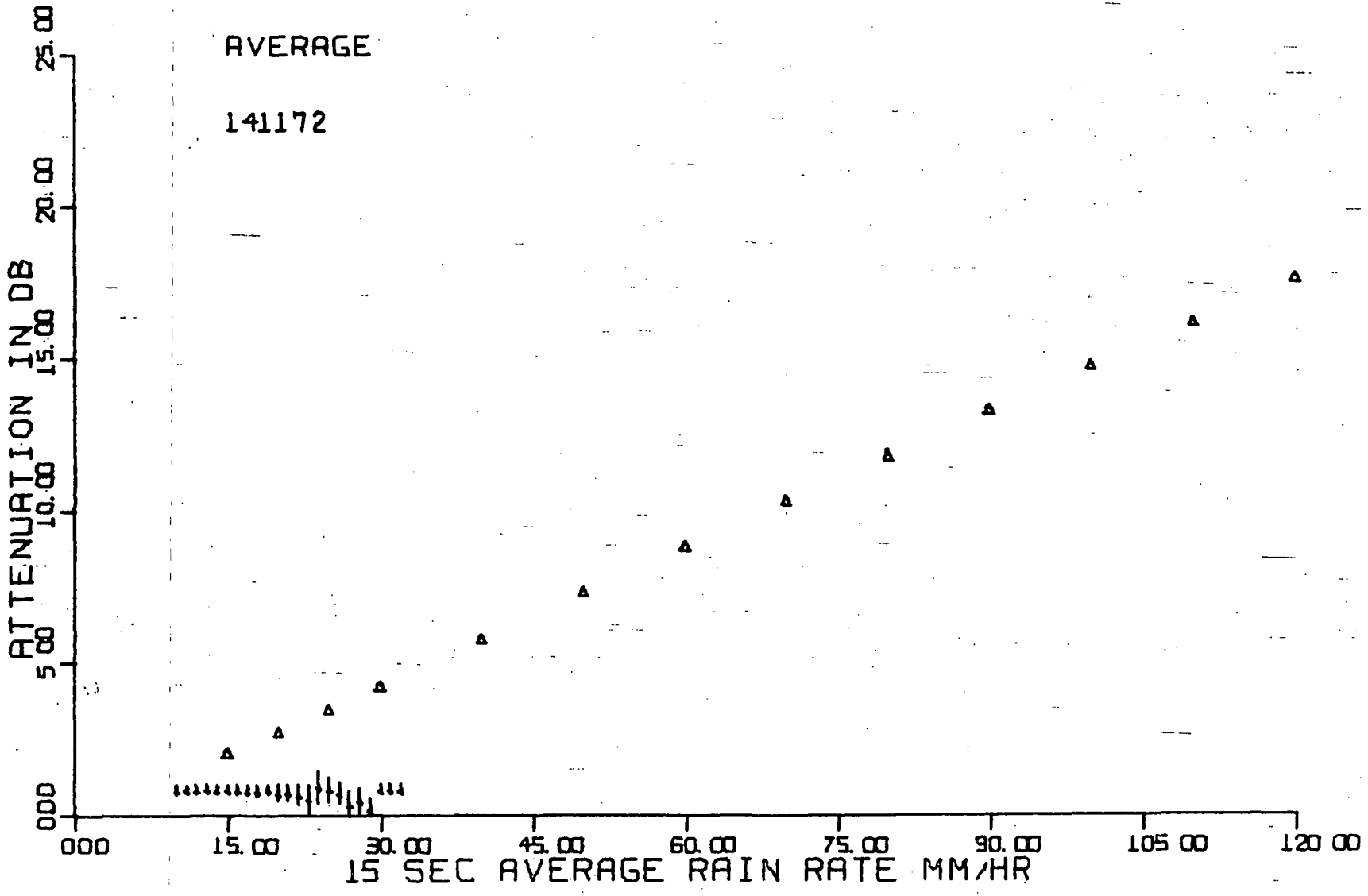

Figure 28. November 14, 1972, average attenuation values for each channel. (All + values were zero.)

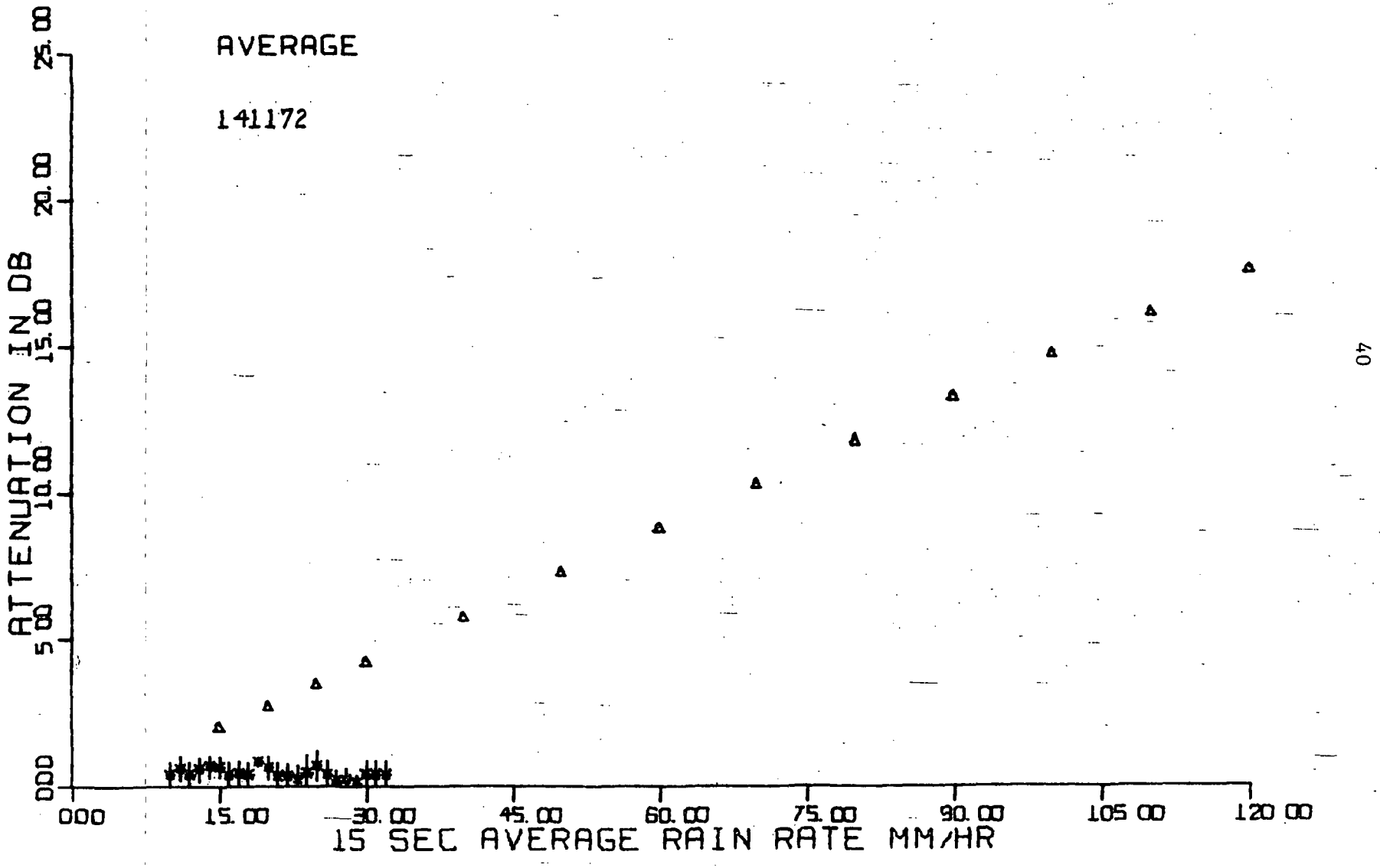

Figure 29. November 14, 1972, average attenuation values.

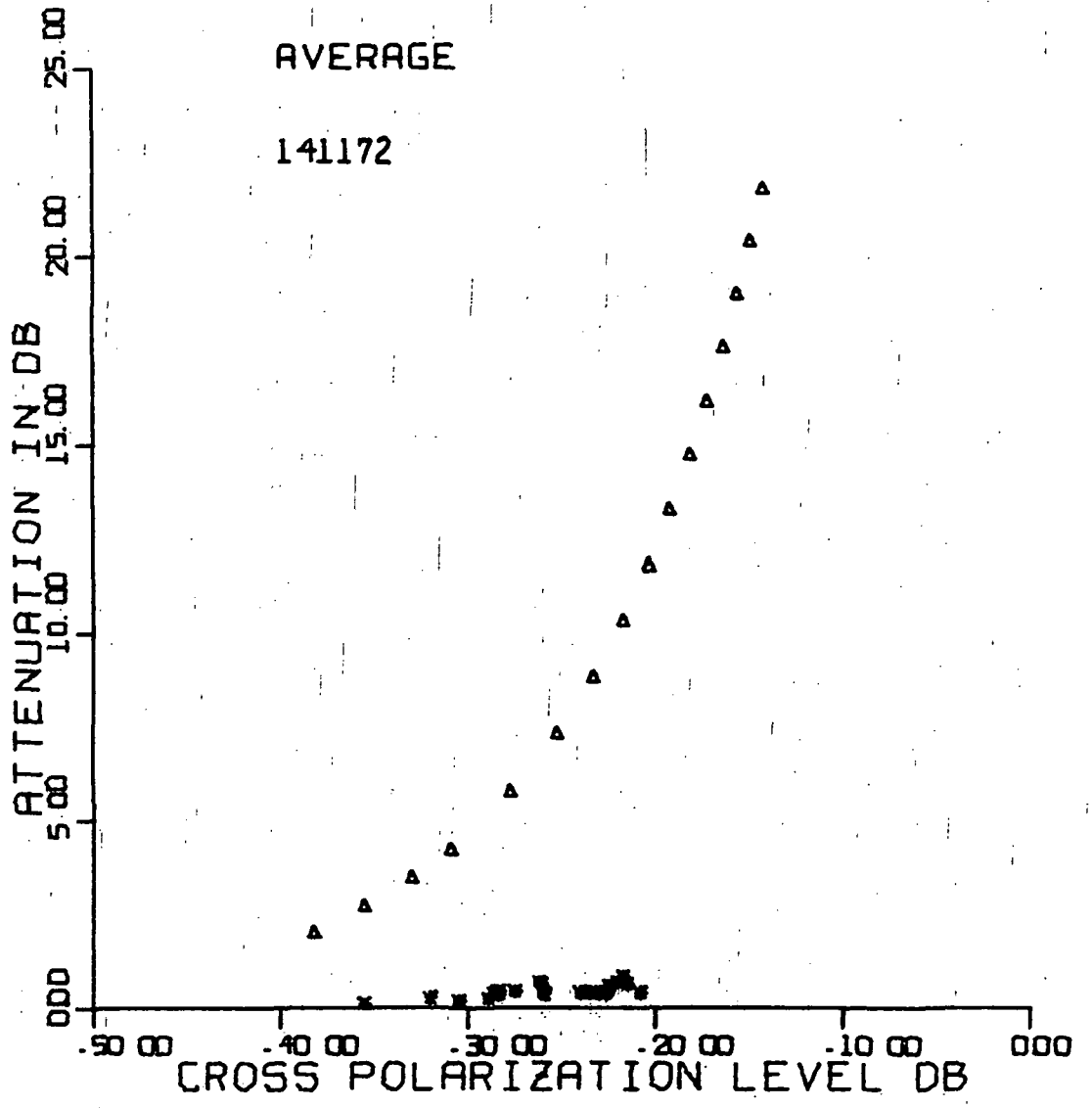

Figure 30. November 14, 1972,
average attenuation versus average cross polarization level.

Table 1. Summary of Storms in this Report Period

Date	Local Starting Time	Local Ending Time	Storm Duration, Seconds	Peak Rain Rate Between Trips for any 1 Gauge, mm/hr.	Peak 15-second Averaged Path Rain Rate, mm/hr.	Total Rain Accumulation, mm					Number of Retained Data Points										
						RG #1	RG #2	RG #3	RG #4	RG #5	RG #1	RG #2	RG #3	RG #4	RG #5	R + T +	R + T -	R + T +/-	R - T +	R - T -	R - T +/-
March 16	16:26:34.4	19:57:08.4	12634	198.6	129.6	22.4	23.4	26.7	24.6	21.8	88	92	105	97	86	288	587	262	932	627	608
March 17	00:38:28.0	06:24:59.4	20791.4	73.7	35.7	7.4	15.5	13.2	16.0	14.5	29	61	52	63	57	105	239	69	939	65	47
April 4	07:29:46.4	09:46:01.6	8175.2	60.9	38.2	7.1	6.6	7.6	8.1	7.1	28	26	30	32	28	57	84	97	127	19	94
May 23	21:26:31.6	21:38:46.2	734.6	66.2	41.7	3.6	4.6	*	3.0	2.8	14	18	0*	12	11	248	27	7	81	8	6
May 26	15:23:57.8	15:39:38.8	941.0	65.2	44.4	2.5	3.3	3.0	2.3	2.3	10	13	12	9	9	7	60	8	49	9	5
May 27	22:32:12.0	23:12:53.6	2441.6	64.3	48.3	6.9	7.1	5.8	6.9	5.3	27	28	23	27	21	11	63	7	100	6	5
May 28	01:03:34.0	02:19:16.2	4542.2	217.6	138.0	23.4	27.2	26.4	27.7	23.4	92	107	104	109	92	25	221	40	41	39	21

* Telephone company disconnected this gauge during line maintenance.

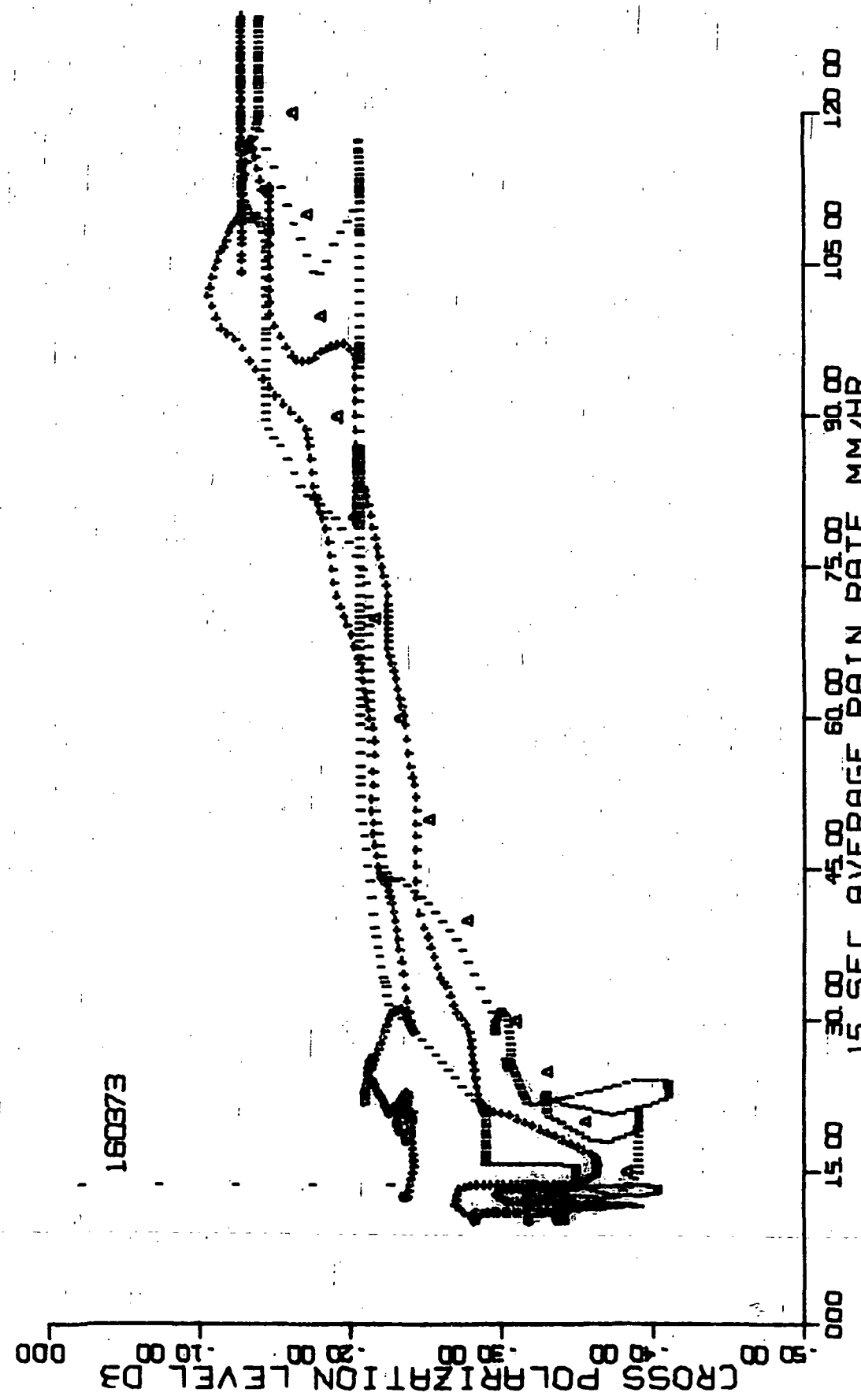

Figure 31. March 16, 1973, cross polarization scatter plot.

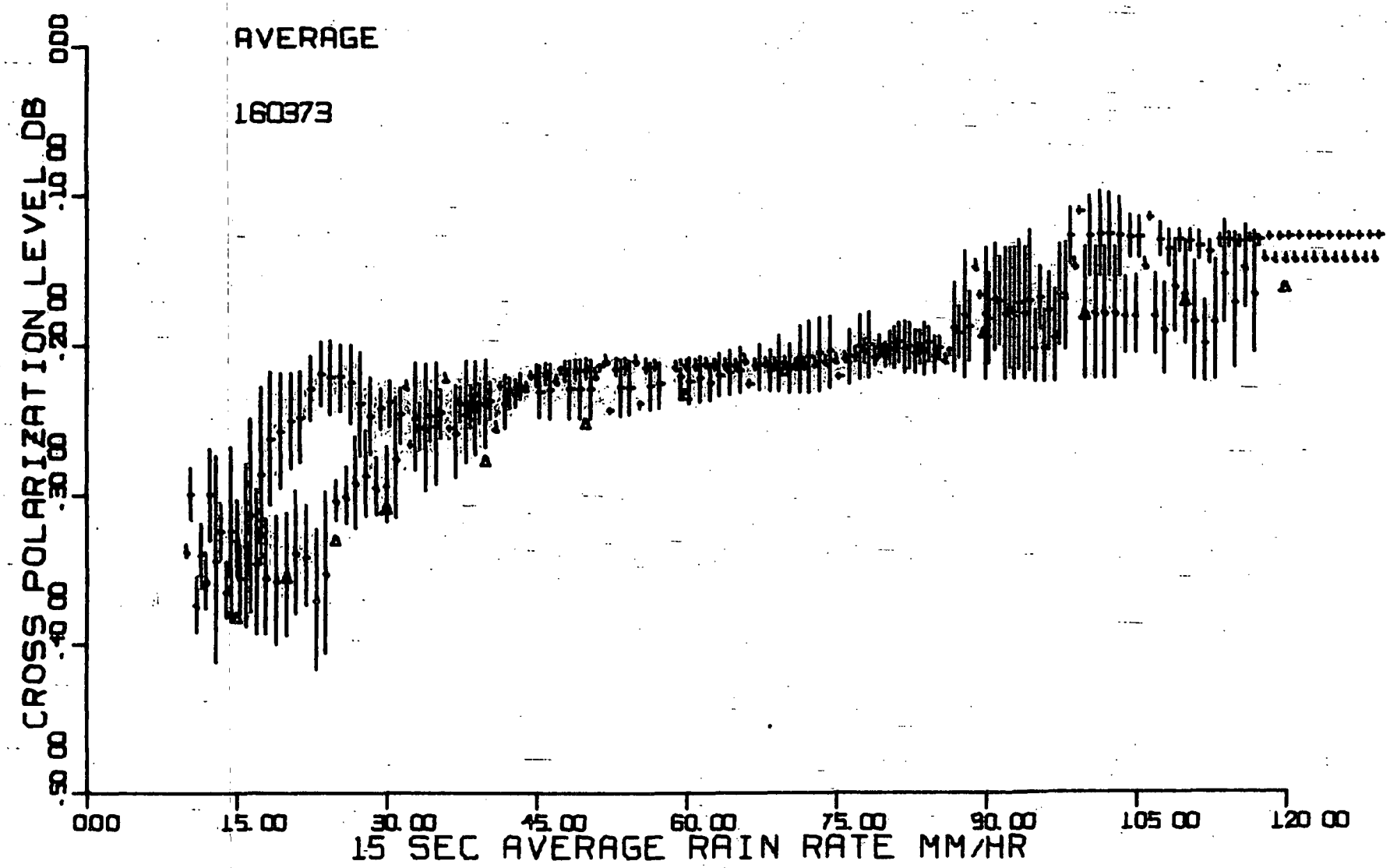

Figure 32. March 16, 1973, average cross polarization levels for each channel.

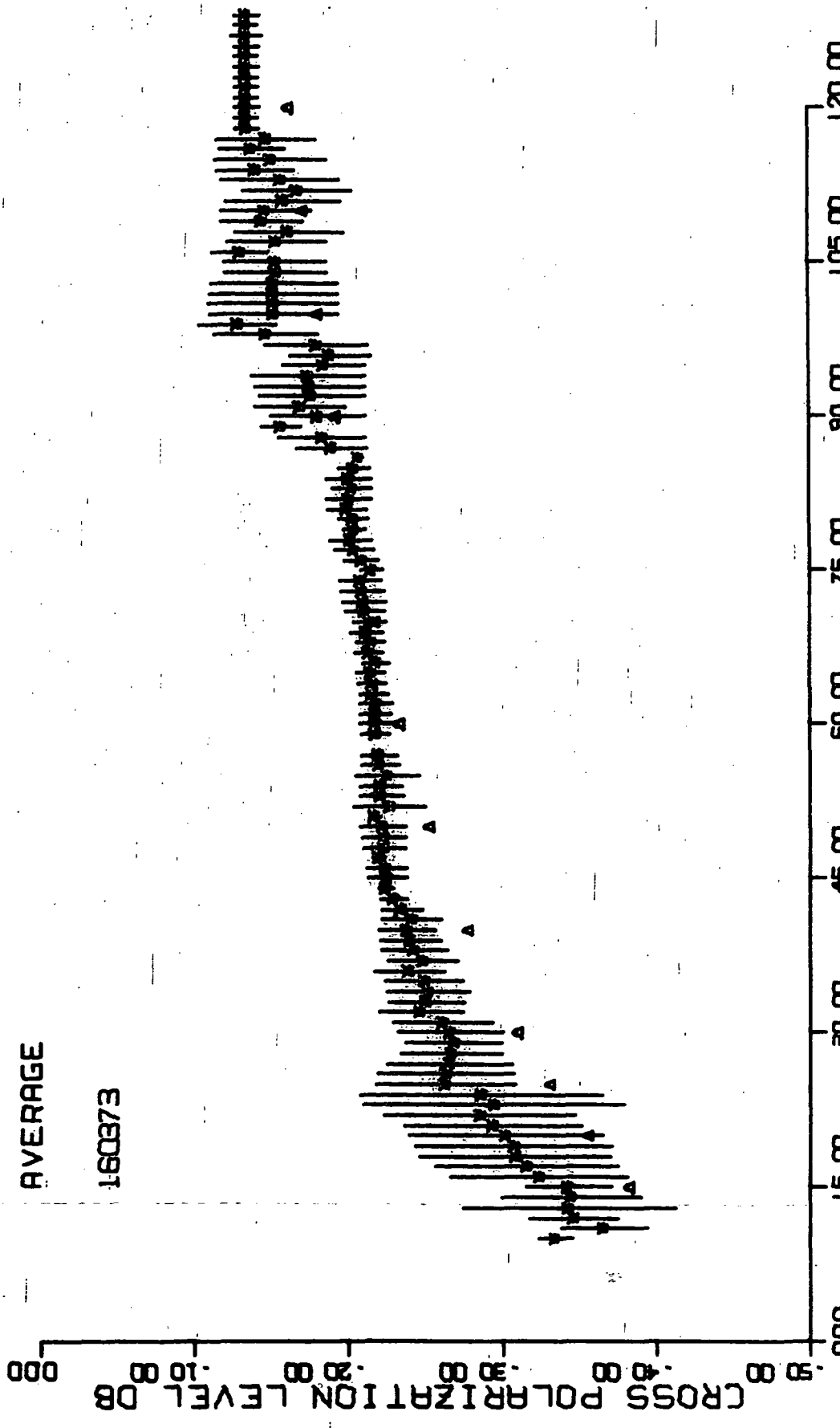

Figure 33. March 16, 1973, average cross polarization levels.

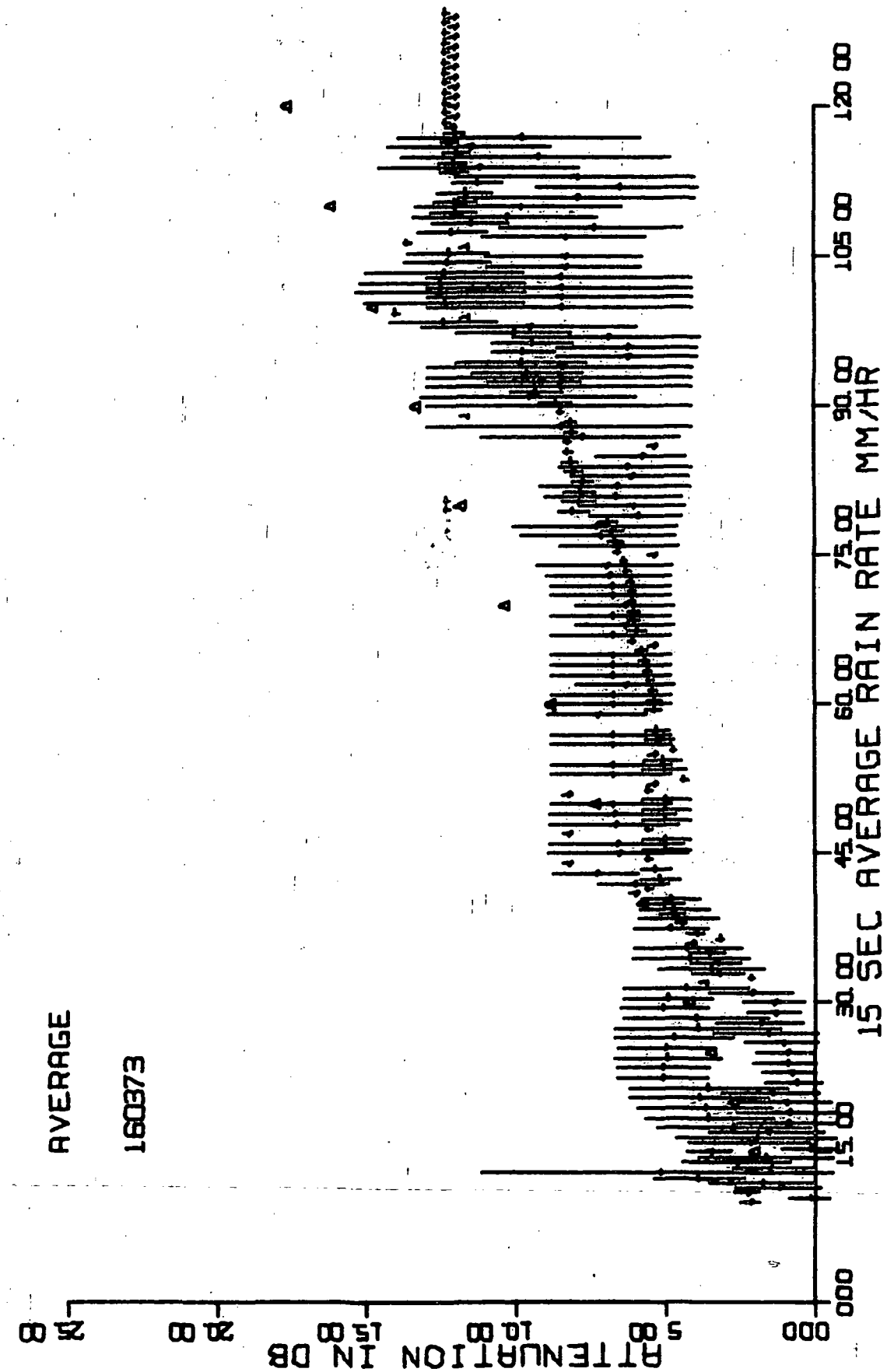

Figure 34. March 16, 1973, average attenuation values for each channel.

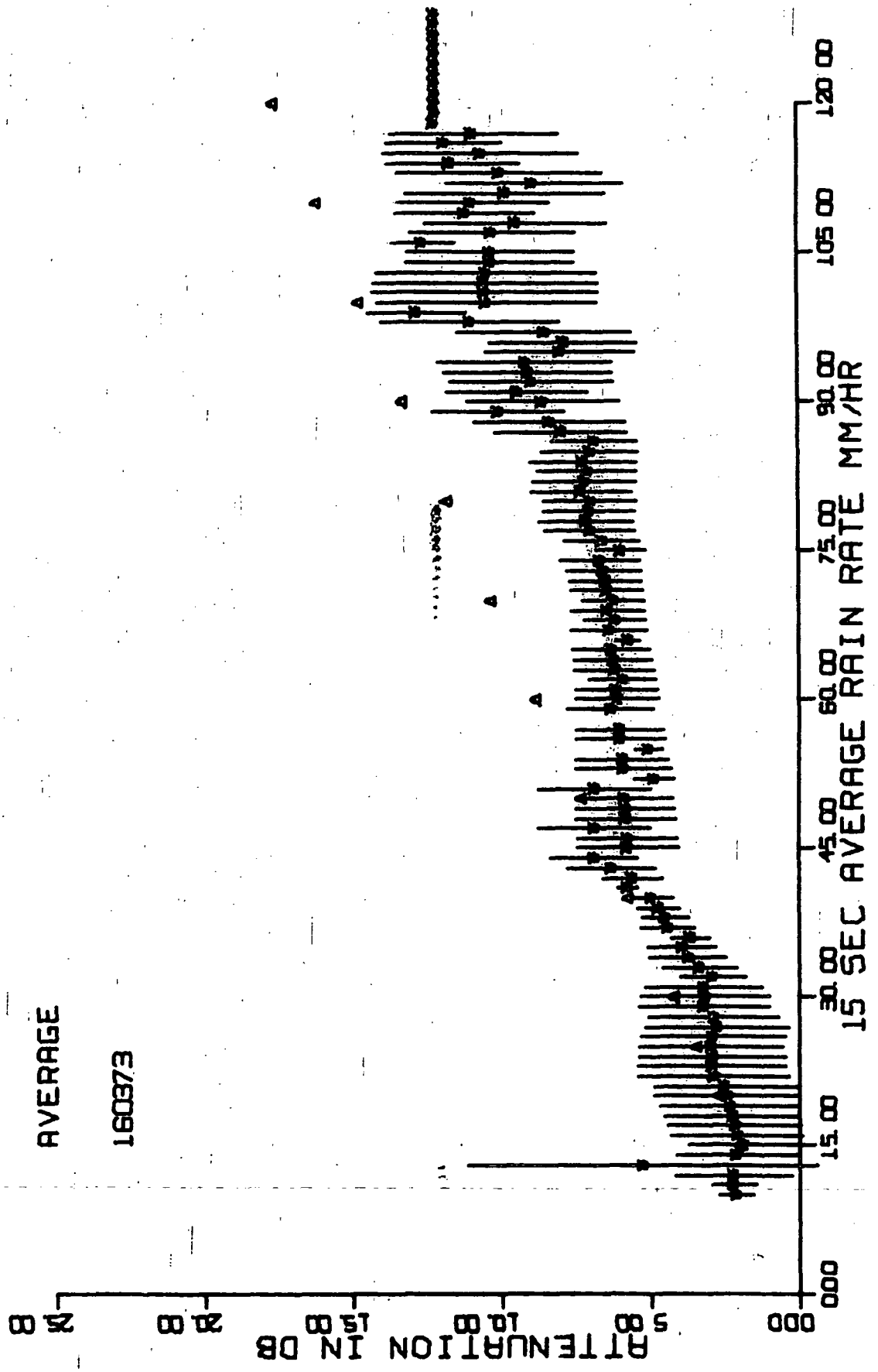

Figure 35. March 16, 1973, average attenuation values.

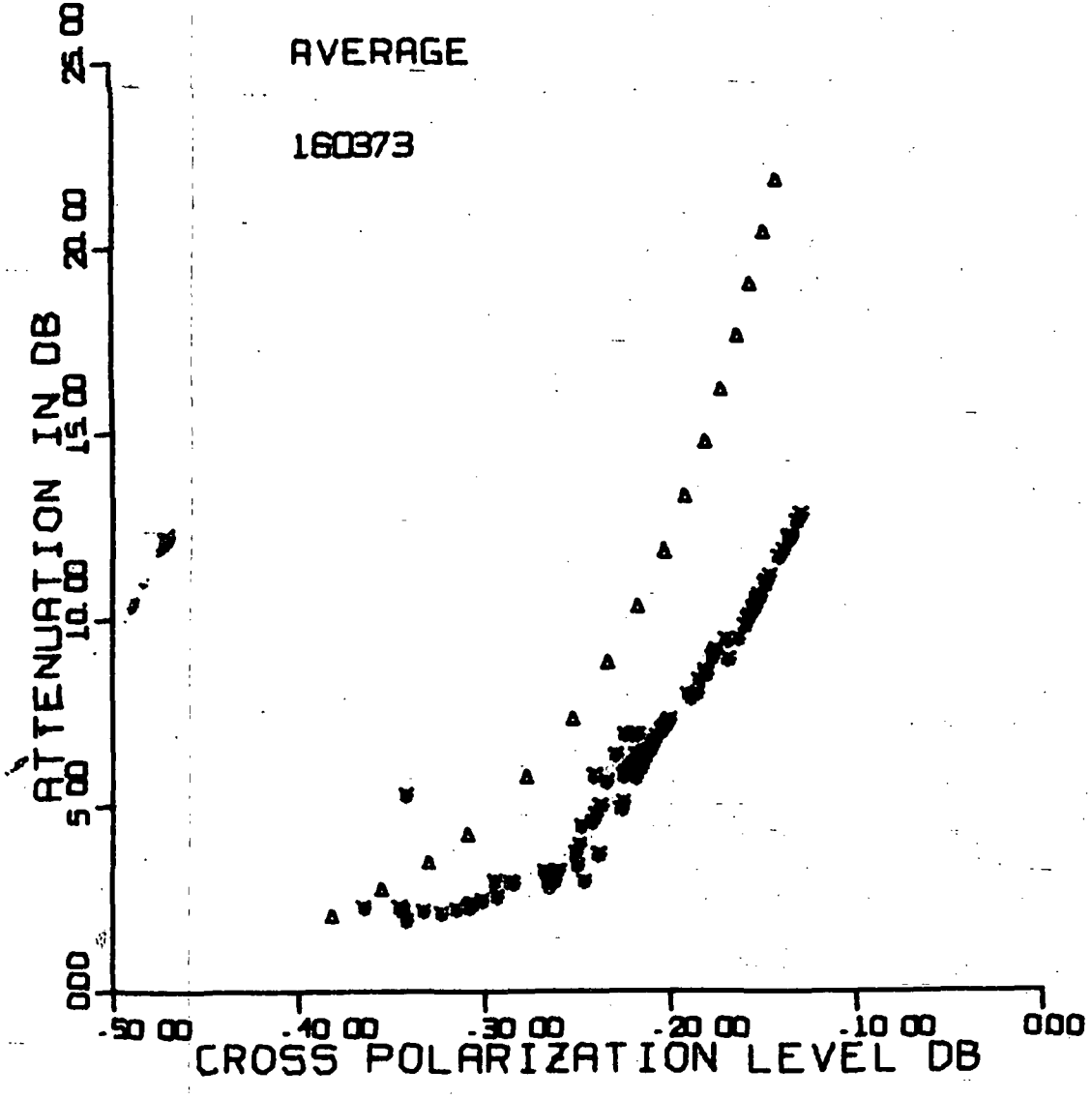

Figure 36. March 16, 1973,
average attenuation versus average cross polarization level.

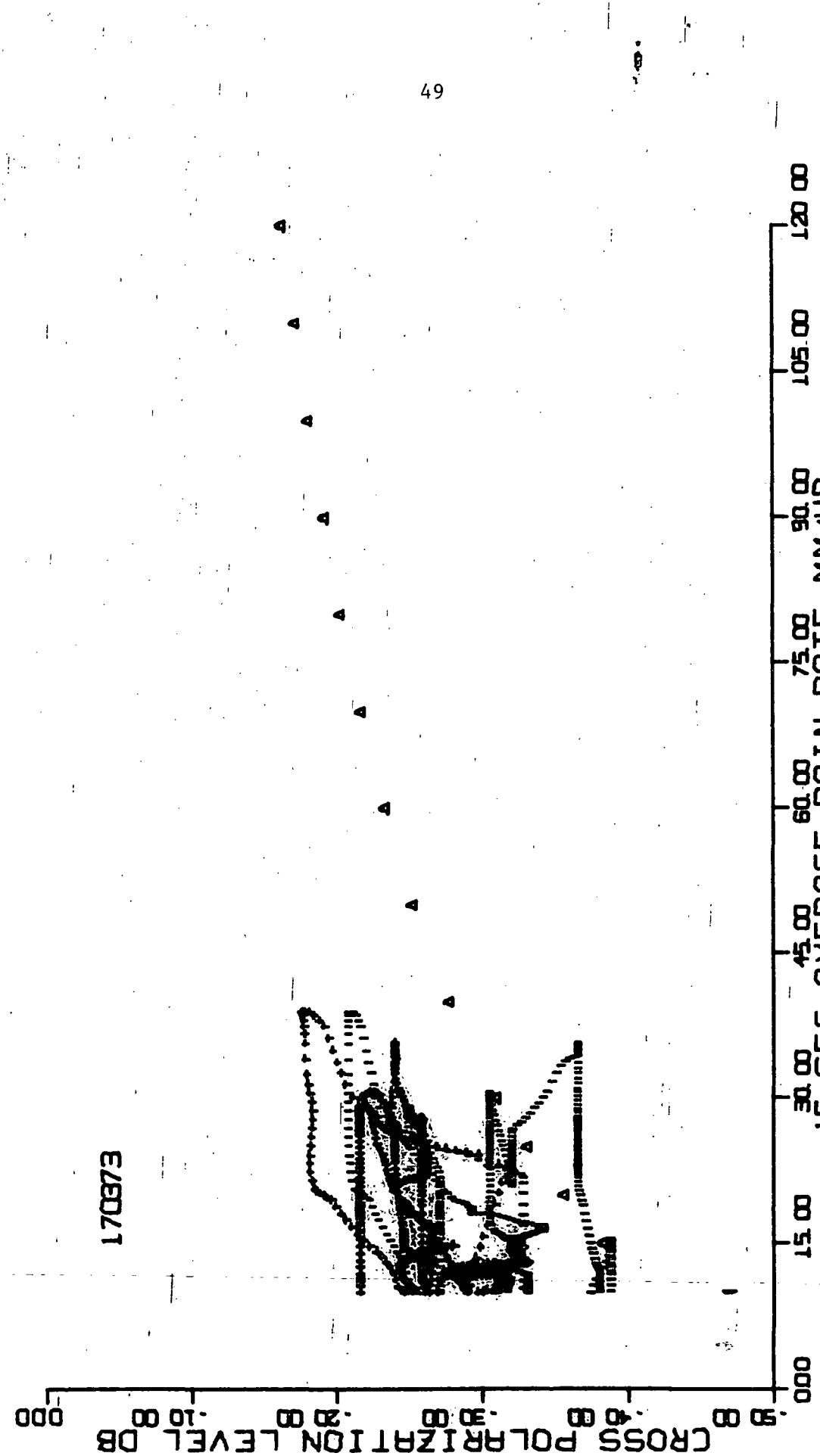

Figure 37. March 17, 1973, cross polarization scatter plot.

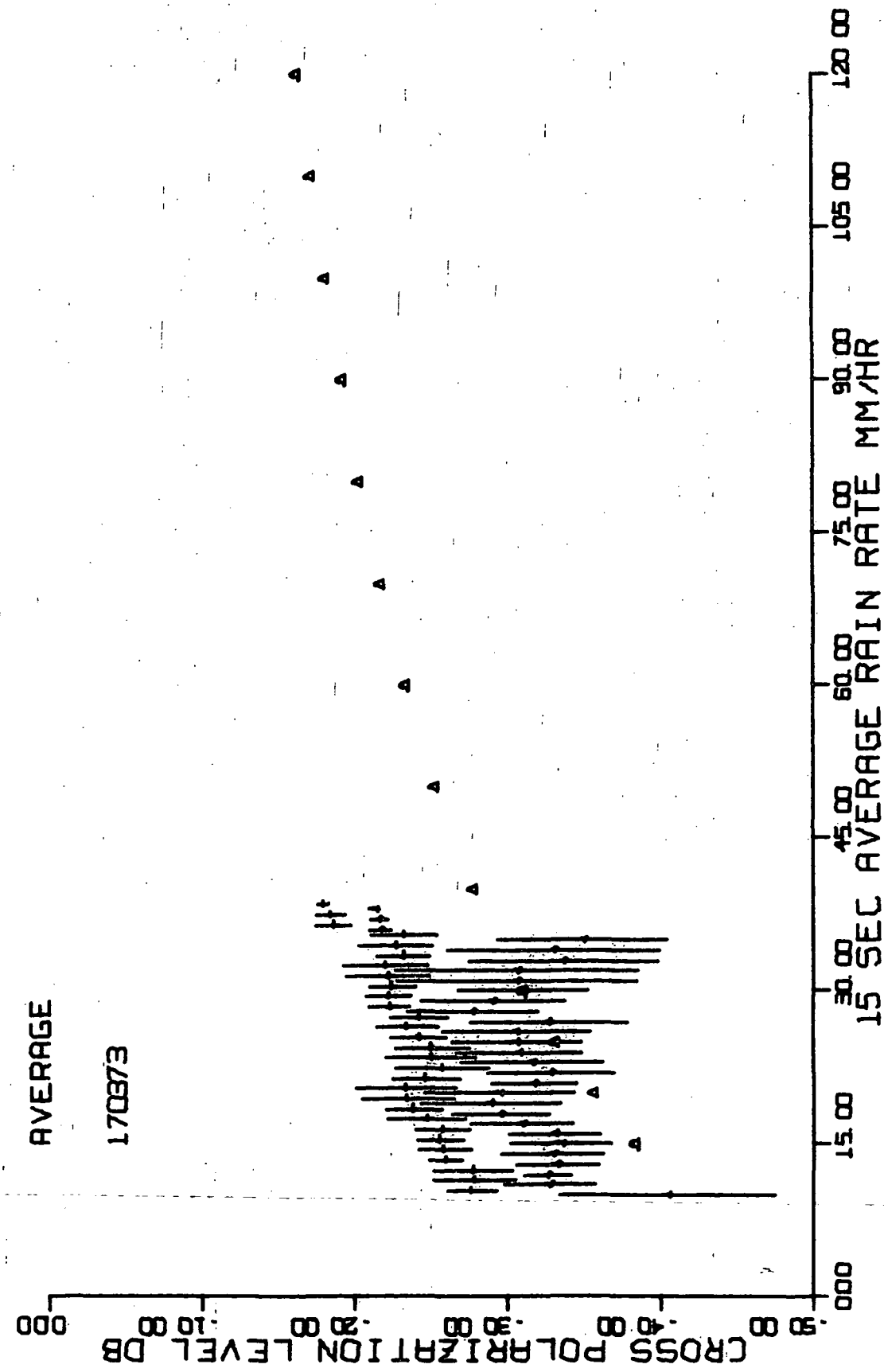

Figure 38. March 17, 1973, average cross polarization levels for each channel.

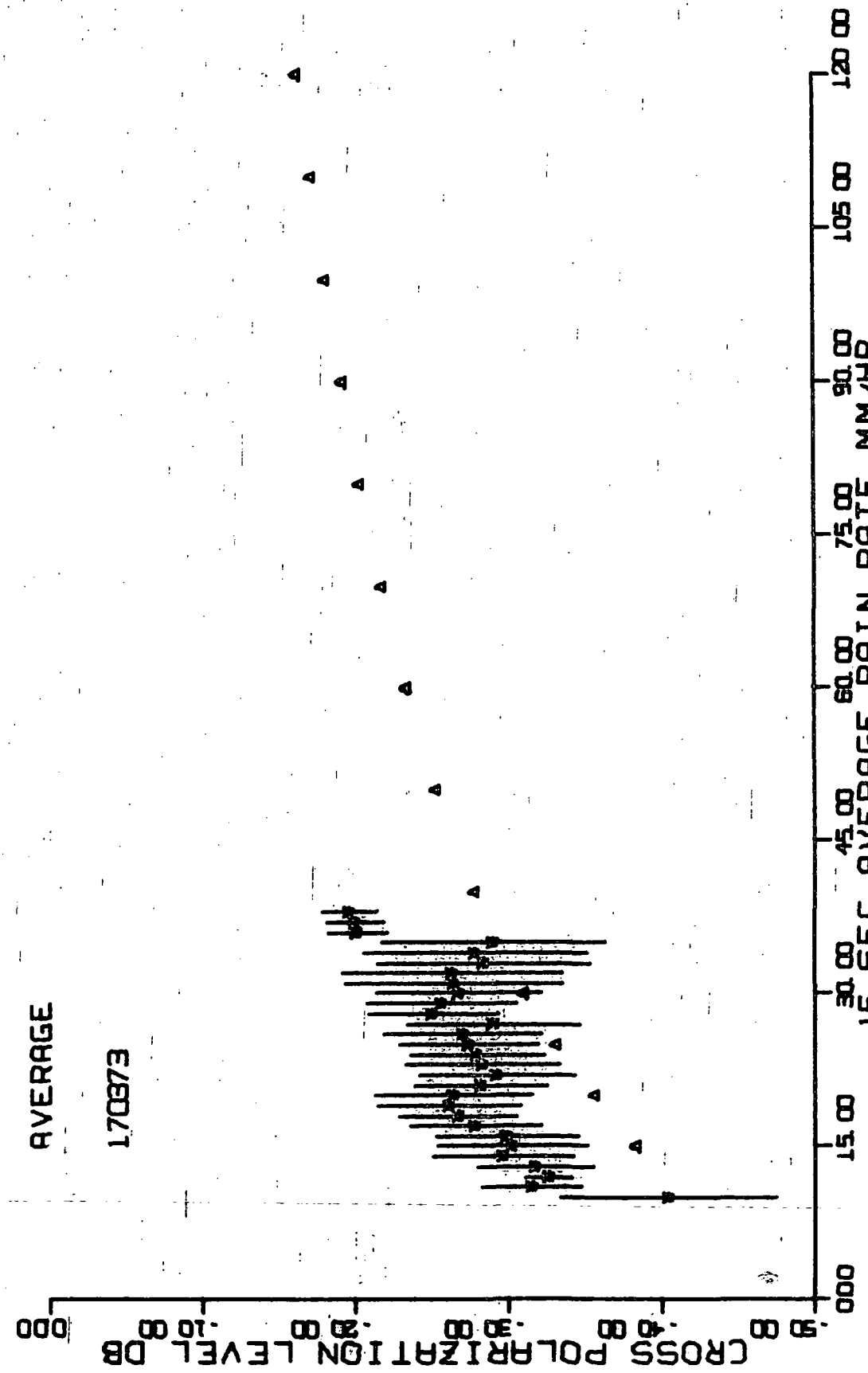

Figure 39. March 17, 1973, average cross polarization levels.

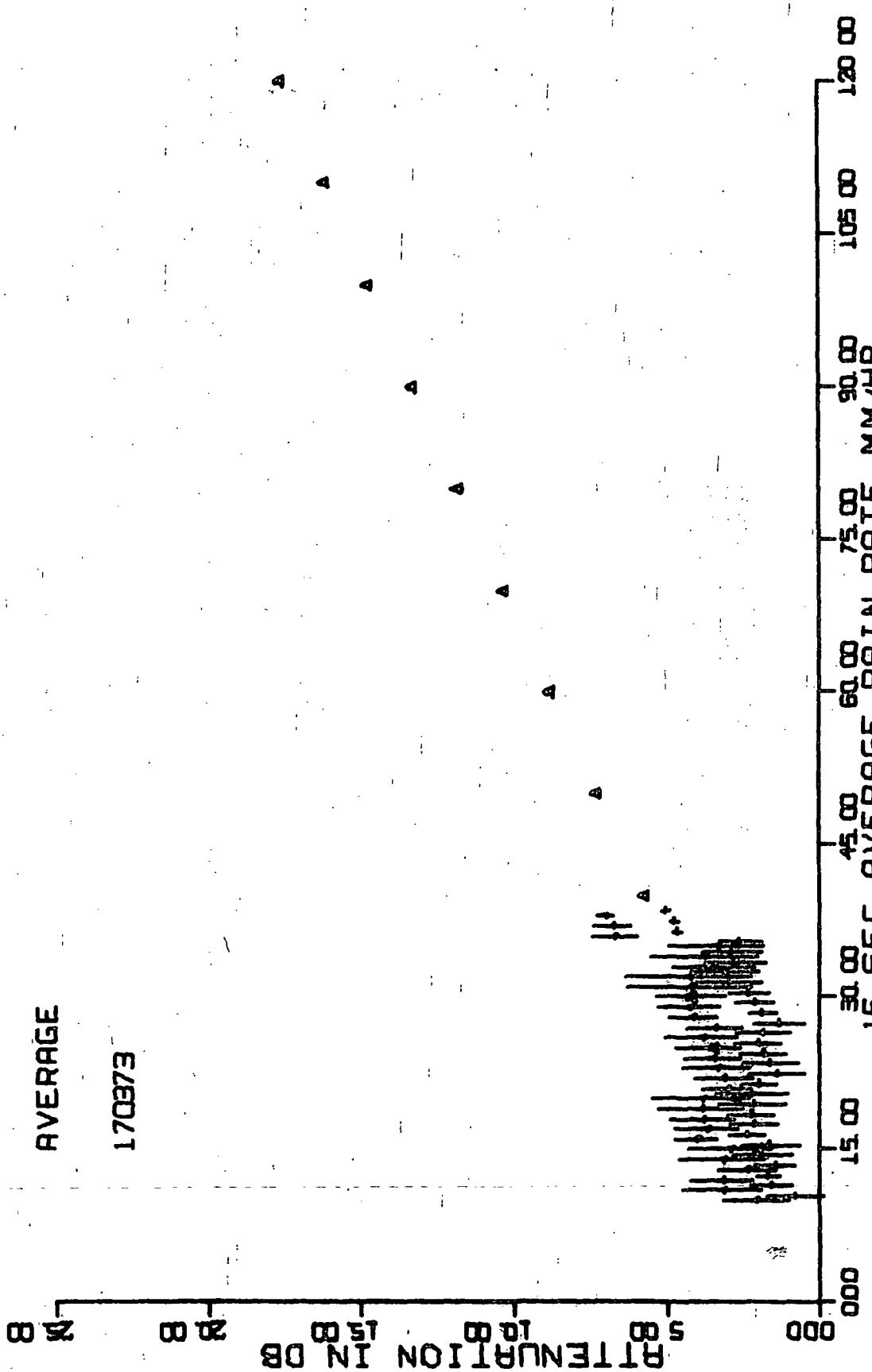

Figure 40. March 17, 1973, average attenuation values for each channel.

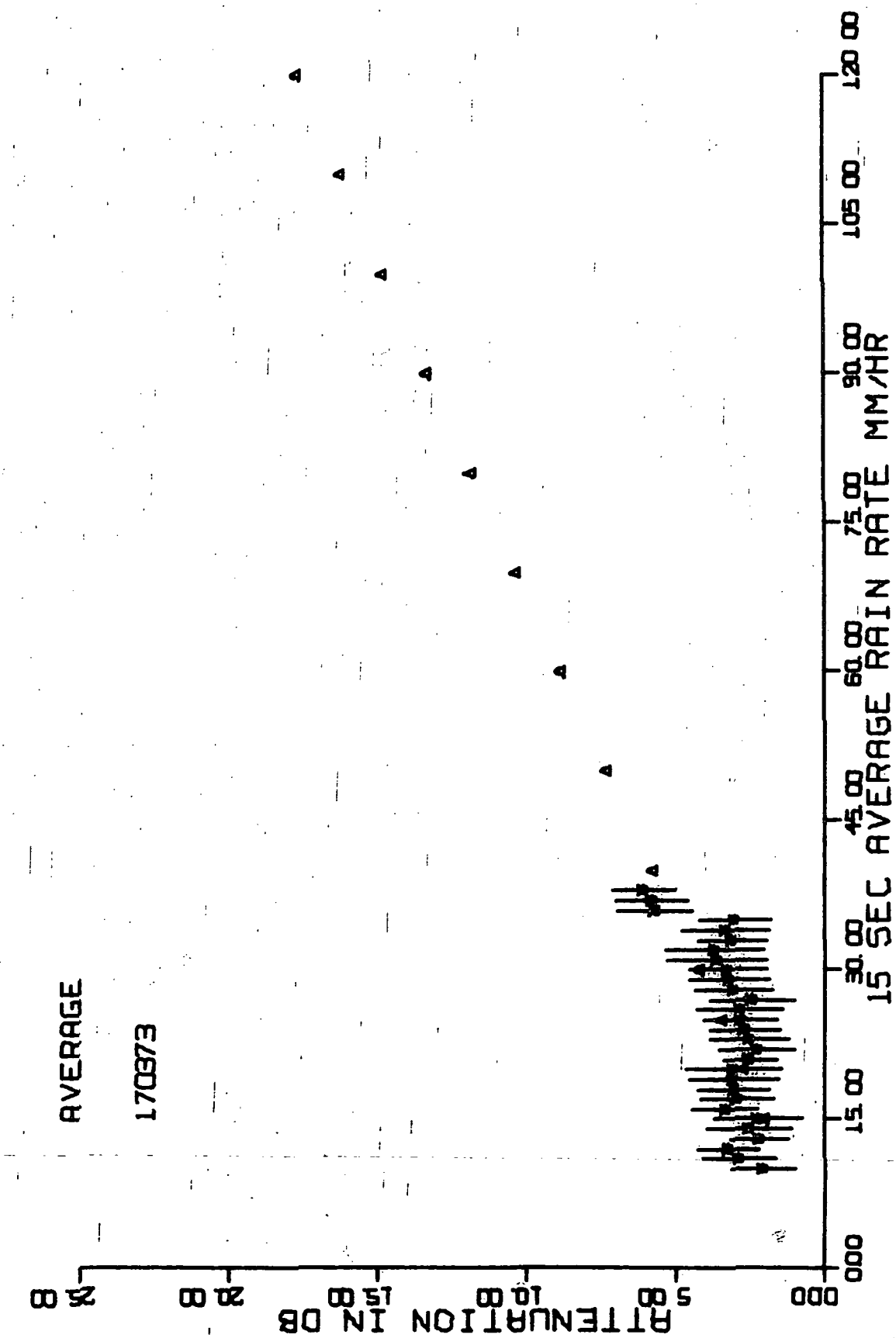

Figure 41. March 17, 1973, average attenuation values.

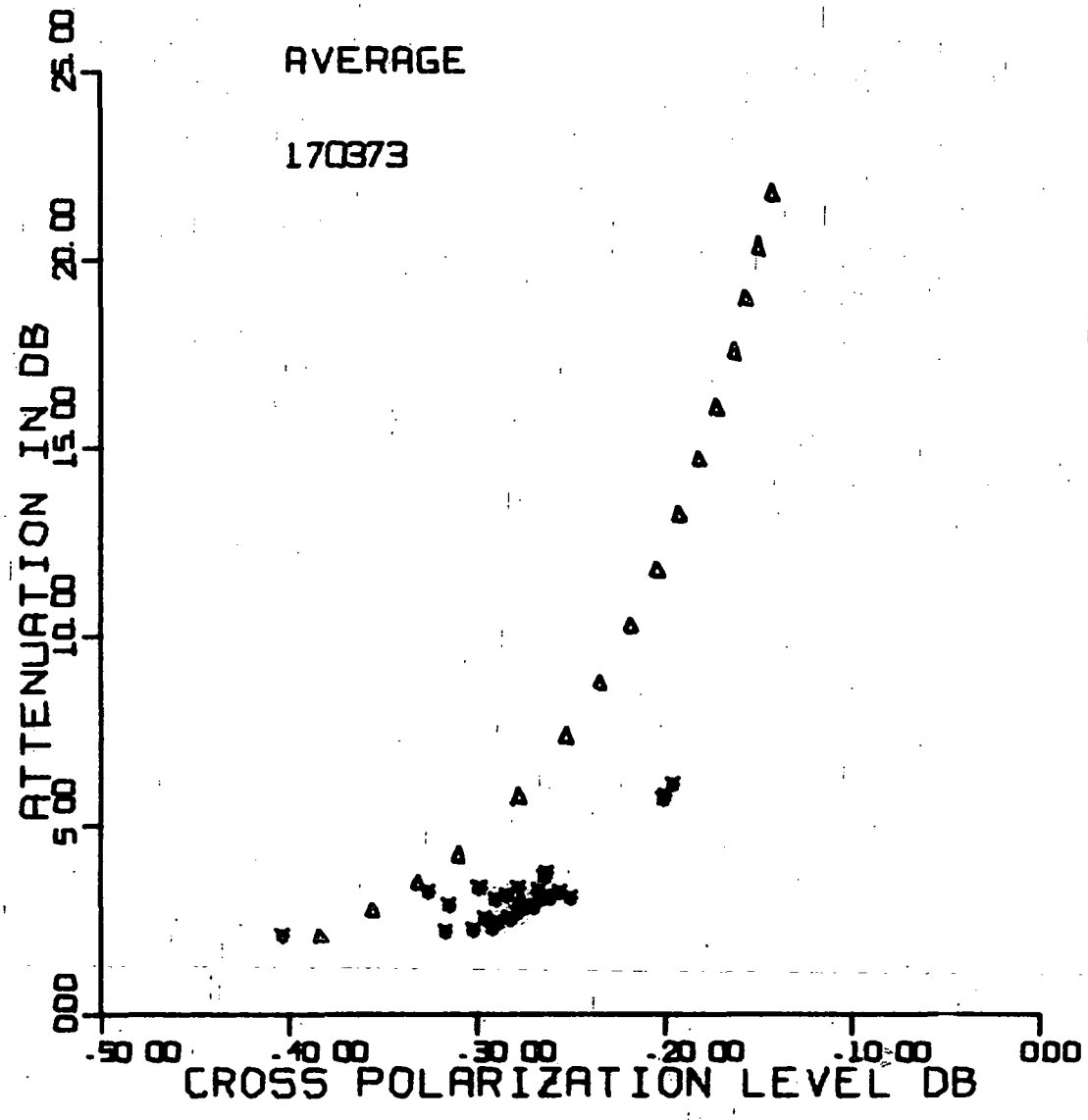

Figure 42. March 17, 1973,
average attenuation versus average cross polarization level.

5.2.5 May 23, 1973

Data for this storm appear in Figures 43 through 48.

5.2.6 May 26, 1973

Figures 49 through 54 present data from this storm.

5.2.7 May 27, 1973

Figures 55 through 58 display data for this storm. Apparently a transient somewhere in the system kept the PB 440 computer from recording sufficient data to generate values for + to - cross polarization and + channel attenuation.

5.2.8 May 28, 1973

Figures 59 through 64 display data from this storm.

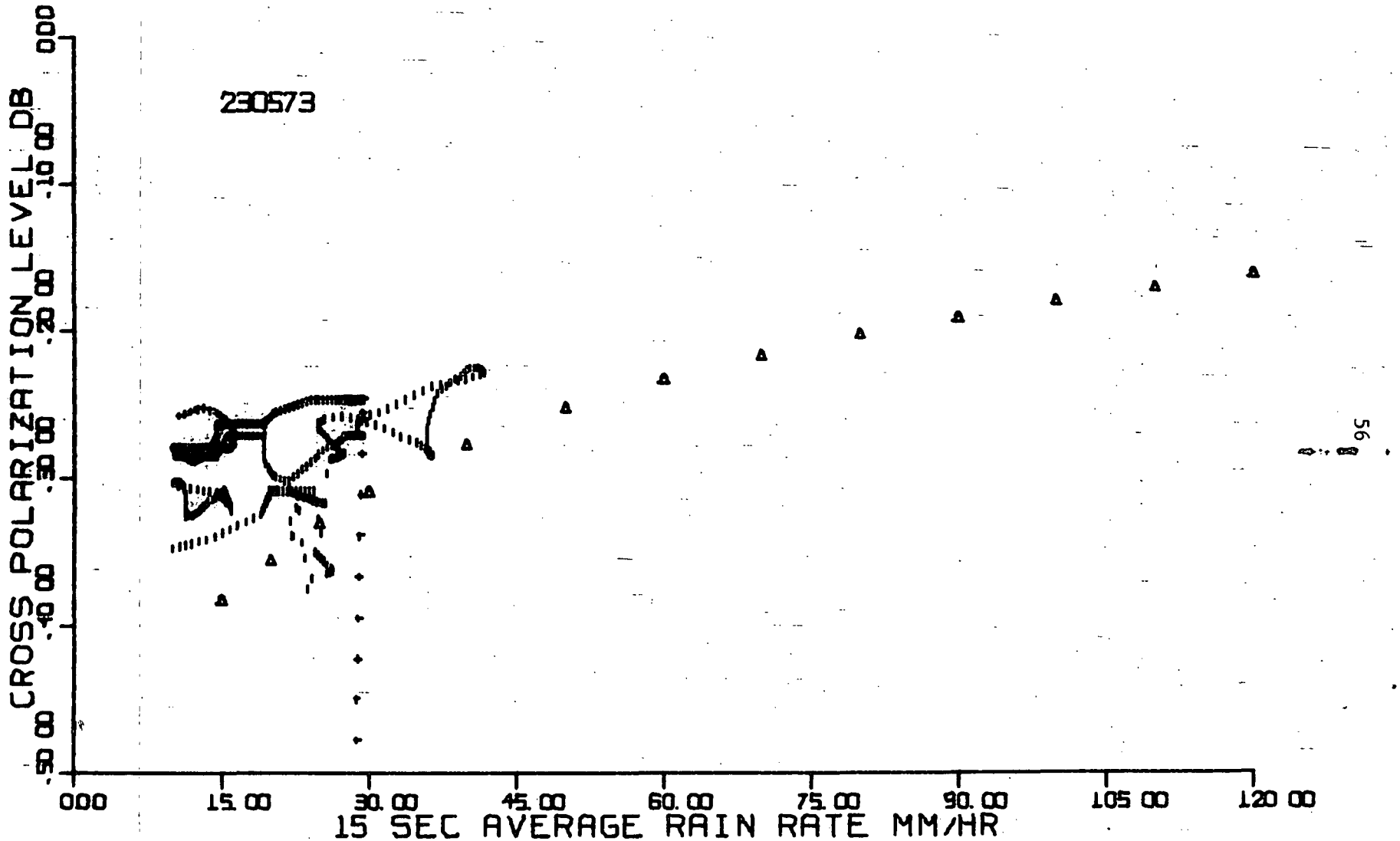

Figure 43. May 23, 1973, cross polarization scatter plot.

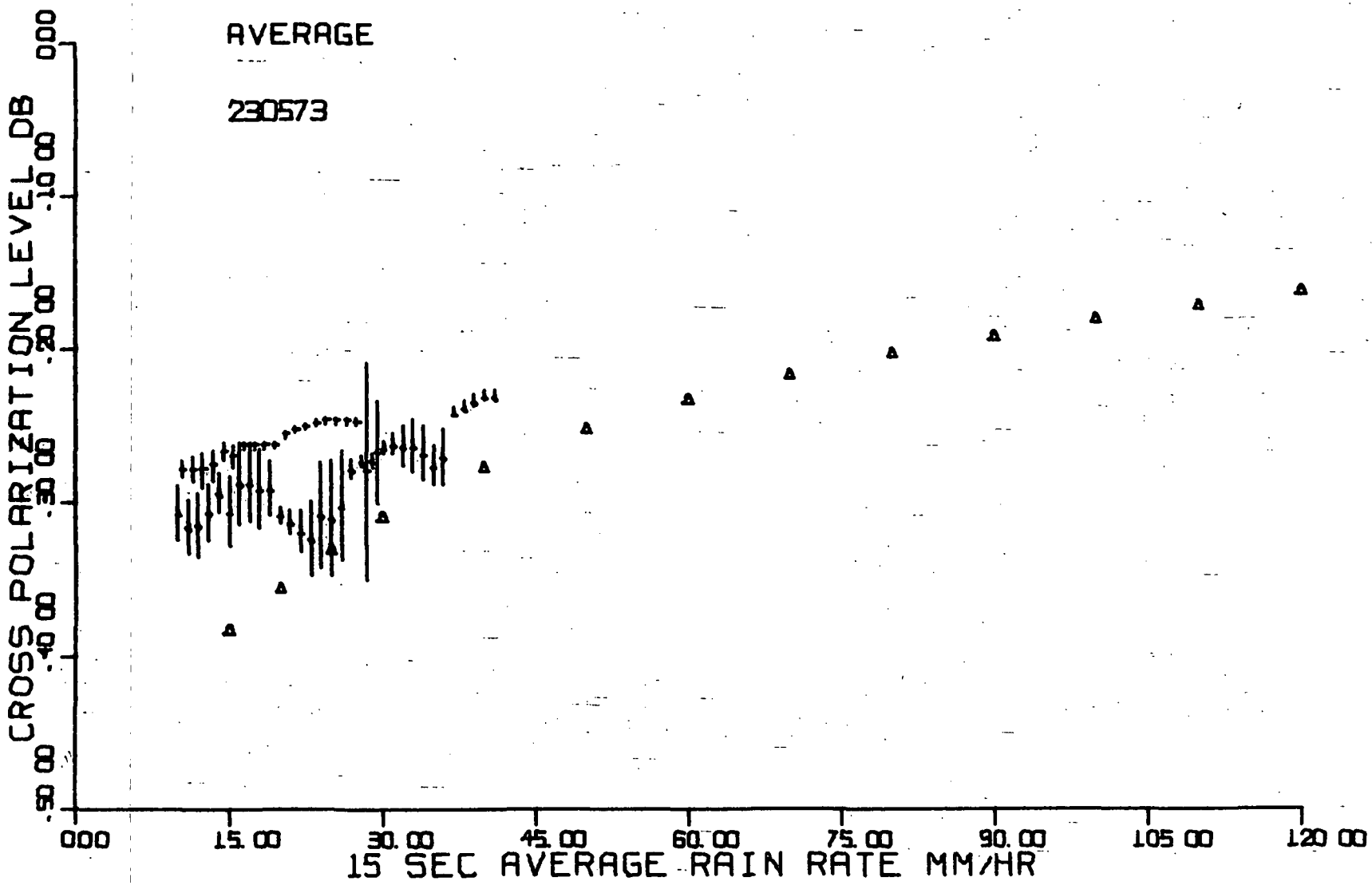

Figure 44. May 23, 1973, average cross polarization levels for each channel.

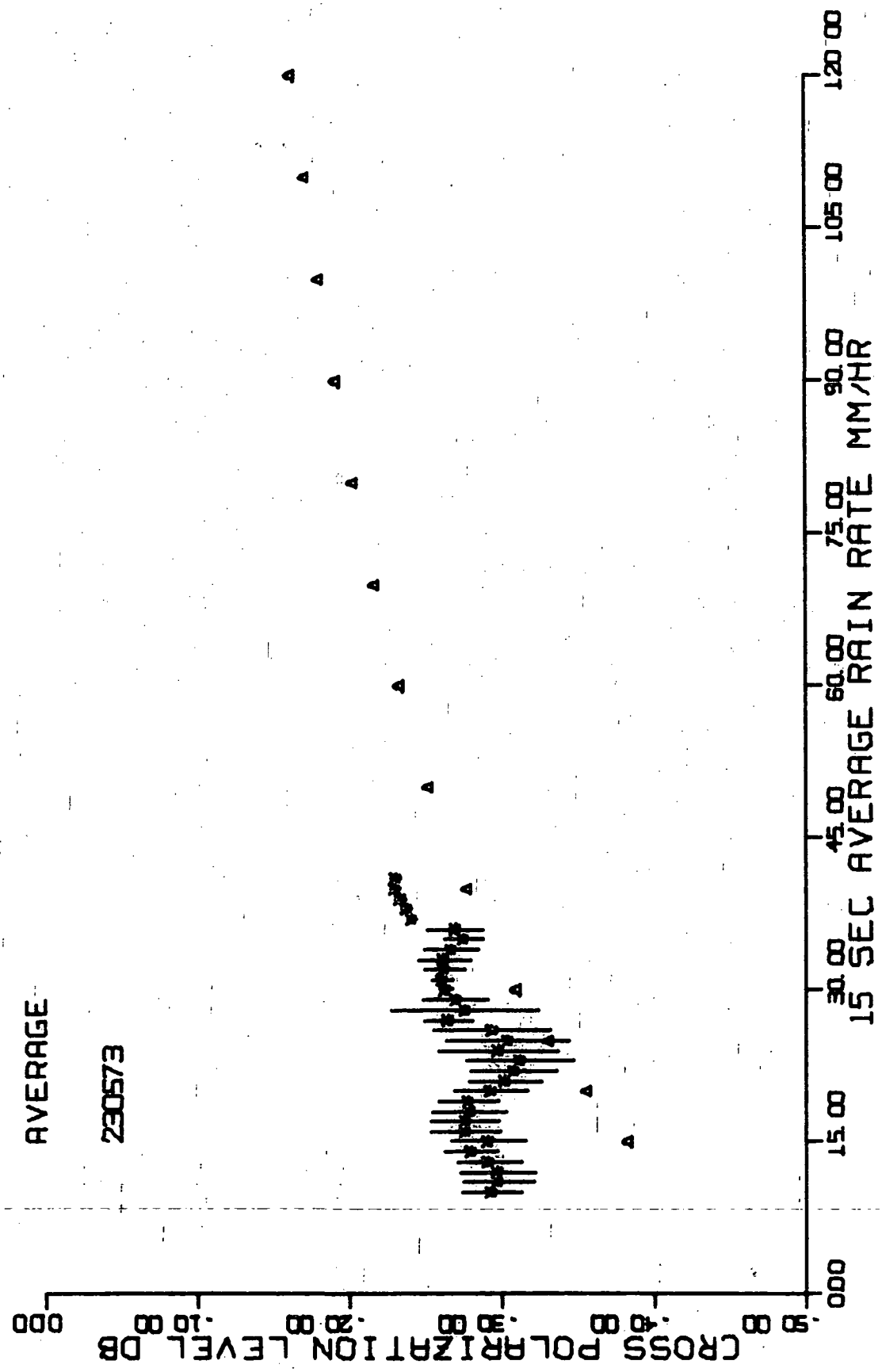

Figure 45. May 23, 1973, average cross polarization levels.

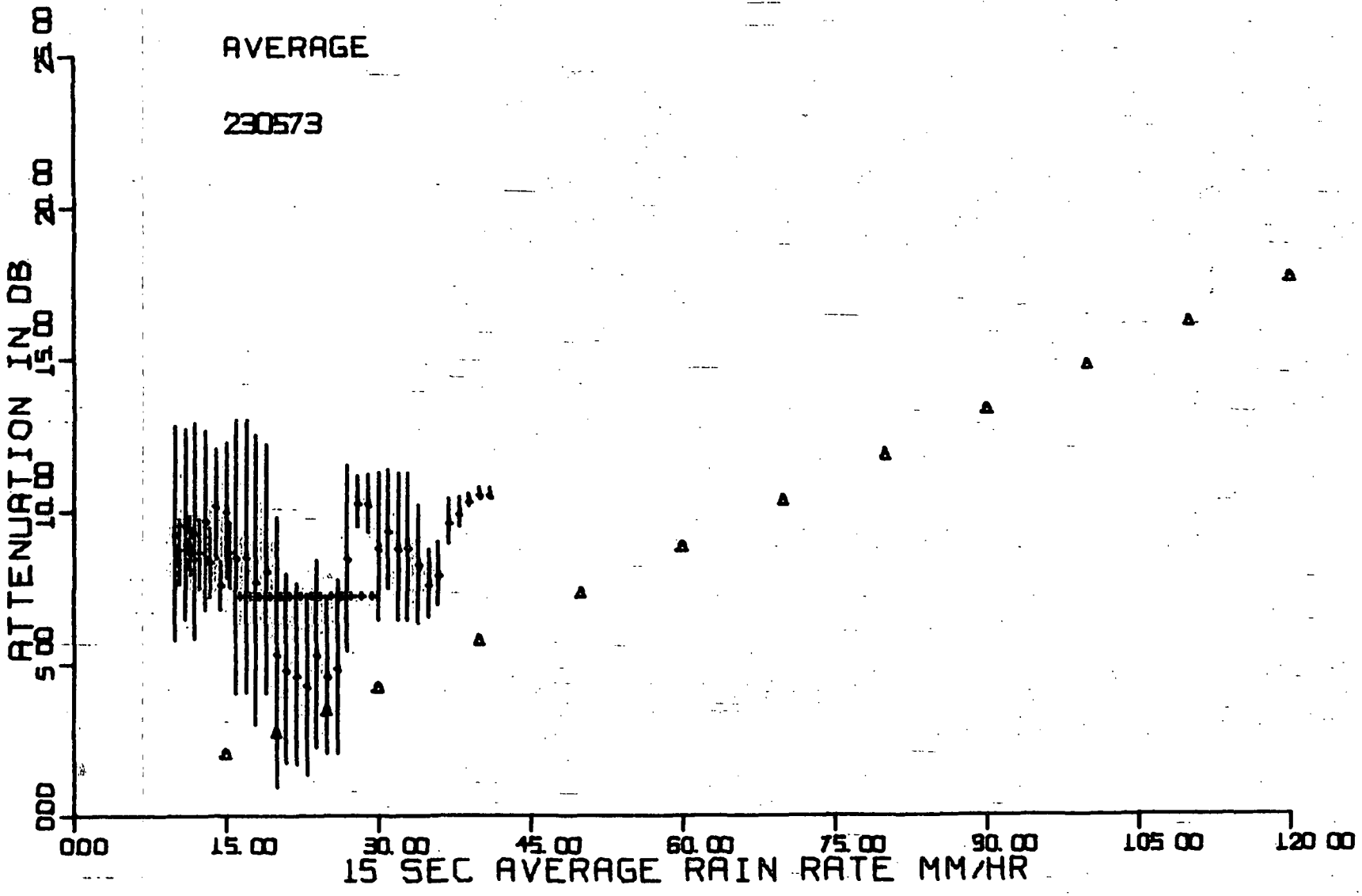

Figure 46. May 23, 1973, average attenuation values for each channel.

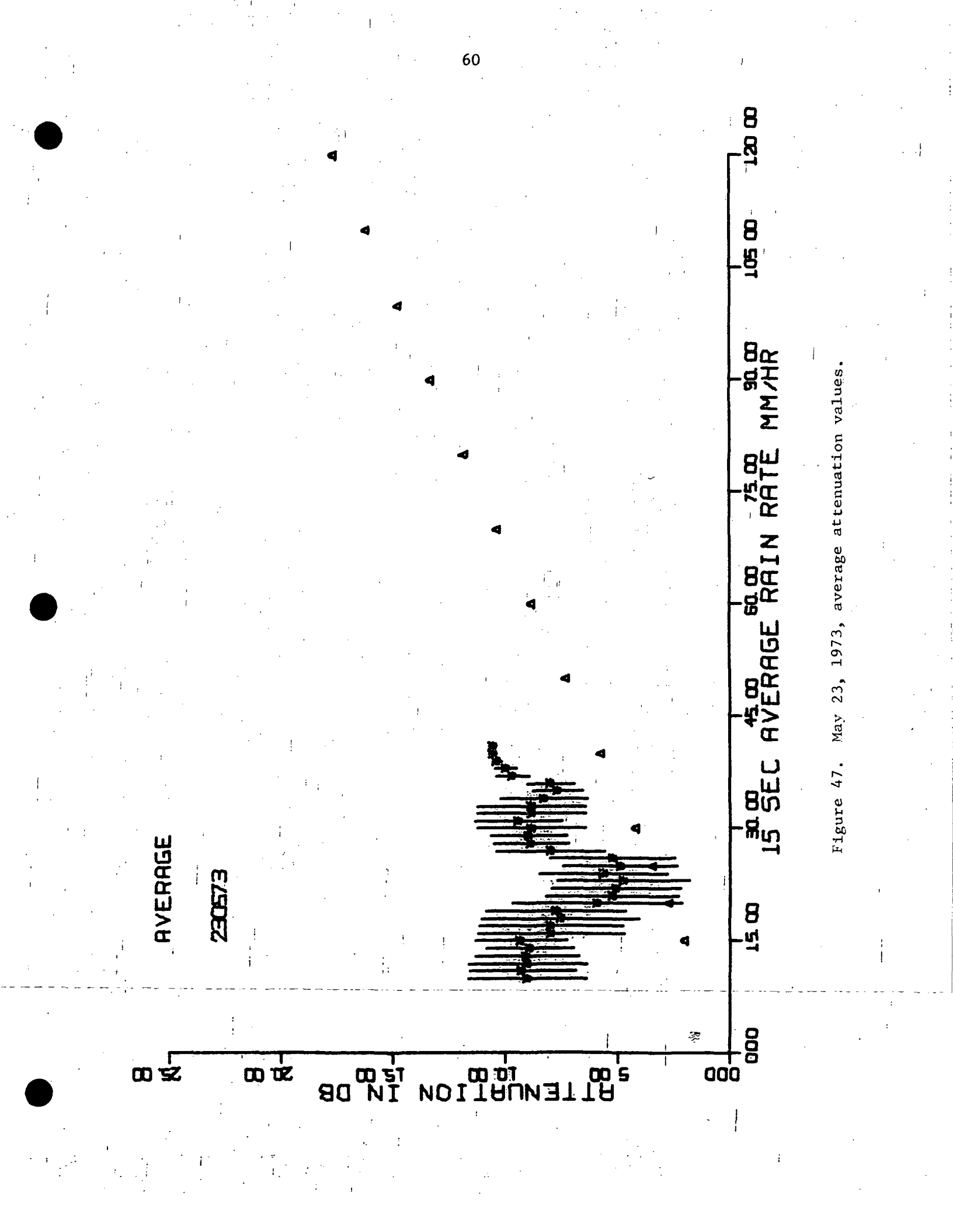

Figure 47. May 23, 1973, average attenuation values.

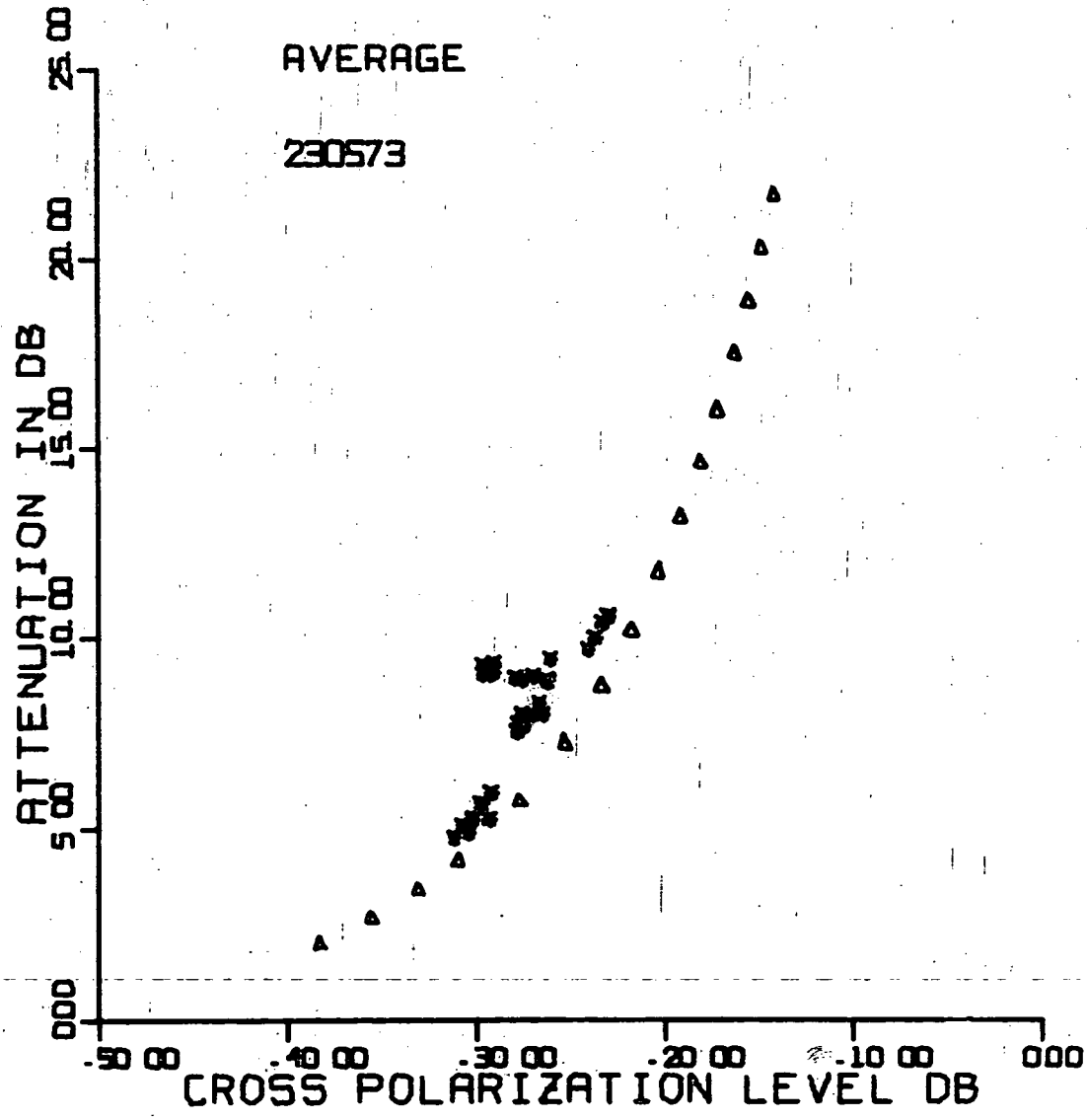

Figure 48. May 23, 1973,
average attenuation versus average cross polarization level.

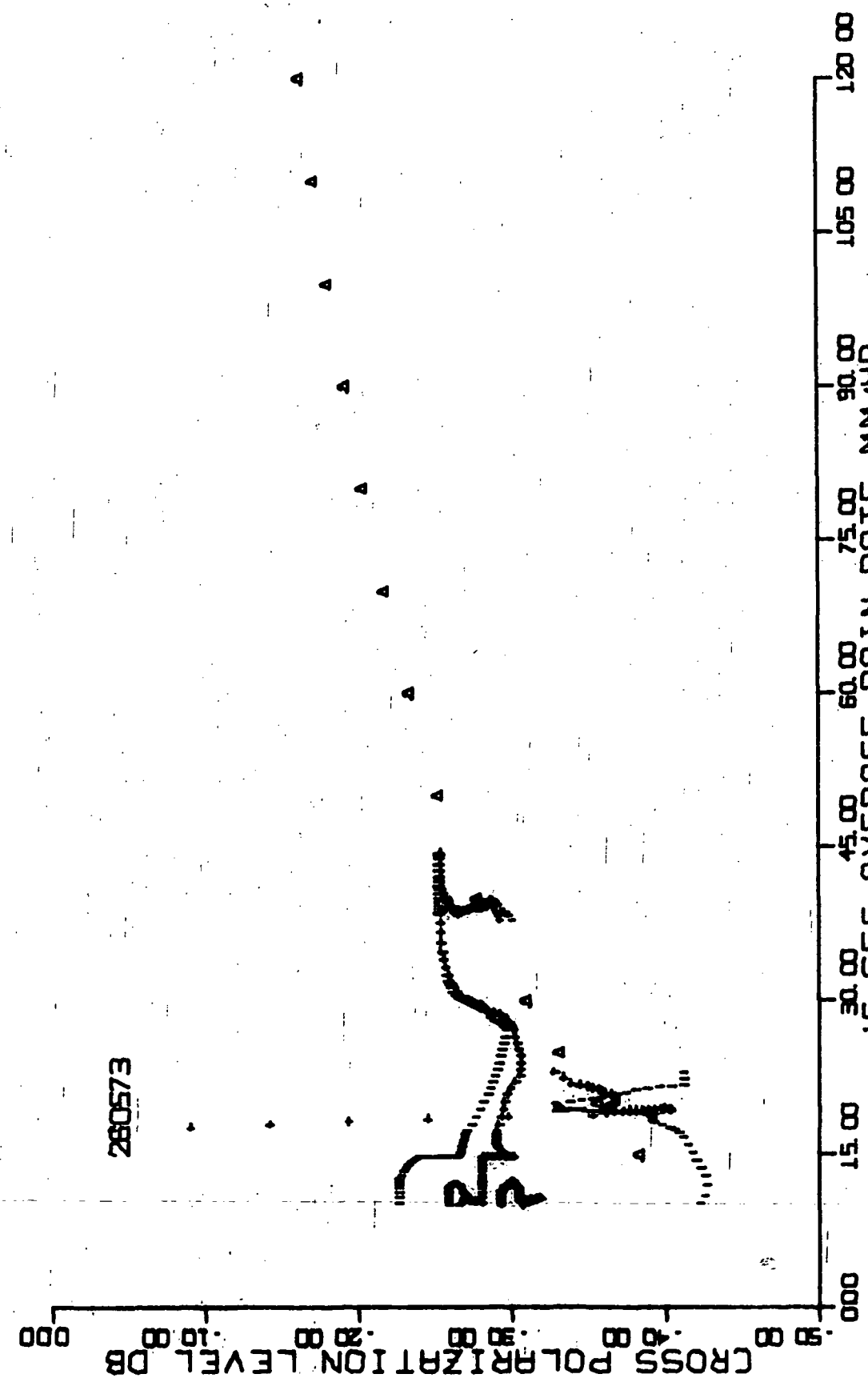

Figure 49. May 26, 1973, cross polarization scatter plot.

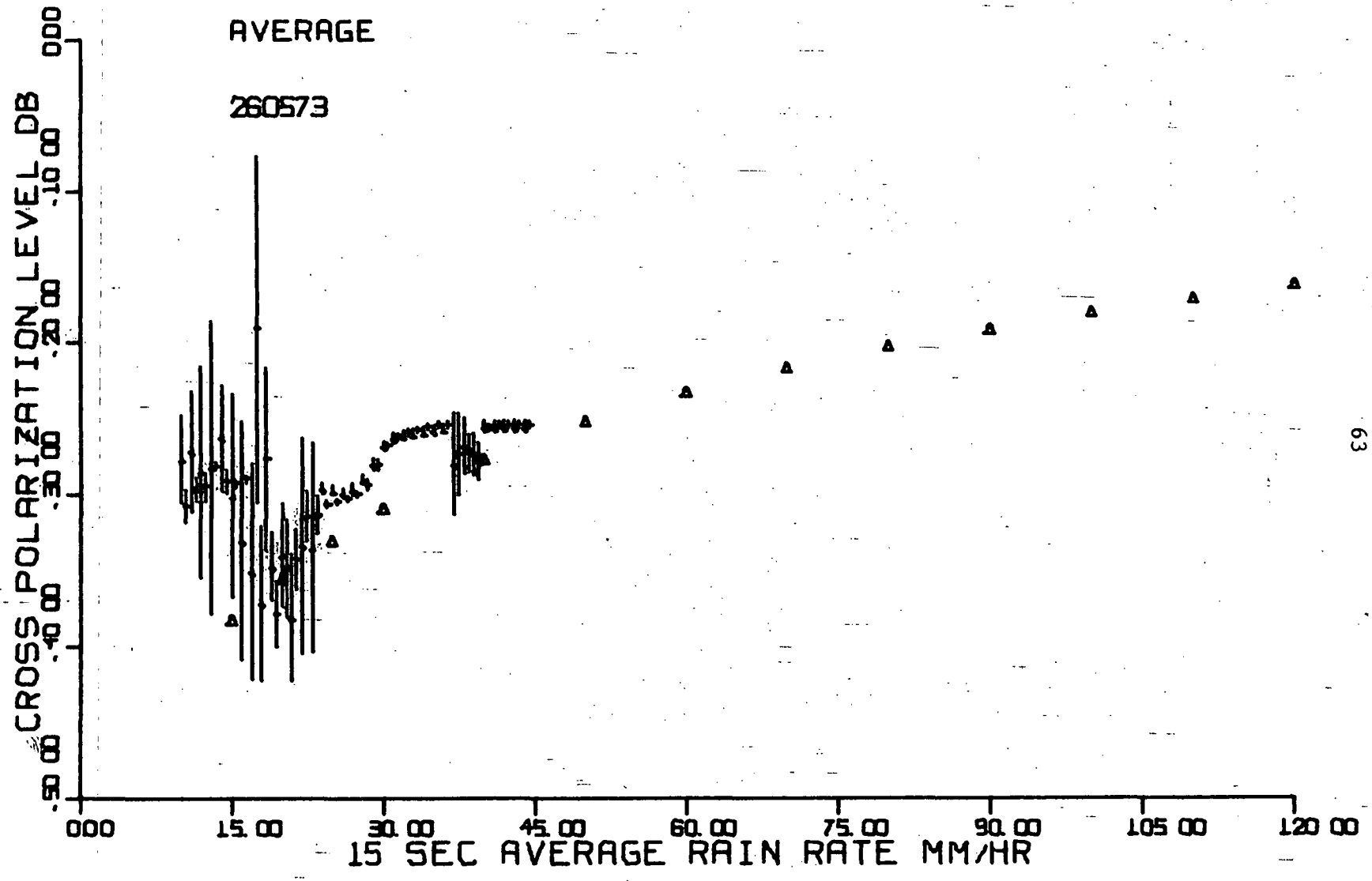

Figure 50. May 26, 1973, average cross polarization levels for each channel.

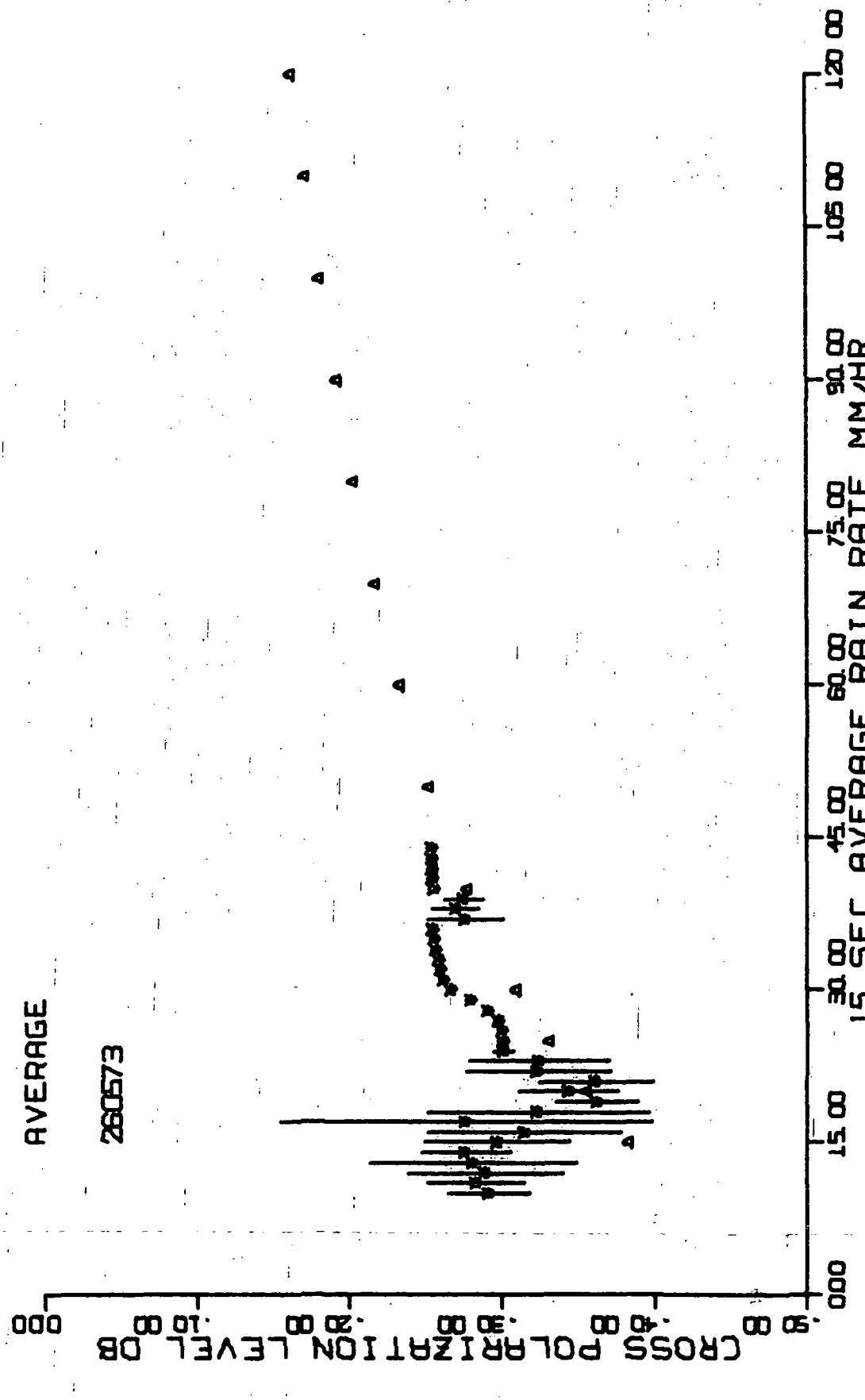

Figure 51. May 26, 1973, average cross polarization levels.

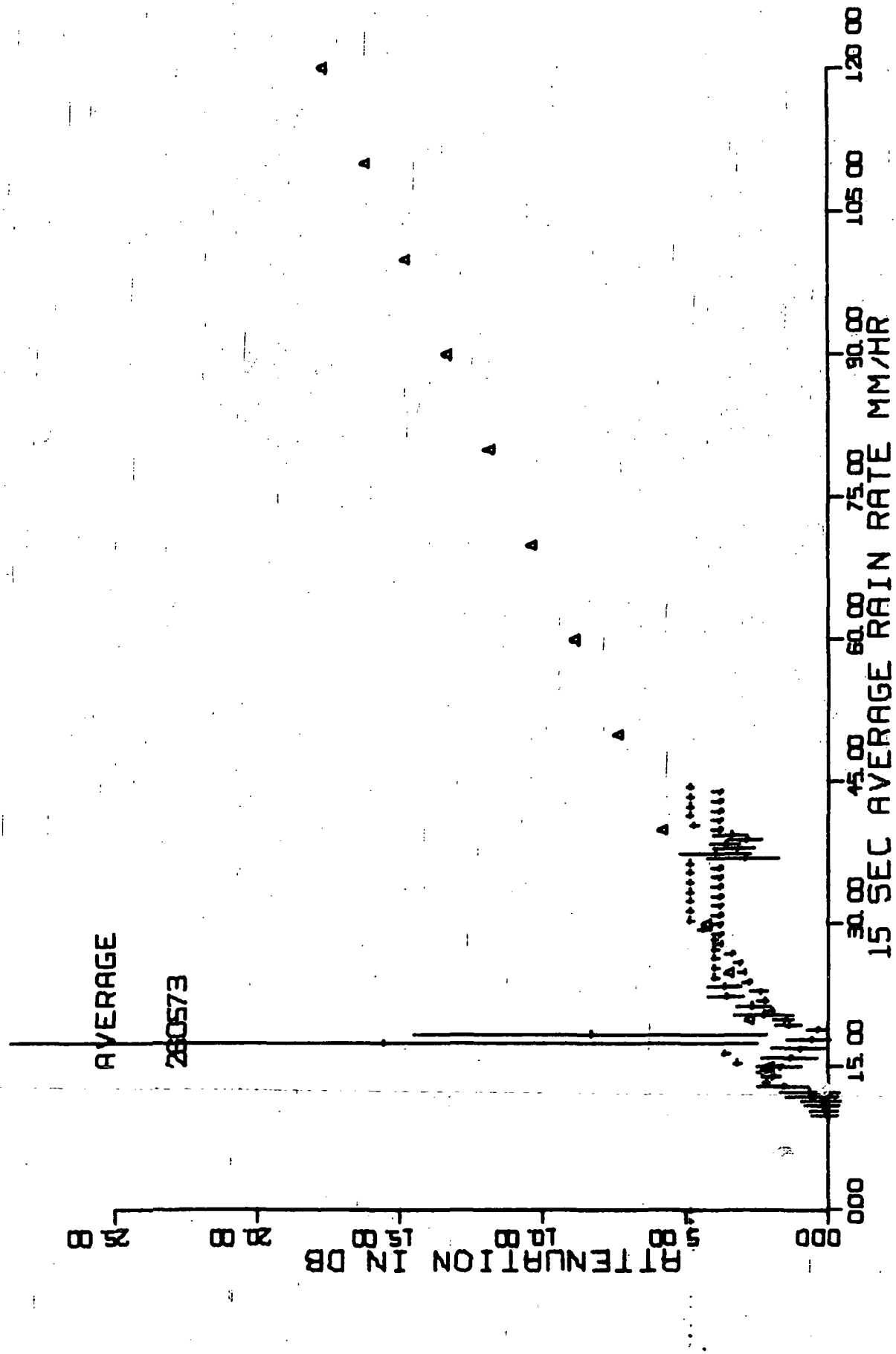

Figure 52. May 26, 1973, average attenuation values for each channel.

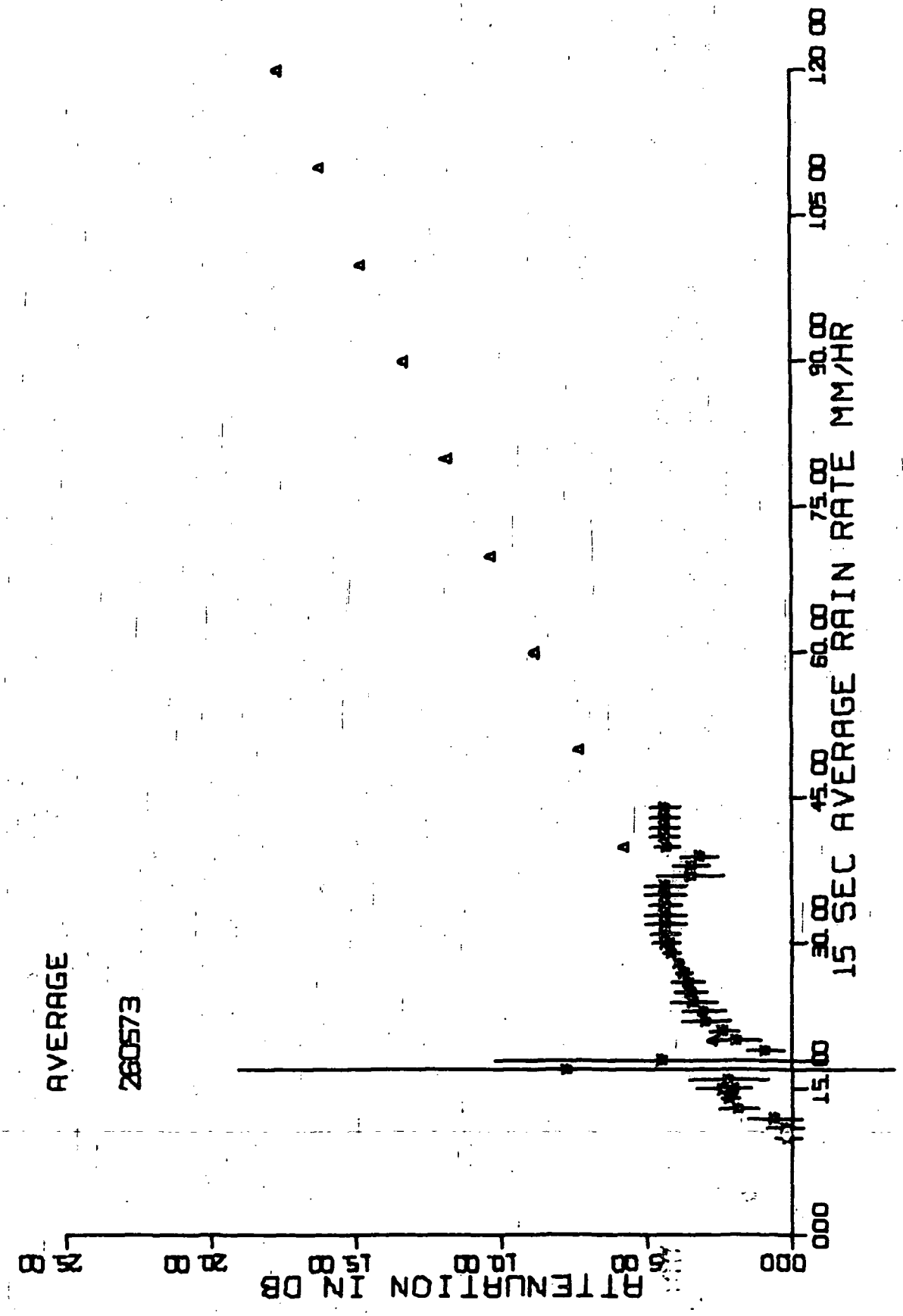

Figure 53. May 26, 1973, average attenuation values.

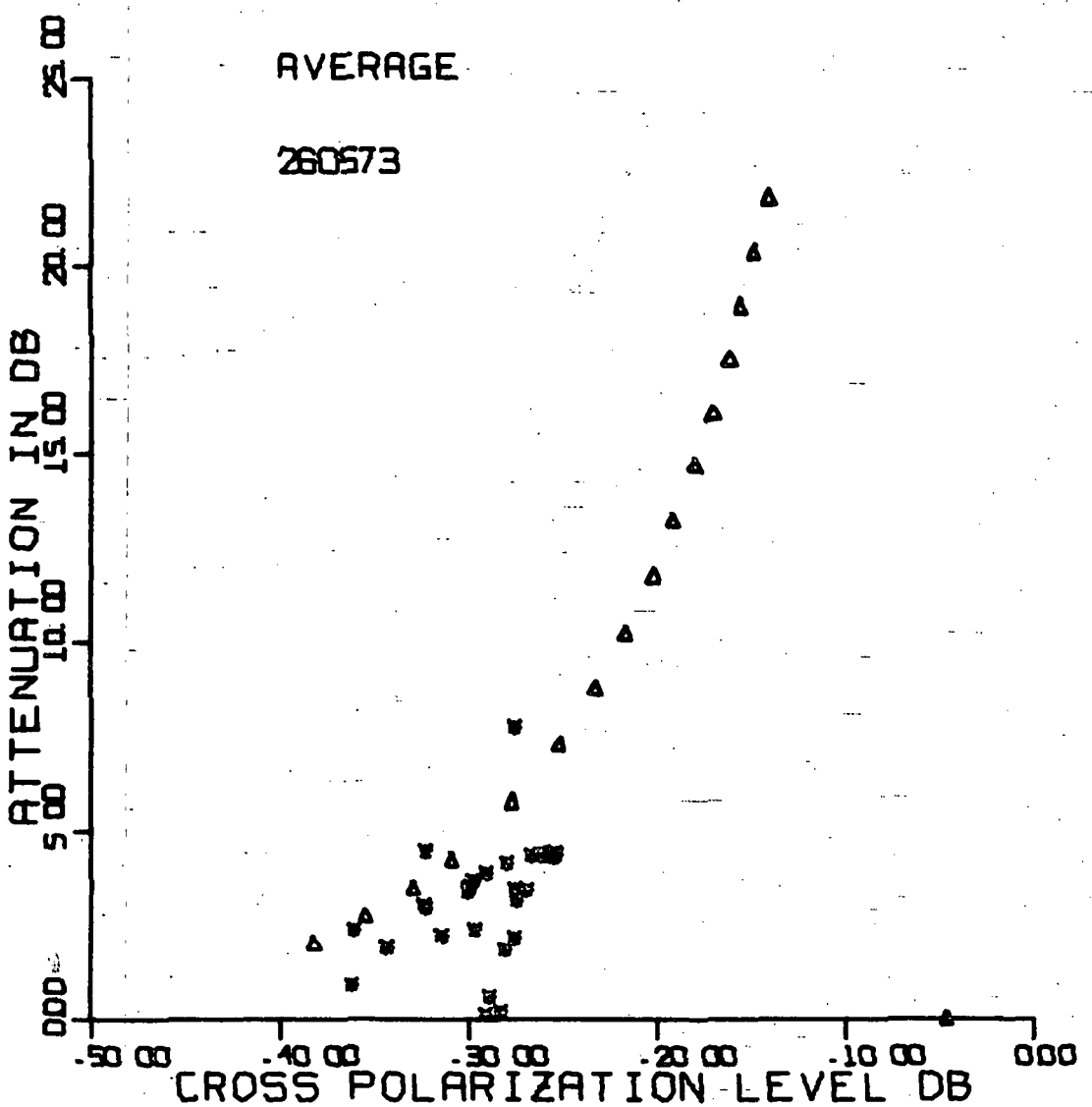

Figure 54. May 26, 1973,
average attenuation versus average cross polarization level.

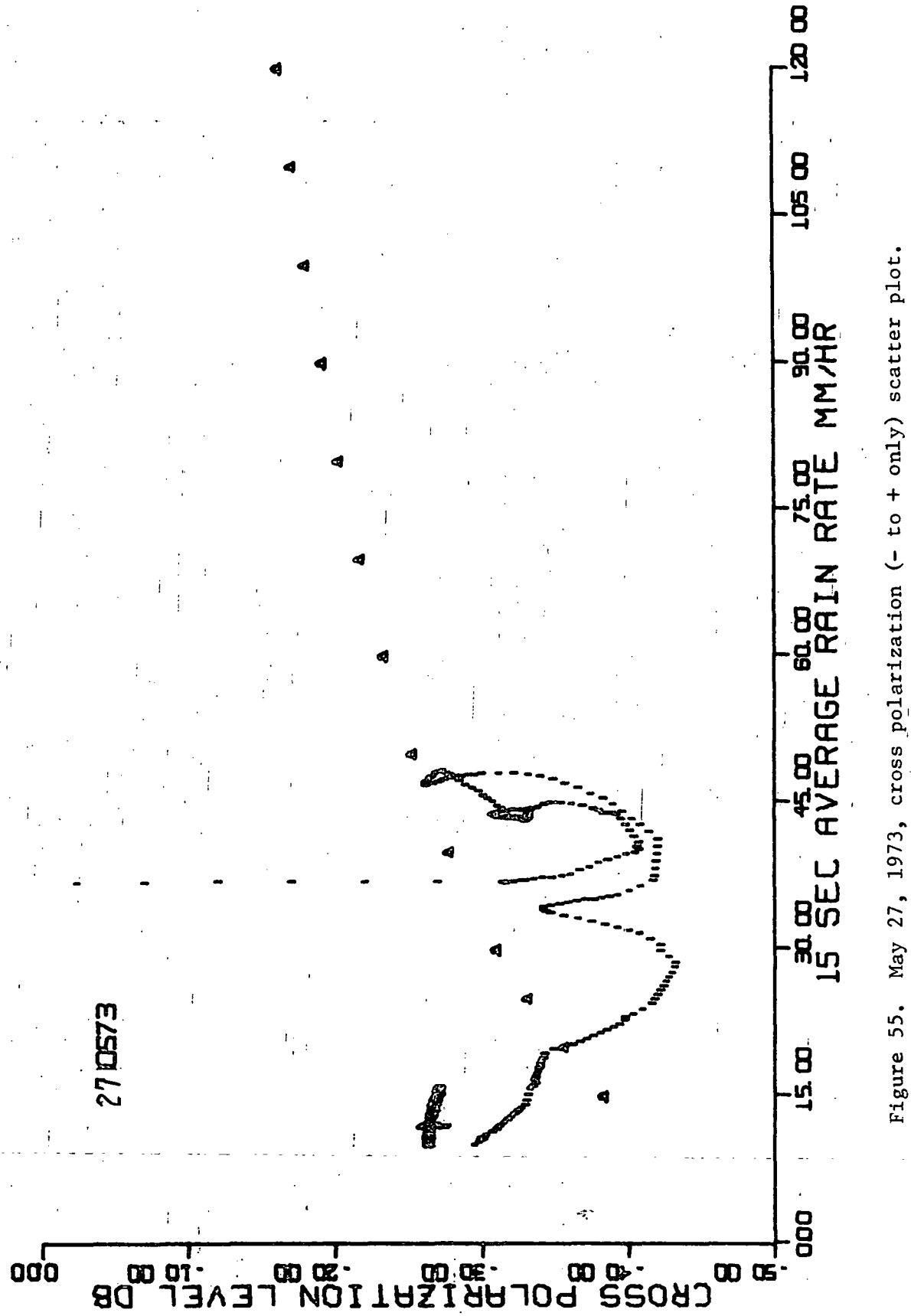

Figure 55. May 27, 1973, cross polarization (- to + only) scatter plot.

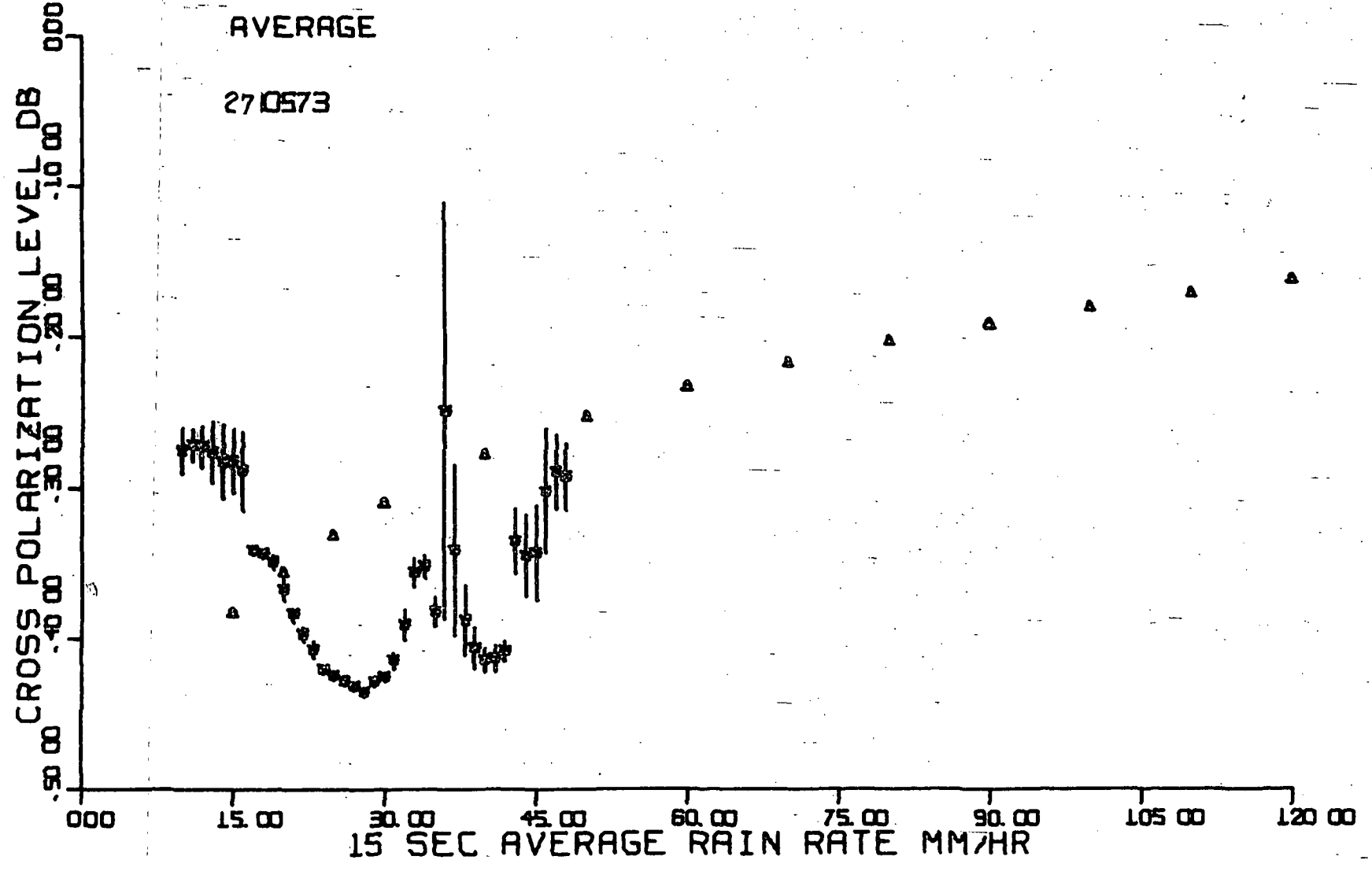

Figure 56. May 27, 1973, average - to + cross polarization levels.

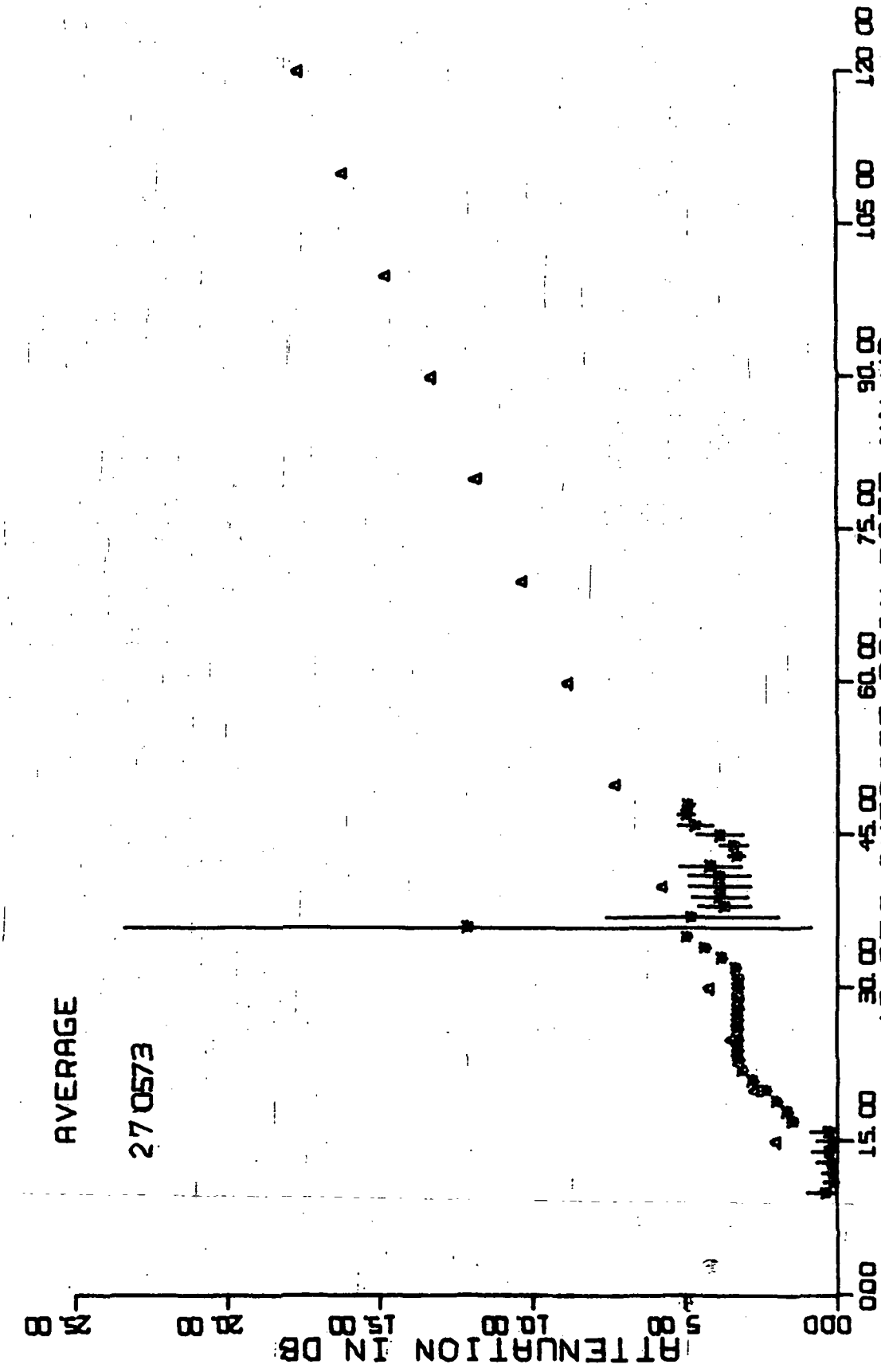

Figure 57. May 27, 1973, average - channel attenuation values.

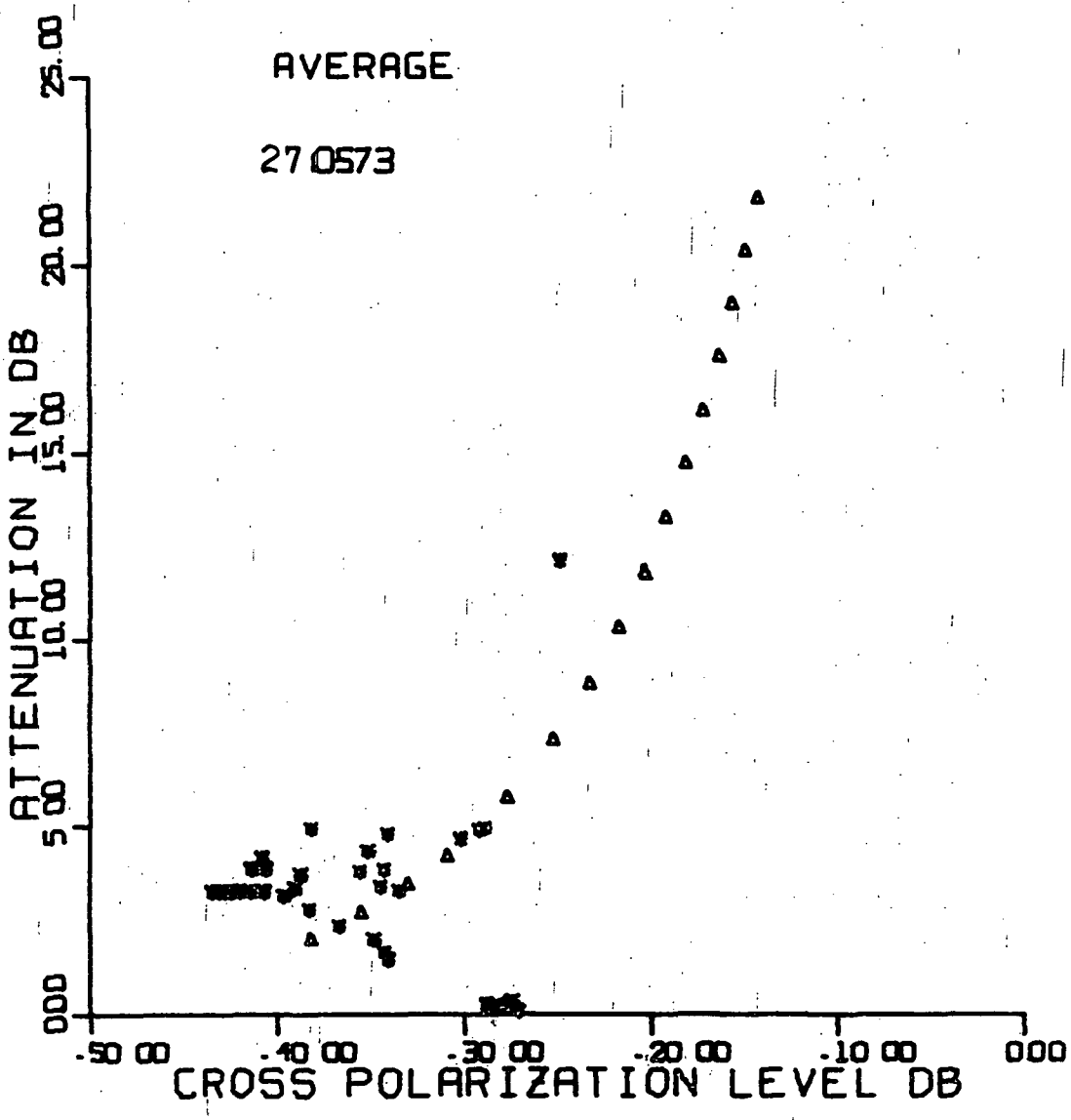

Figure 58. May 27, 1973,
average - channel attenuation versus average - to + cross polarization levels.

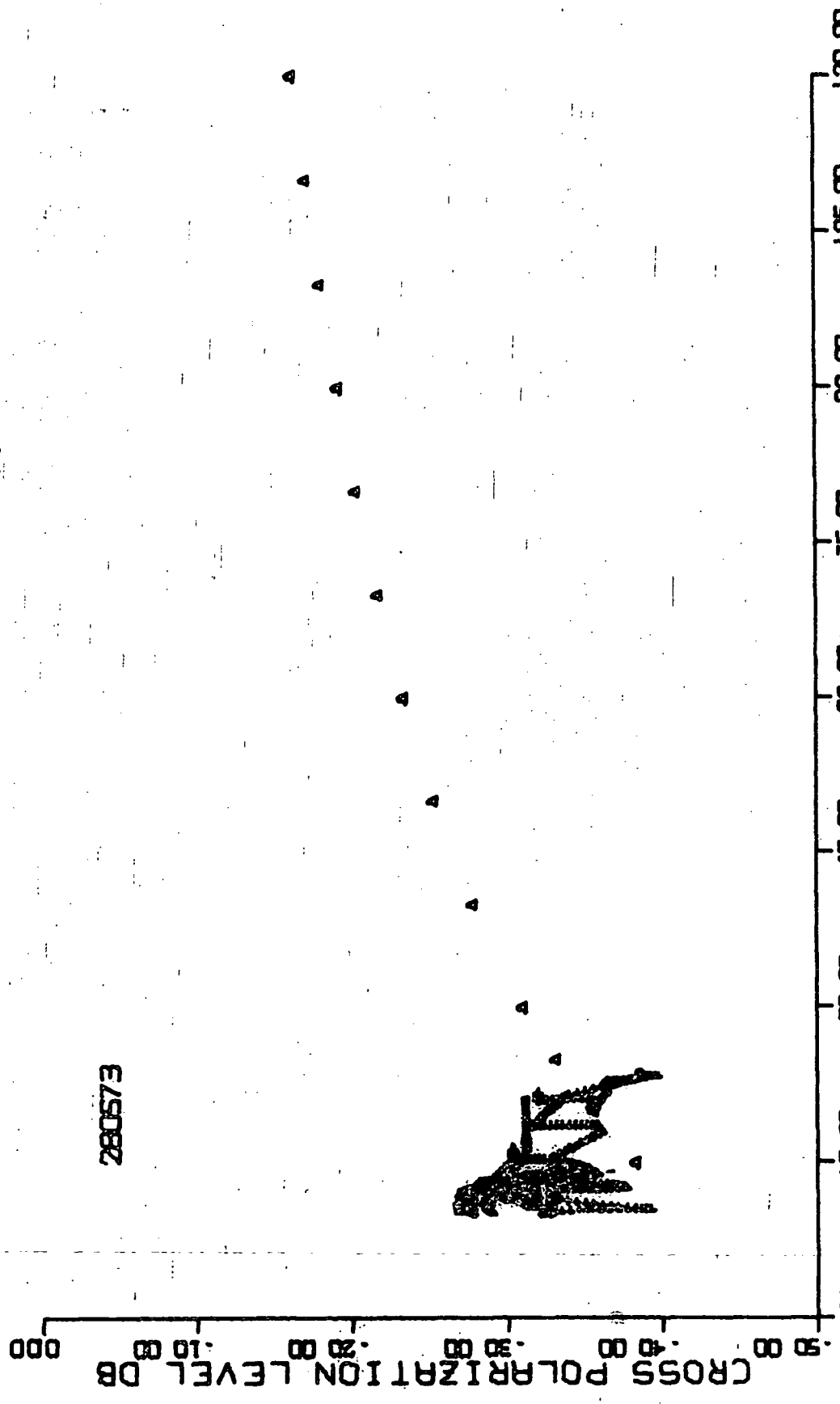

Figure 59. May 28, 1973, cross polarization scatter plot.

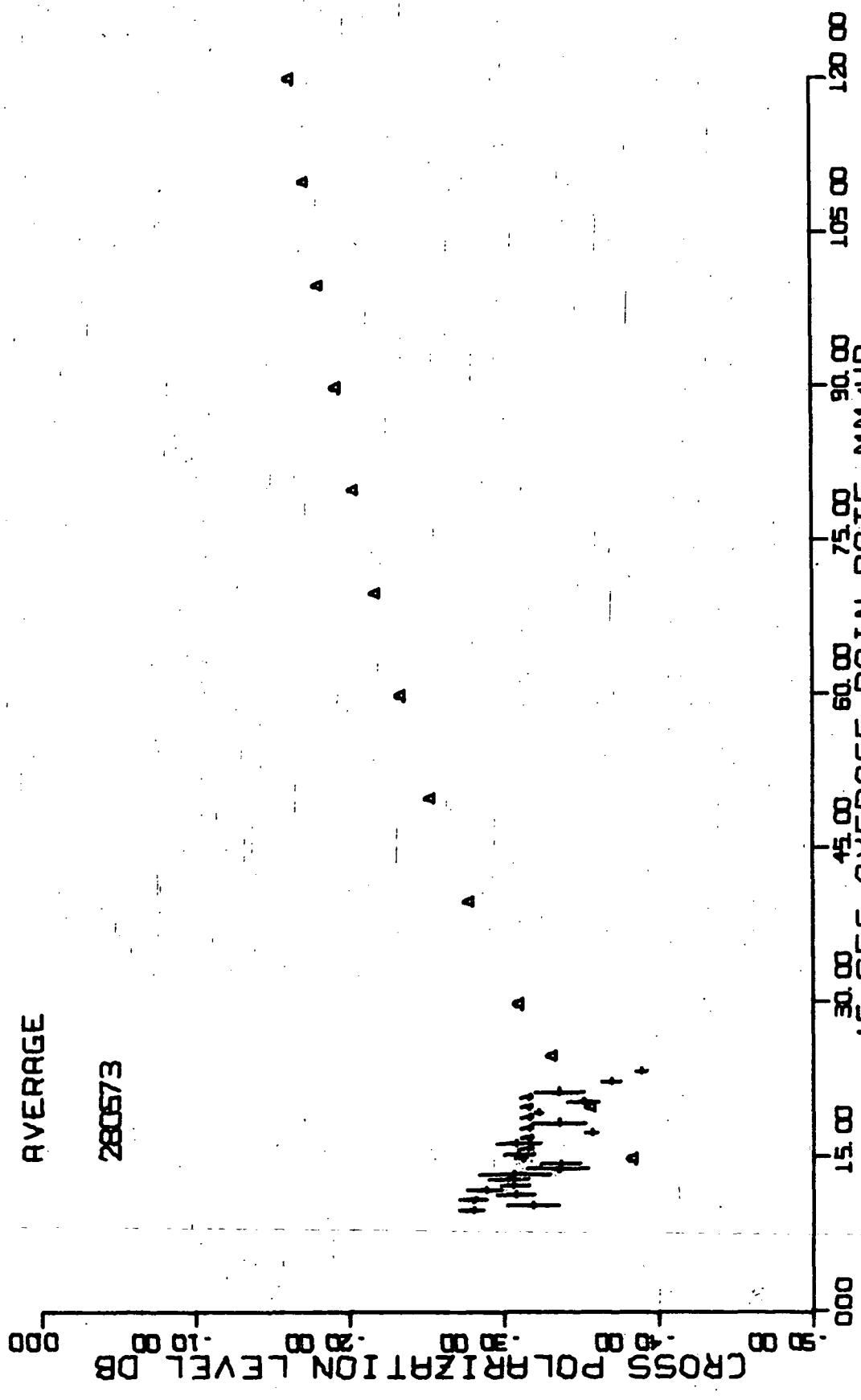

Figure 60. May 28, 1973, average cross polarization levels for each channel.

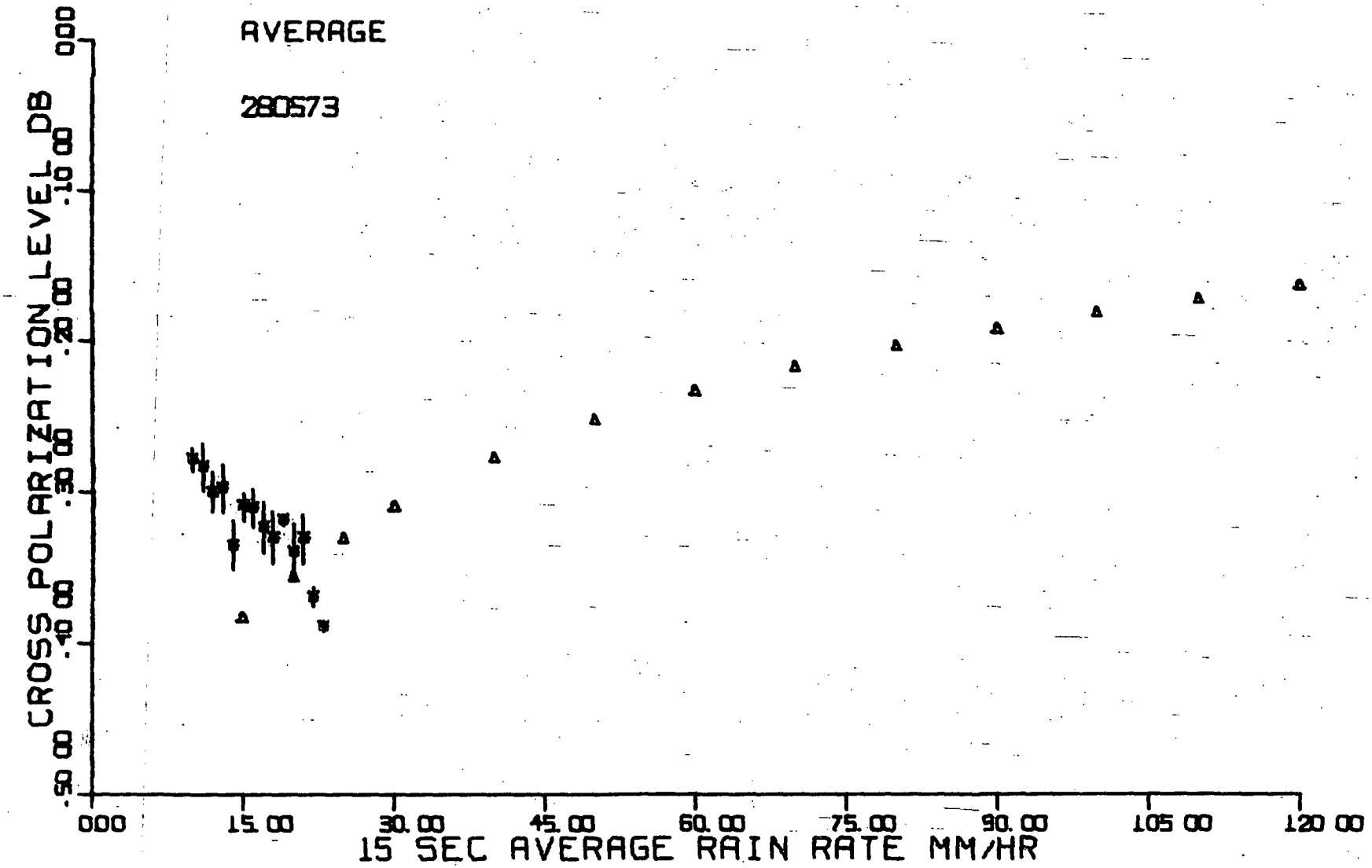

Figure 61. May 28, 1973, average cross polarization levels.

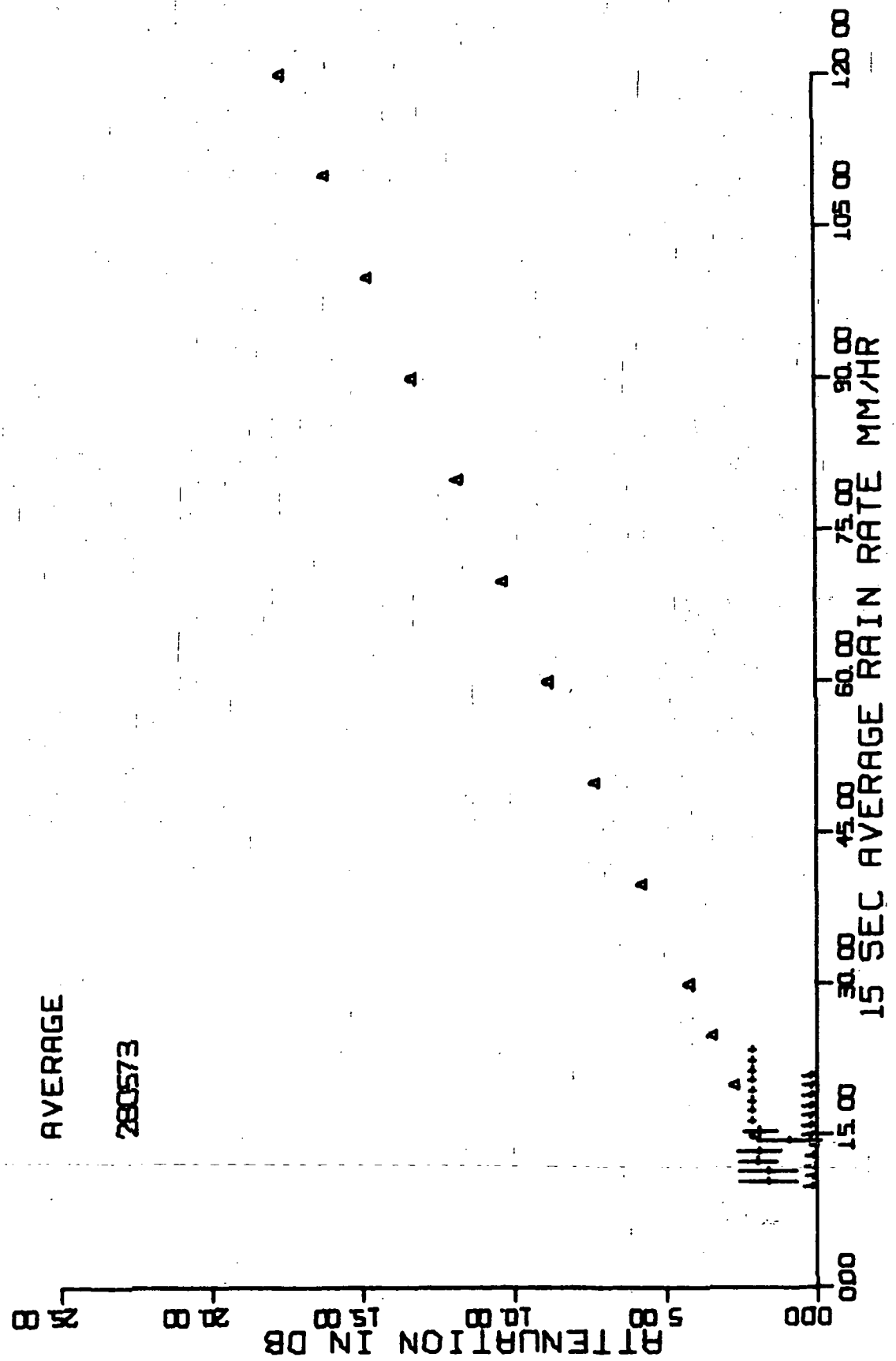

Figure 62. May 28, 1973, average attenuation values for each channel.

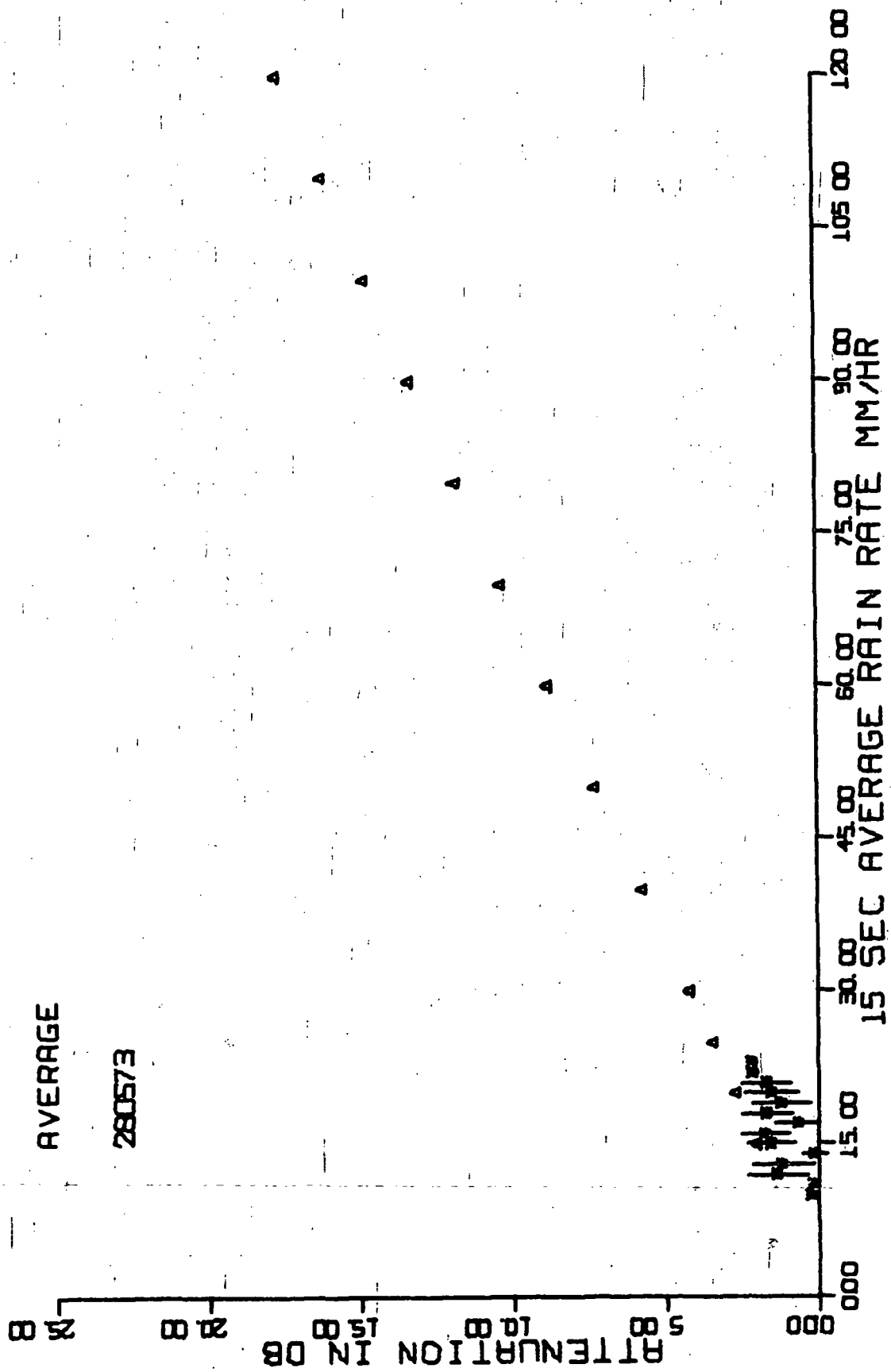

Figure 63. May 28, 1973, average attenuation values.

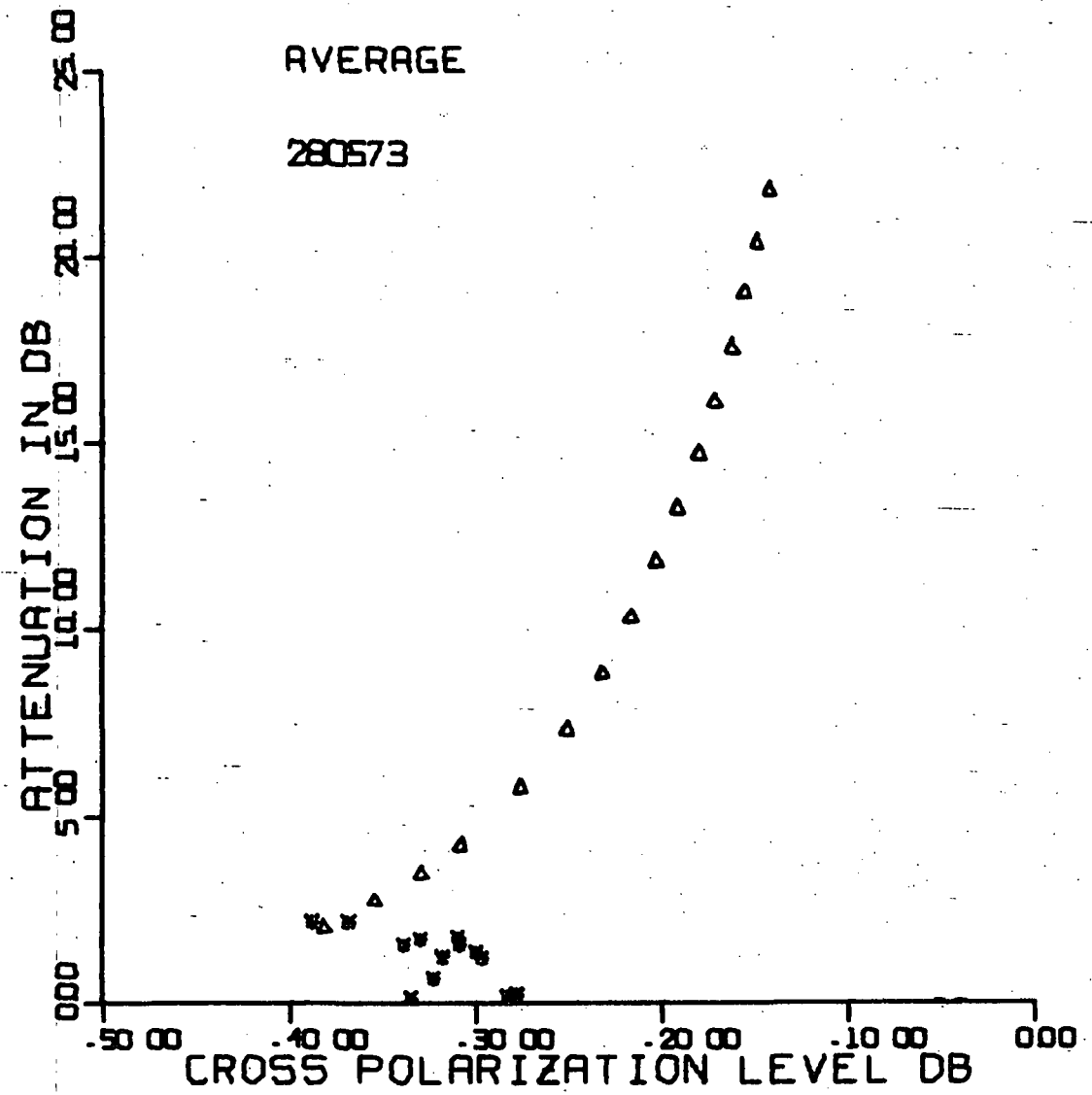

Figure 64. May 28, 1973,
average attenuation versus average cross polarization level.

5.3 Summary

Figure 65 is a cumulative scatter plot of all the 1973 depolarization data presented in this report.

Figures 66 and 67 illustrate the average cross polarization levels by channel for all of the 1972 and presently available 1973 data respectively. Figures 68 and 69 present similar data for both channels together.

Figures 70 and 71 display the 1972 and 1973 average attenuation values for each channel and Figures 72 and 73 illustrate the average values resulting when data from both channels are combined.

Figures 74 and 75 are plots of average attenuation versus average cross polarization level for 1972 and 1973 respectively.

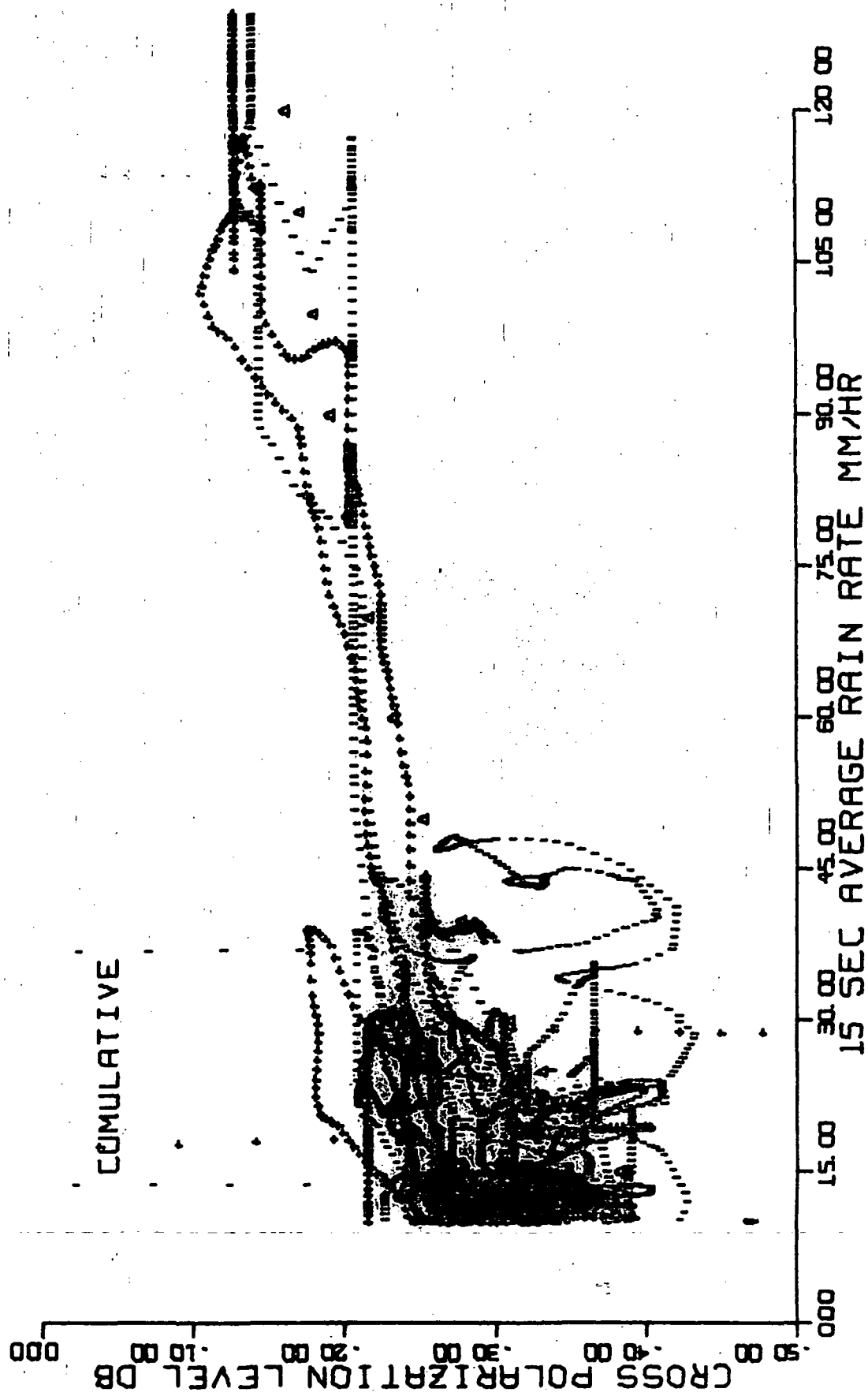

Figure 65. Cross polarization scatter plot for all six 1973 storms.

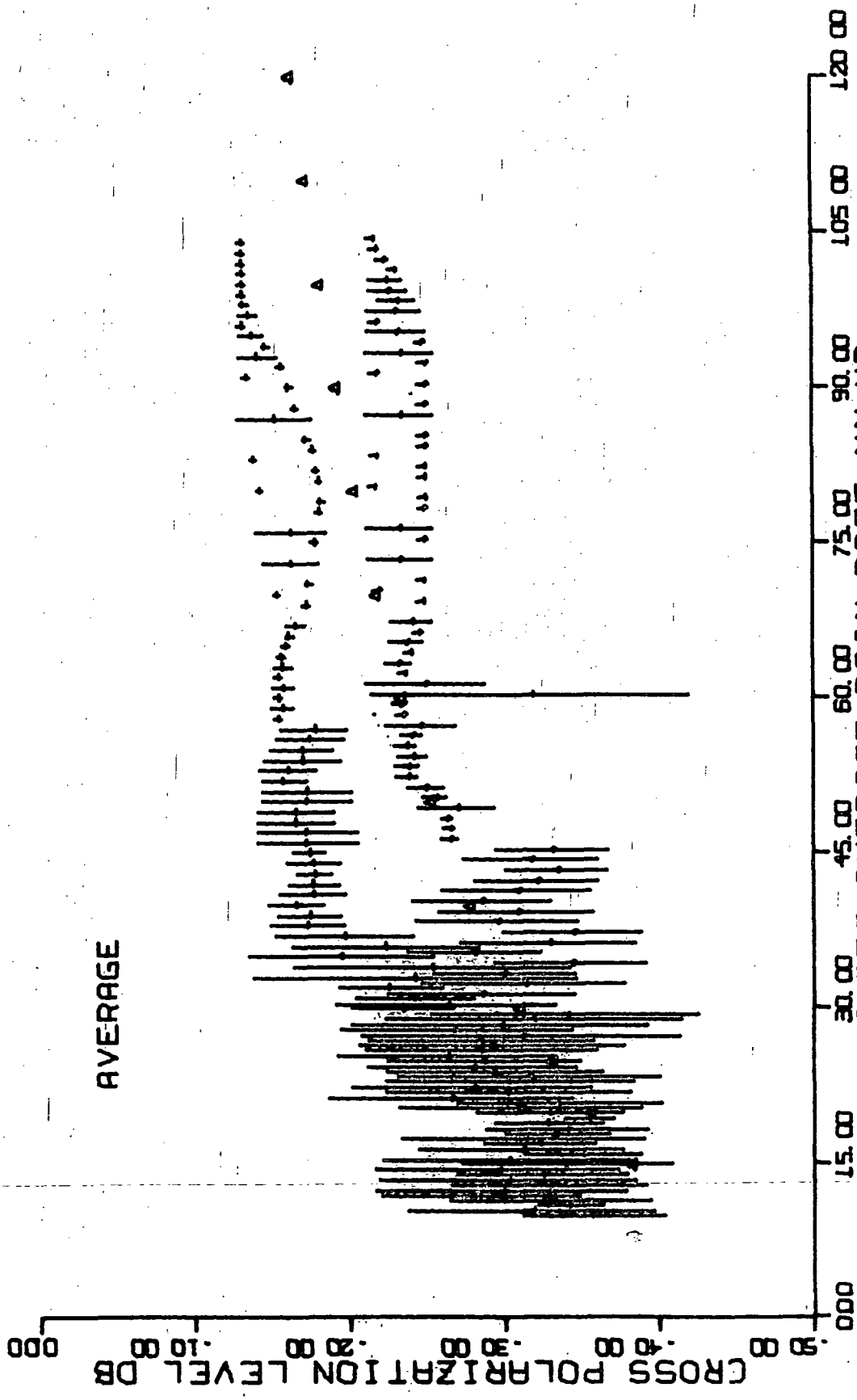

Figure 66. 1972 average cross polarization levels for each channel.

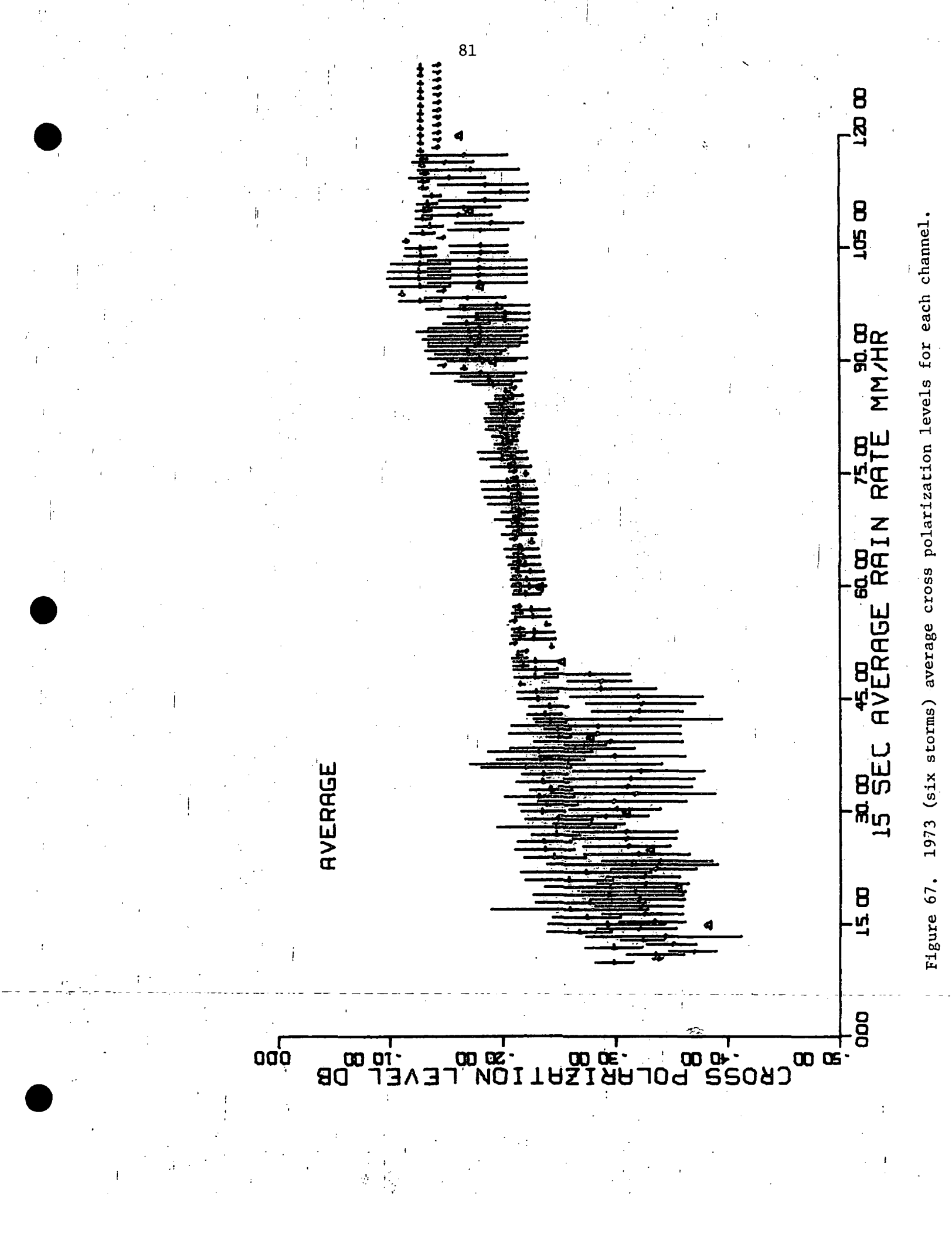

Figure 67. 1973 (six storms) average cross polarization levels for each channel.

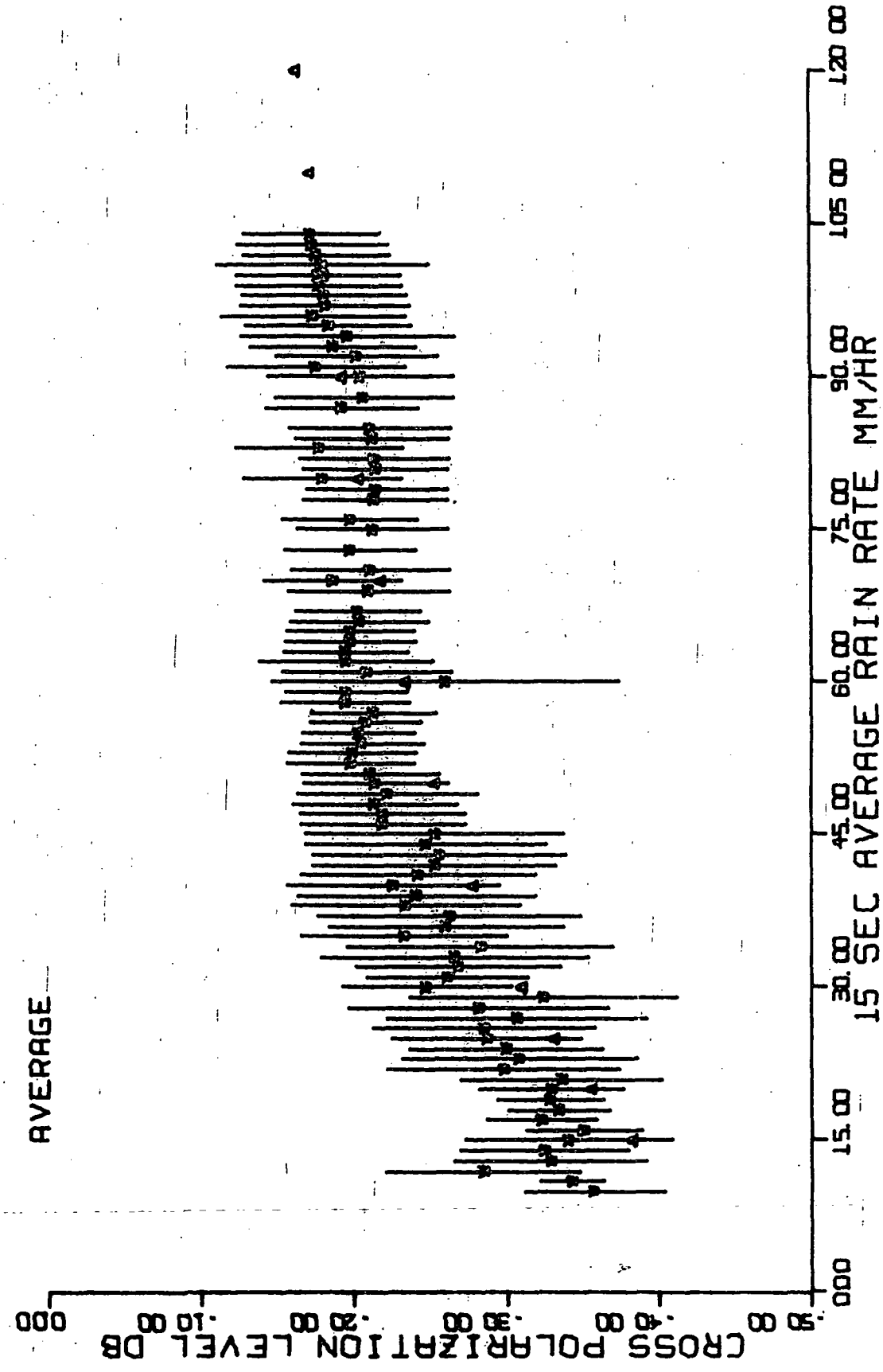

Figure 68. 1972 average cross polarization levels.

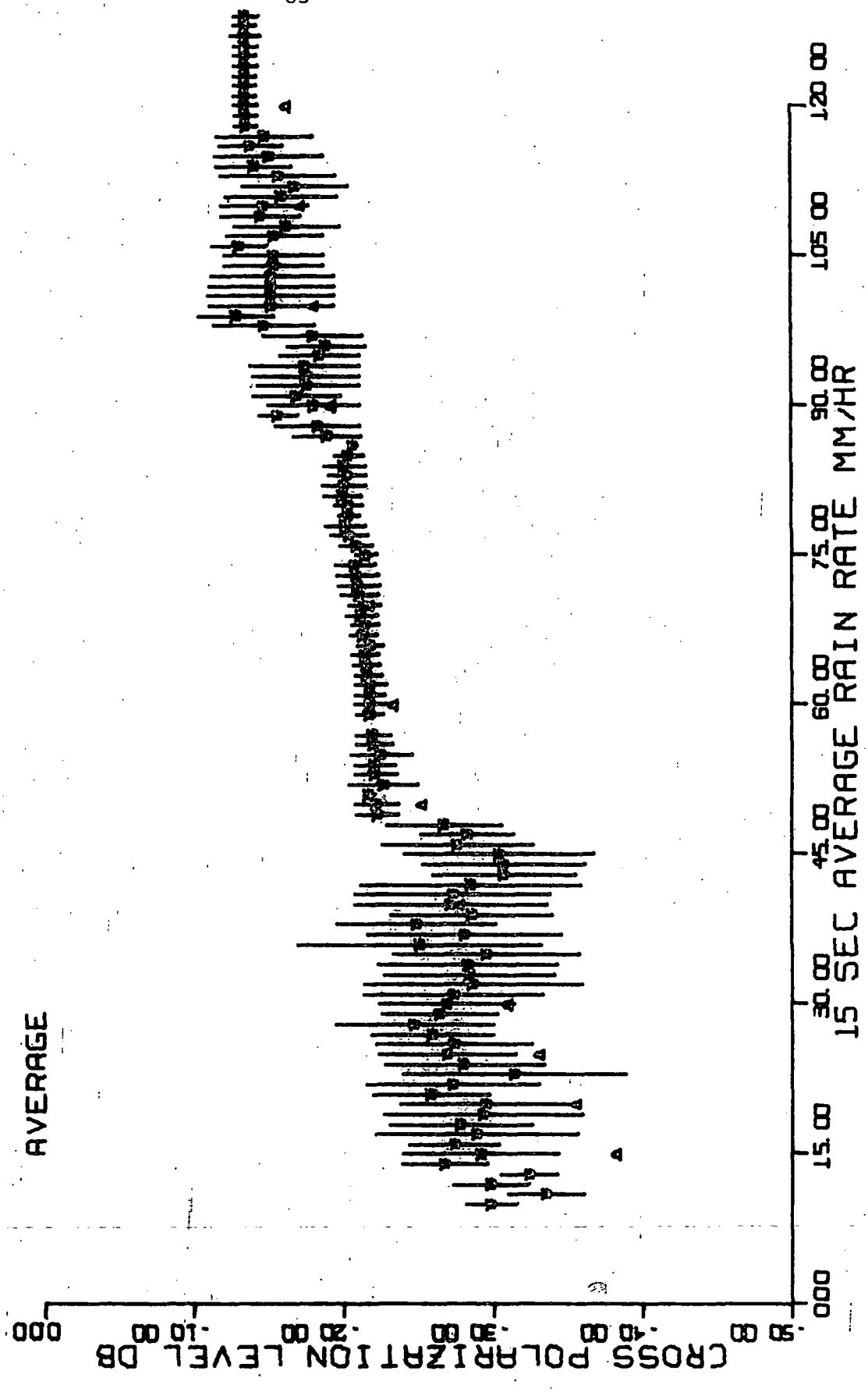

Figure 69. 1973 (six storms) average cross polarization levels.

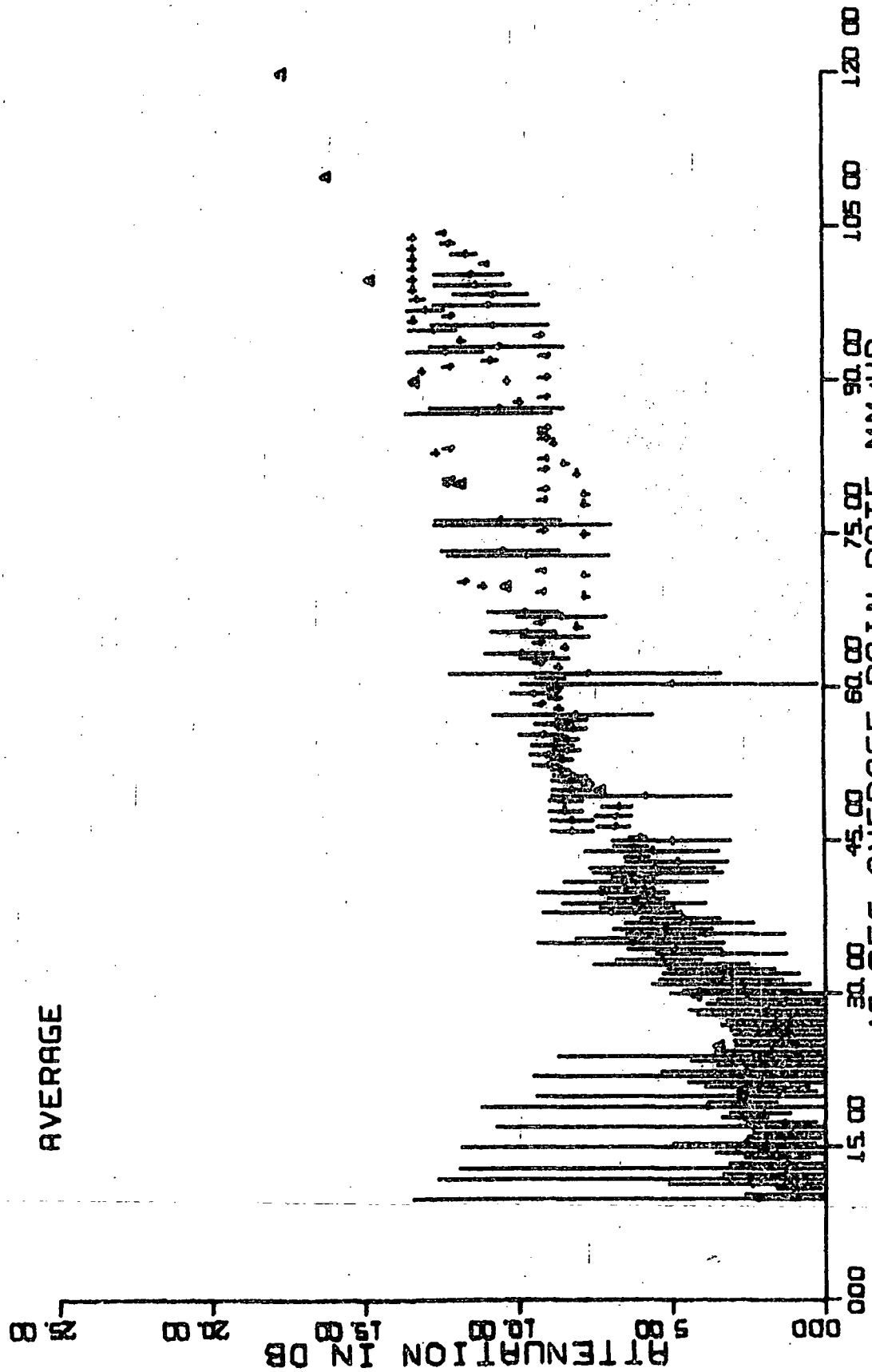

Figure 70. 1972 average attenuation values for each channel.

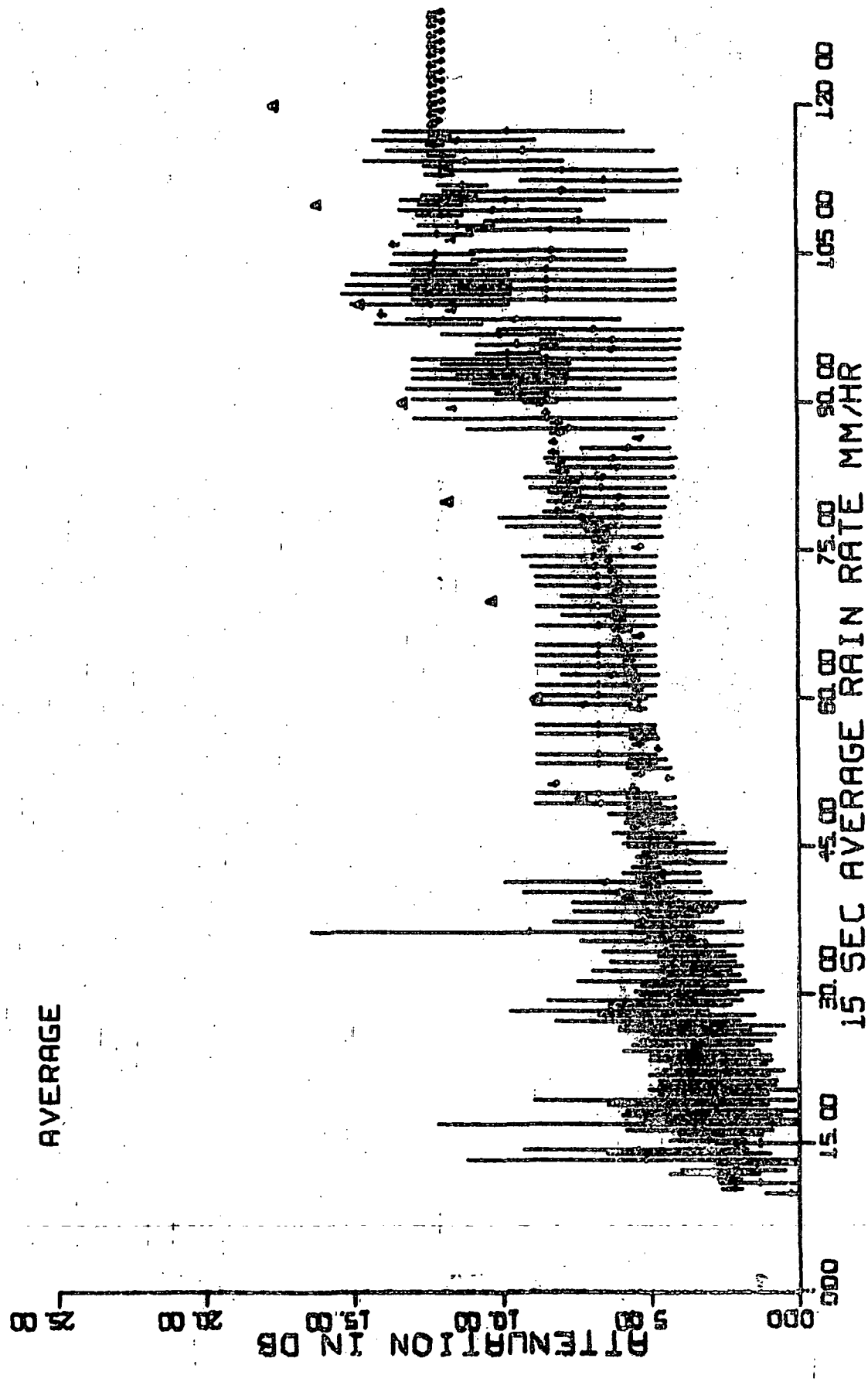

Figure 71. 1973 (six storms) average attenuation values for each channel.

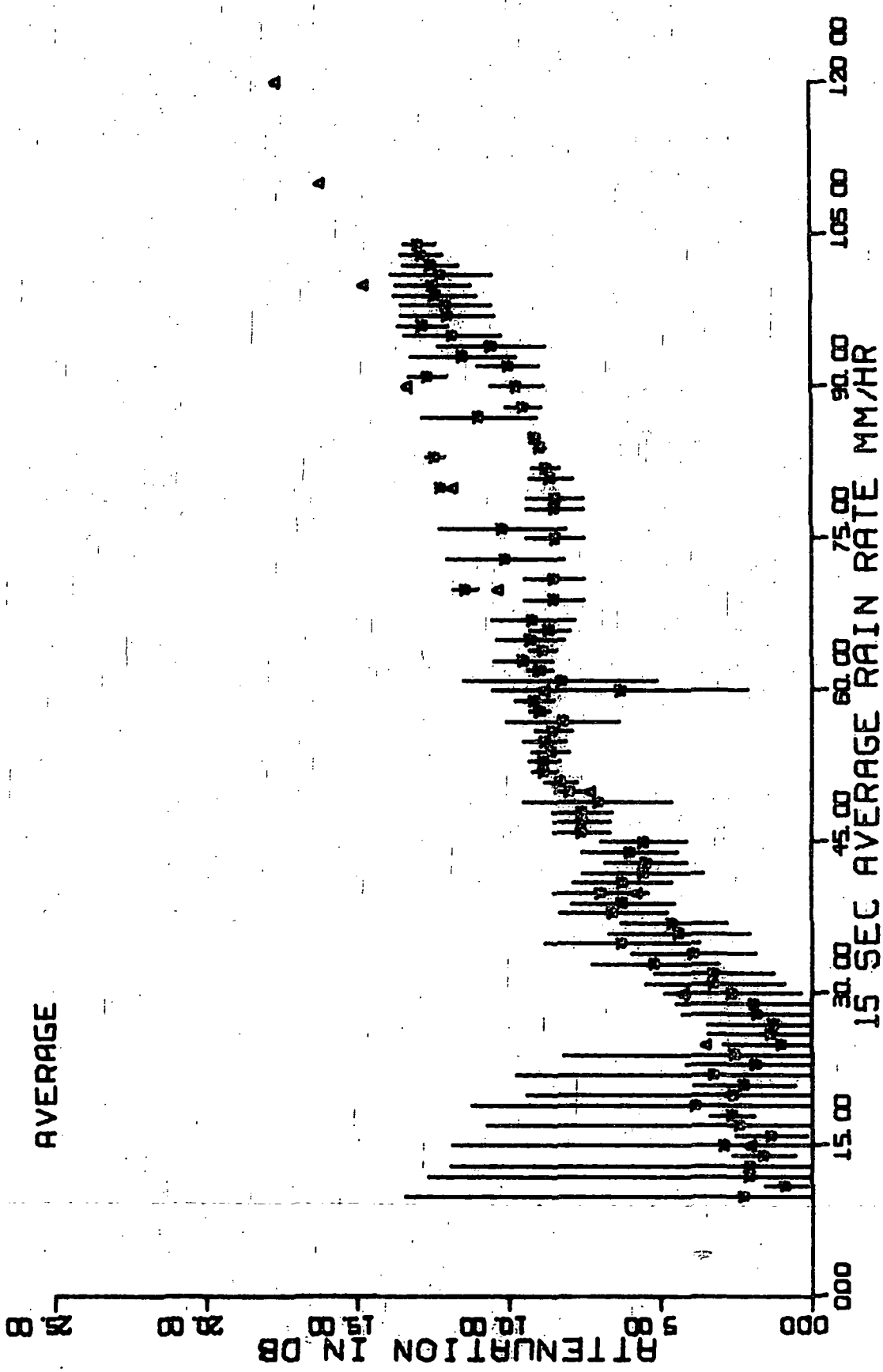

Figure 72. 1972 average attenuation values.

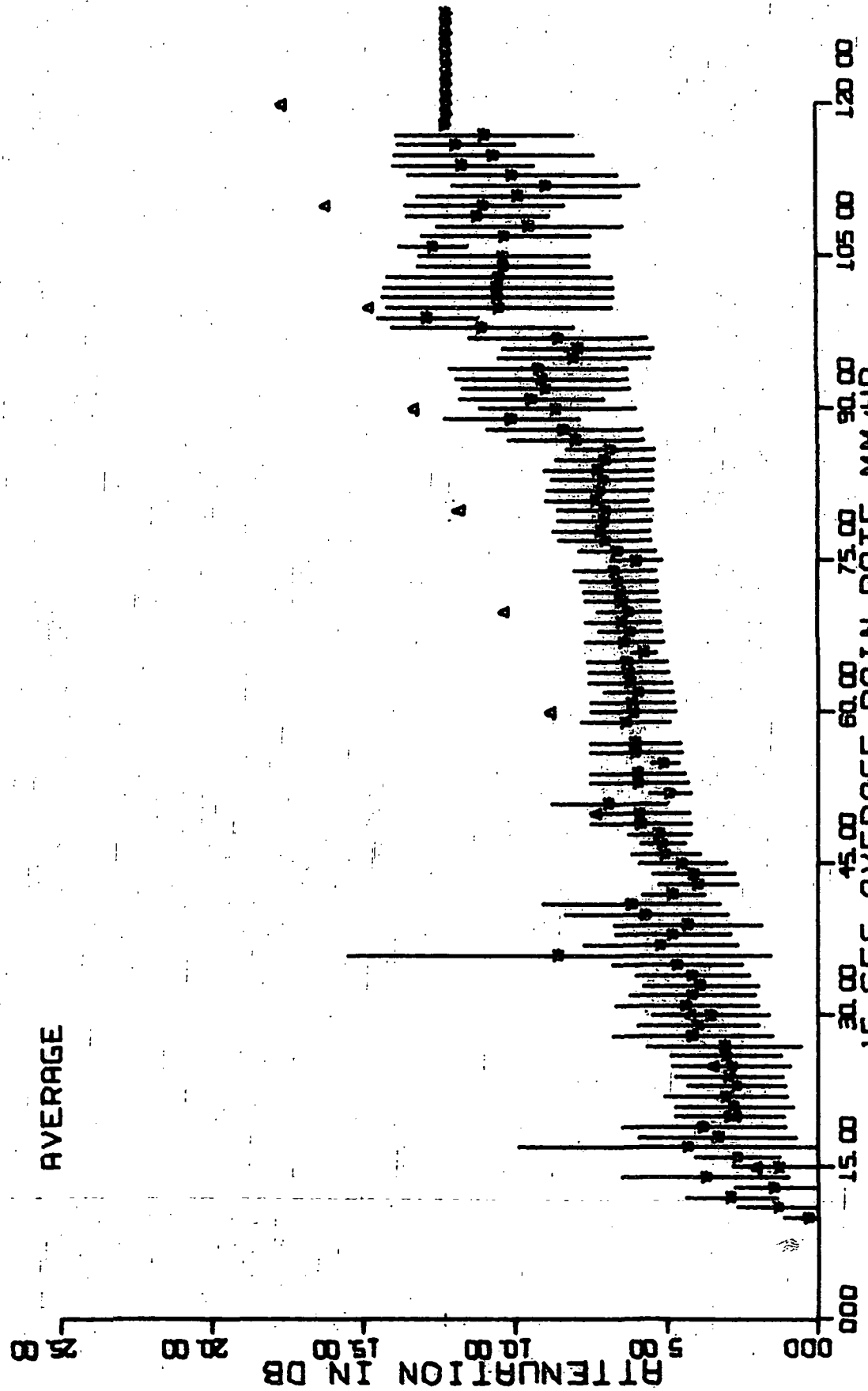

Figure 73. 1973 (six storms) average attenuation values.

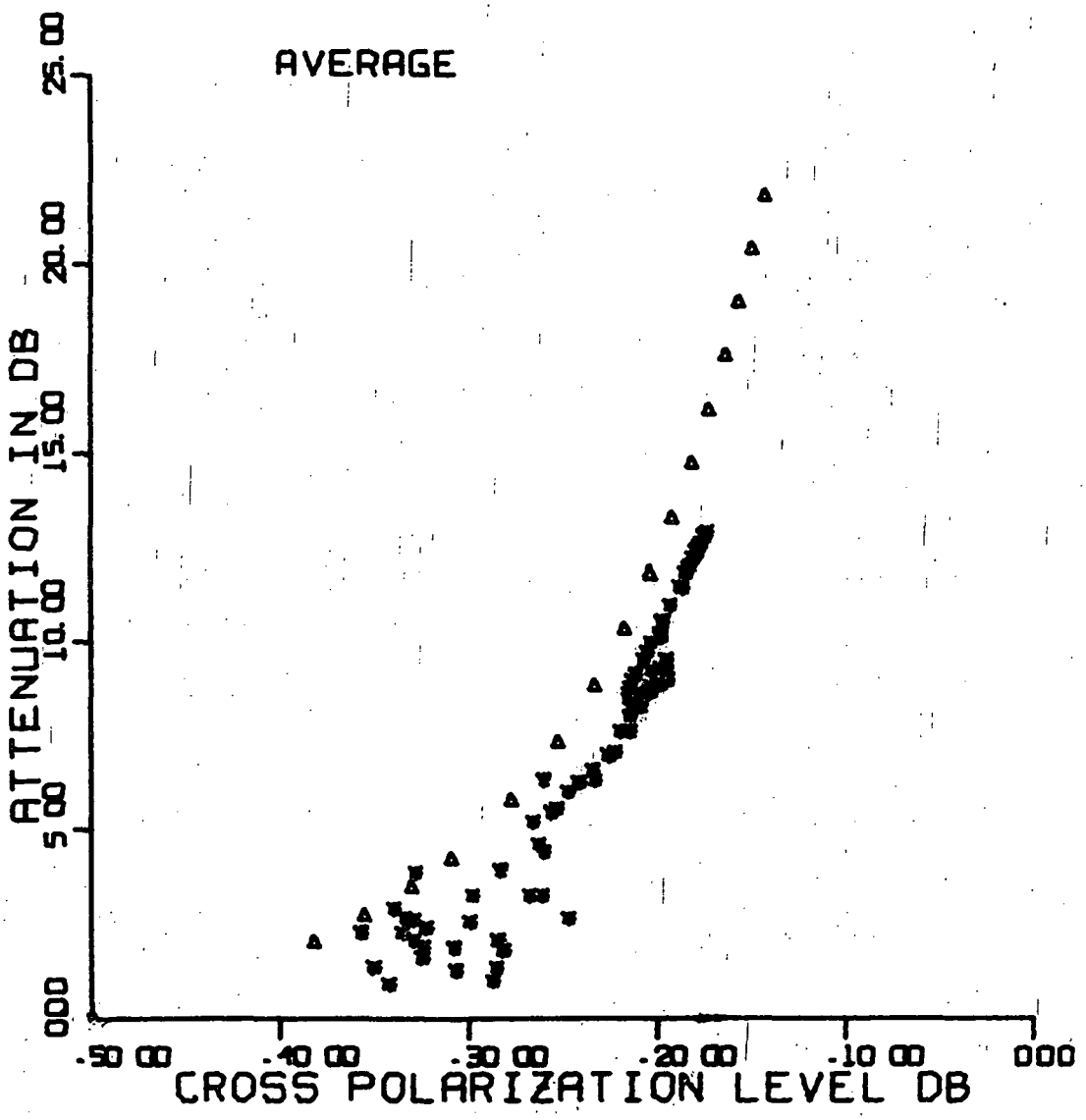

Figure 74. 1972 average attenuation versus average cross polarization level.

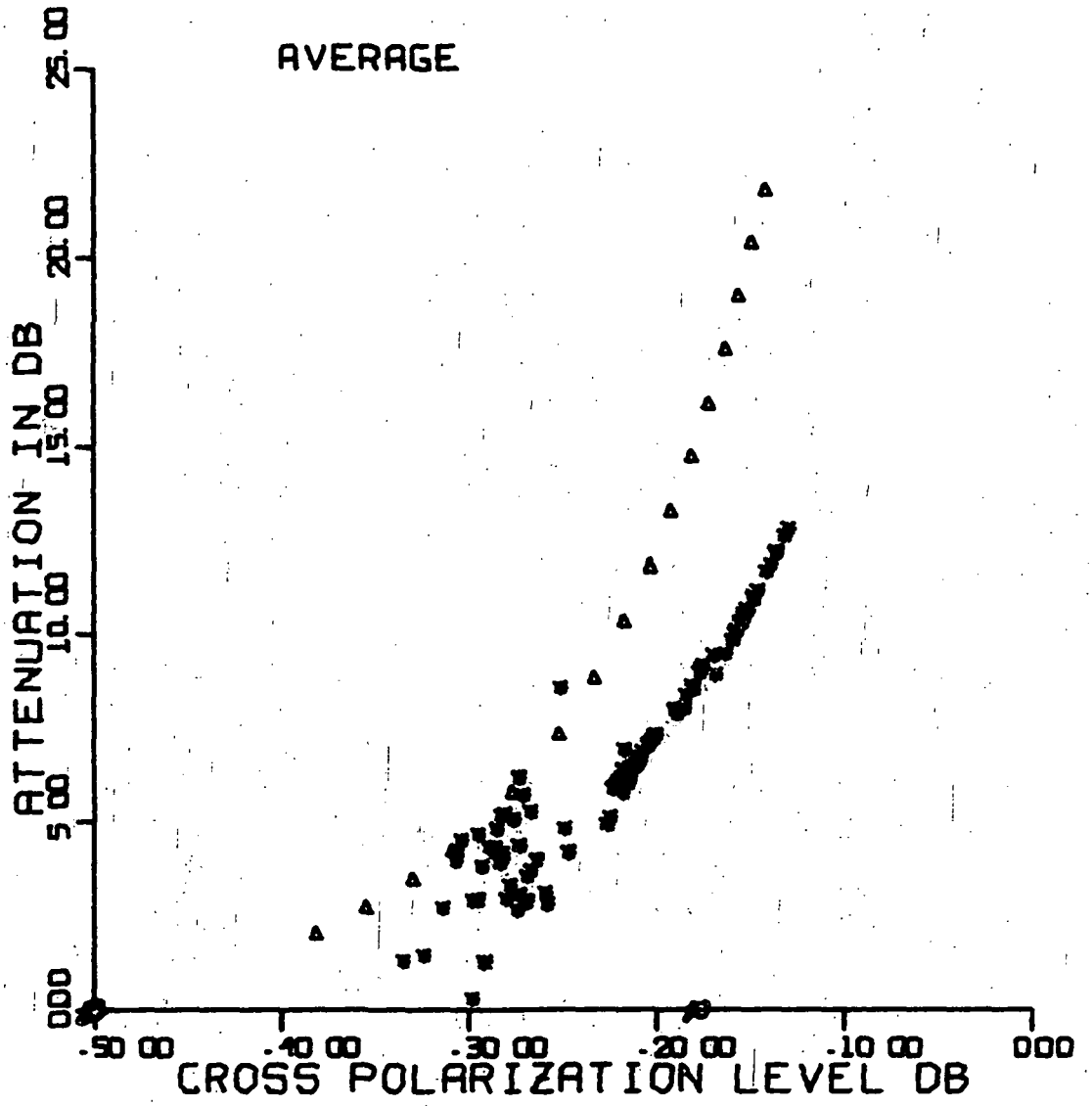

Figure 75. 1973 (six storms)
average attenuation versus average cross polarization level.

6. Literature Cited

1. C. W. Bostian and W. L. Stutzman, "The Influence of Polarization on Millimeter Wave Propagation Through Rain," Semi-Annual Status Report II, NASA Grant NGR-47-004-091, VPI&SU, Blacksburg, January 1973.

2. C. W. Bostian and W. L. Stutzman, "The Influence of Polarization on Millimeter Wave Propagation Through Rain," Semi-Annual Status Report I, NASA Grant NGR-47-004-091, VPI&SU, Blacksburg, July 1972.

3. J. A. Morrison, M. J. Cross, and T. S. Chu, "Rain-Induced Differential Attenuation and Differential Phase Shift at Microwave Frequencies," BSTJ, Vol. 52, pp. 599-604, April 1973.

4. T. Oguchi, "Attenuation of Electromagnetic Waves Due to Rain with Distorted Drops," J. Radio Res. Lab. Japan, Vol. 11, pp. 19-44, January 1964.

5. T. Oguchi, "Attenuation and Phase Rotation of Radio Waves Due to Rain: Calculations at 19.3 and 34.8 GHz," Radio Science, Vol. 8, pp. 31-38, January 1973.

6. A. F. Stevenson, "Solution of Electromagnetic Scattering Problems as Power Series in the Ratio (Dimension of Scatterer)/Wavelength," JAP, Vol. 24, pp. 1134-1142, September 1953.

7. D. T. Thomas, "Cross Polarization Distortion in Microwave Radio Transmission Due to Rain," Radio Science, Vol. 6, pp. 833-840, October 1971.

8. H. C. van de Hulst, Light Scattering by Small Particles, New York: John Wiley and Sons, Inc., 1957, pp. 28-34.

9. P. A. Watson and M. Arbabi, "Rainfall Cross Polarization at Microwave Frequencies," Proc. IEE (London), Vol. 120, April 1973.

10. P. H. Wiley, C. W. Bostian, and W. L. Stutzman, "The Influence of Polarization on Millimeter Wave Propagation Through Rain," Interim Report I, NASA Grant NGR-47-004-091, VPI&SU, Blacksburg, June 1973.

7. Appendix: Considerations in RF System Design for Cross Polarization Measurements

7.1 Introduction

The RF system design, construction, and testing for this project were done by R. E. Marshall. Mr. Marshall wrote an M.S. thesis about the RF system and included in it both new information developed by this project and information from widely scattered sources in the literature. As Mr. Marshall's thesis will be of considerable interest to other designers of depolarization experiments, most of it is reproduced in the pages which follow. It involves the design of a transmitter and receiver to meet the following criteria:

Transmitter

1. Operating independent channels: 2(+45° and -45° polarization)
2. Switching capability: transmit or no transmit remotely selected for each channel
3. Polarization isolation: > 40.0 dB

Receiver

1. Operating independent channels: 2(+45° and -45° polarization)
2. Polarization isolation: > 40.0 dB
3. Dynamic range: > 41.0 dB
4. Easily interpreted transfer function

SECTION 7.2

RECEIVER

7.2.1 Scope of Section

Presented in this section are typical receivers for attenuation and depolarization measurements, design calculations for the VPI&SU 17.65 GHz transmitter, and suggested improvements.

7.2.2 Typical Receivers

Once the path is defined, the receiver design is primary. Optimum receiver performance is obtained easily if one is not working under the restriction of a specific received signal level. This restriction fixes the upper bound of the dynamic range and forces the designer to find hardware that will fit the situation. It is simpler to design the receiver and then provide the proper transmitted power.

Figure 2.1 is a block diagram of a receiver that will measure attenuation. Single conversion is used because it is economical, introduces less noise, and is easily accomplished with available millimeter wave components. The RF amplifier and mixer are usually found commercially in a single "black box." Noise associated with wide bandwidths and high noise figures is a major cause of shortened receiver dynamic range. Bandwidths as low as 10 MHz are available with most commercial millimeter wave mixer-preamplifiers. Typical noise figures are from 9.0 to 10.0 dB. The local oscillator must be stable because of the narrow bandwidth requirement. A 50% savings is usually realized when mechanical tuning is chosen over voltage tuning; voltage tuned

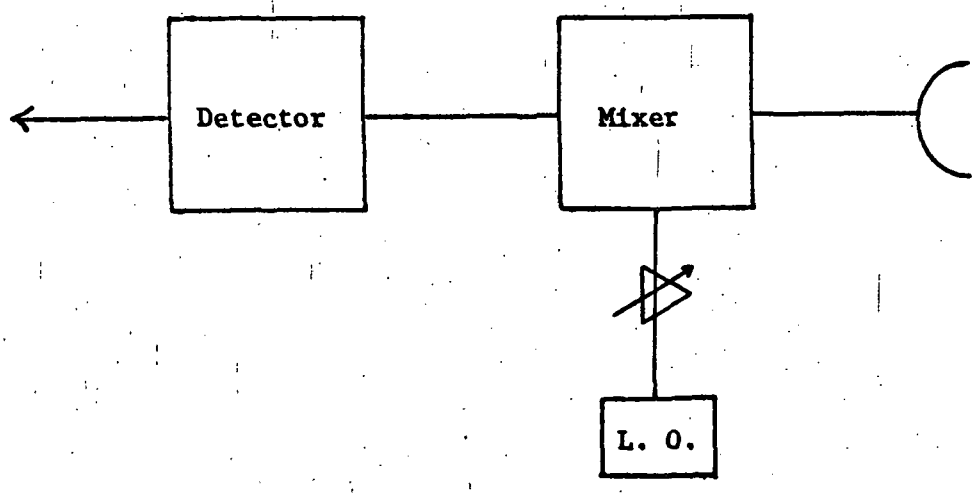

Figure 2.1. Attenuation Receiver

oscillators also require more expensive and stable power supplies. Detector choice is based mainly on the transmission mode used, but a linear transfer function will result in easier data analysis.

Figure 2.2 is a block diagram of a dual channel receiver used for cross-polarization measurements. The mixers, preamplifiers, local oscillator, and detectors are identical to the components used in the attenuation receiver. The local oscillator is shared by both channels, which greatly reduces cost and tuning difficulties. The relative cost of the local oscillator allows the addition of another channel for about 70% of the cost of a single channel receiver.

Figure 2.3 is a block diagram of the VPI&SU 17.65 GHz, CW, receiver. The isolators insure polarization isolation, and the attenuators control local oscillator power to the mixers. The use of uncalibrated attenuators here will save about $300.00 per attenuator.

7.2.3 Choosing Receiver Components

The elimination of cost and noise due to a transmission line between a pre-amplifier and a mixer warranted the use of commercially available mixer-preamplifiers for the VPI&SU receiver. A balanced mixer with an orthomode coupling mechanism was chosen because of its high isolation between the local oscillator port and the RF port.[5] Local oscillator noise suppression also prompted the use of a balanced mixer[6], because local oscillator noise reduces the dynamic range of the receiver.

The mixer-preamplifier chosen was an RHG MP015/2C. The specifications are listed below.

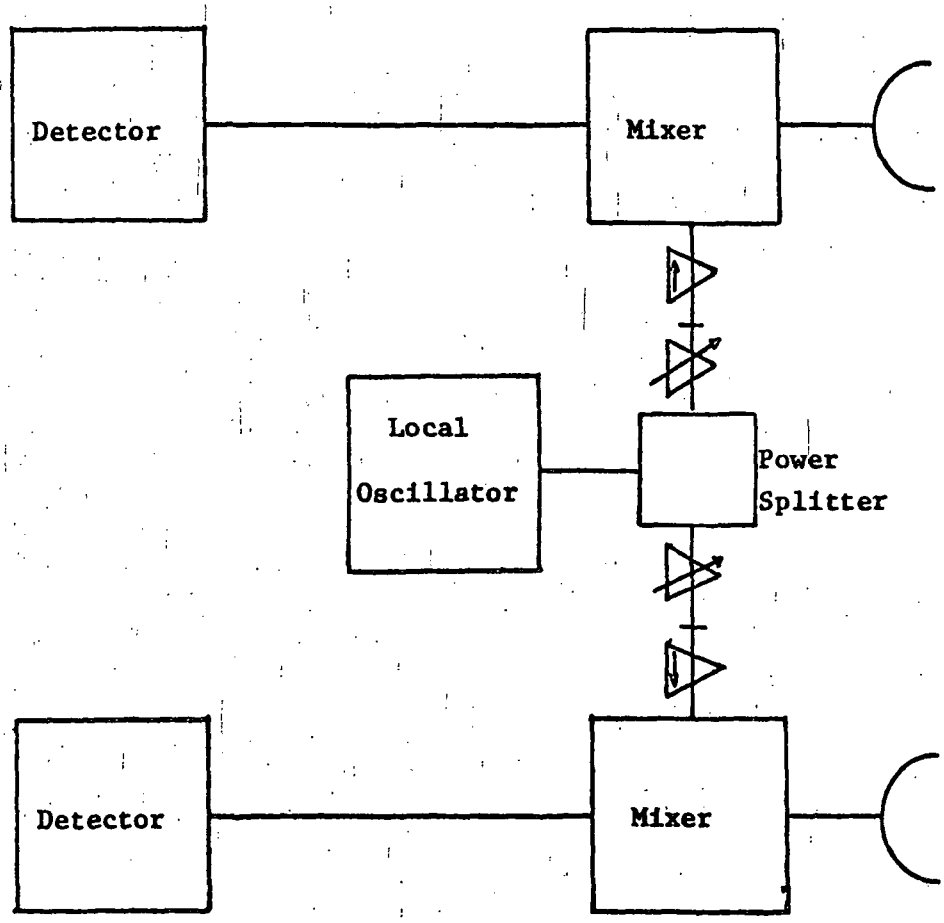

Figure 2.2. Depolarization Receiver

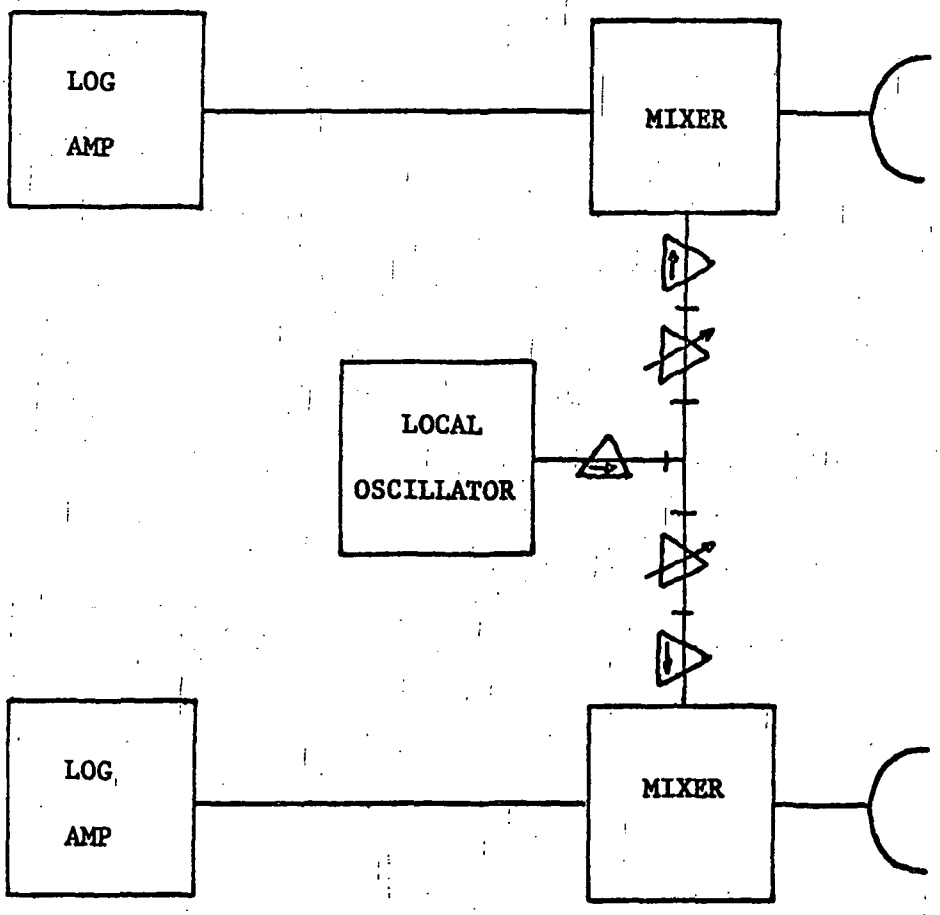

Figure 2.3. VPI & SU Receiver

Gain: 25 dB

LO Injection: 0 to +3 dBm

LO to RF Isolation: 20 dB

Input VSWR: 3/1

IF: 30 MHz

IF Bandwidth: 10 MHz

Noise Figure: 9.8 dB

An ideal figure can now be placed on the receiver sensitivity. This sensitivity will be a best case value and will be adjusted by local oscillator noise.

$$S = -174 \text{ dBm} + 10 \log(BWXF)$$ [7]

S = CW sensitivity in dBm

BW = IF bandwidth in MHz

F = noise figure expressed as a ratio

Diode conversion loss is included in the noise figure.

S = -94.2 dBm

The orthomode coupling system does introduce the problem of a 3 to 1 VSWR. The mixer must receive a 0 to +3 dBm local oscillator signal above the reflected local oscillator power. Below is a calculation of minimum LO power required for proper operation.

$|p|$ = magnitude of the reflection coefficient

$|p| = (\text{VSWR} - 1)/(\text{VSWR} + 1) = 1/2$

$t+r = 1.0$

t ≡ transmitted power coefficient

r ≡ reflected power coefficient

$$r = |p|^2 = 1/4$$

$$t = 3/4$$

$P_{LO} \equiv$ local oscillator power

$P_{LO}t = 1$ mw

$P_{LO} = 4/3$ mw (minimum value)

$P_{LO} = 8/3$ mw (maximum value)

$P_{LO}(\text{total}) = 16/3$ mw (maximum value)

Since commercial specifications tend to reflect the best possible values of VSWR, it is best to buy more LO power than is needed and then put an attenuator in series with the mixer LO input. This also allows the receiver to operate longer if the LO power decreases with age.

Receiver stability is almost completely dependent upon local oscillator stability with a fixed frequency CW receiver. The bandwidth of the receiver is 10 MHz and if the LO drifts 5.0 MHz or more, an attenuation measurement error of at least 3 dB would occur. Cross-polarization data would not be erroneous because each channel would fade equally. The danger to cross-polarization measurements results from a loss in dynamic range. As the LO drifts, the IF will drift out of the bandwidth and the detector output will drop. This forces the upper end of the dynamic range to move towards the lower end and jeopardizes the lower rainfall rate data. Below is a calculation of required LO stability.

Frequency = 17.62 GHz

$$\text{Stability} = \pm(BW/2)(100/F) = \pm \frac{.5}{17.62} = \pm\ 0.0284\%$$

This value of stability must be good over the temperature range

the LO will experience. If temperatures are extreme, an environmental chamber may be more economical than buying an LO that is stable over the extreme temperature range.

Noise generated by the LO causes a reduction in the dynamic range of the receiver, by causing a detector output when no RF is applied to the mixer. Noise problems can be minimized by choosing the most stable LO available and picking an IF bandwidth as small as possible for that stability. This also aids in tuning because the detector output will have a sharper maximum for the smaller bandwidths. The value for allowable LO noise will vary depending on the type of detector used, and for that reason, a more detailed discussion of LO noise will be presented after the section on detectors. Below is a list of LO specifications defined to this point.

Frequency: 17.62 GHz

Stability: $\pm$ 0.0284%

Power: 4/3 to 8/3 mw (per channel)

Tuning: Mechanical

Detectors

As stated before, the dynamic range of the receiver must be greater than 42 dB, and the transfer function should be as elementary as possible. For these two reasons, the logarithmic amplifier is an ideal detector for attenuation and cross-polarization measurements. Figure 2.4 represents the input vs output characteristic of an RHG LST 3010 MAT log amplifier chosen for the VPI&SU receiver. The linear D.C. output vs input dBm is "tailor made" for attenuation or cross-polarization

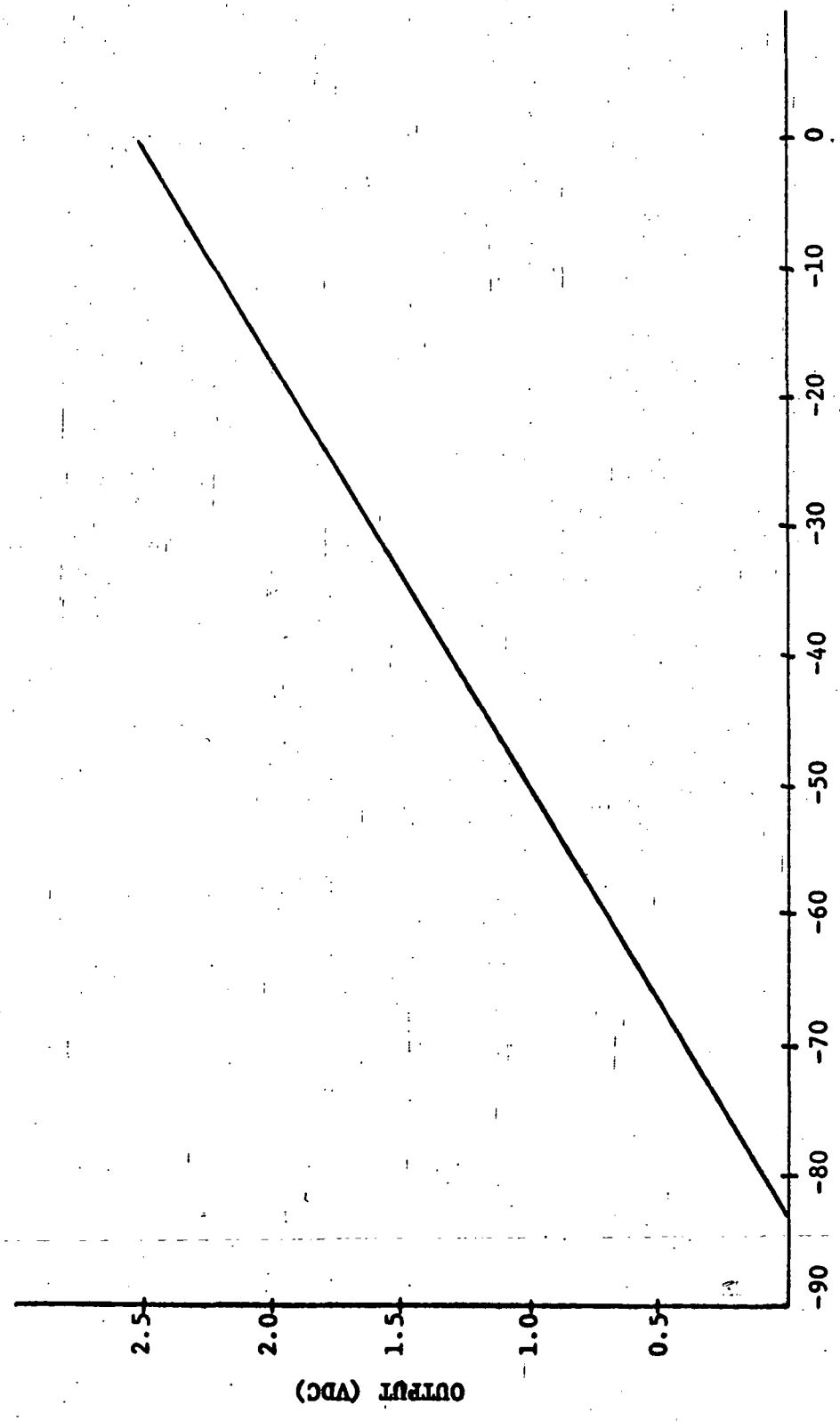

Figure 2.4. Logarithmic Amplifier

measurements. Below is a list of the RHG log amplifier specifications.

Frequency:	30 MHz
Bandwidth:	10 MHz
Input Impedance:	50 Ω
Input VSWR:	< 1.5-1
Dynamic range:	> 80 dB
Log accuracy:	± 1 dB over 80 dB range

It is now possible with the aid of Figure 2.4 to calculate the maximum allowable LO noise. A dynamic range of 50 dB was used instead of 42 to insure that all the data is observed. A 50 dB dynamic range corresponds to a -50.0 dBm LO noise signal.

DETECTOR INPUT VSWR = 1.5 to 1

$$|\rho| = \frac{1.5-1}{1.5+1} = \frac{0.5}{2.5} = 1/5$$

$t + r = 1.0$

$r = |\rho|^2 = \frac{1}{25}$

$t = 24/25$

p_{ND} = noise power incident to the detector = $\frac{25}{24}$ (10^{-5}) mw

p_{ND} = -49.8 dBm

IF gain = 25 dB

p_{NLO} = -49.8 dBm - 25 dB = -74.9 dBm ≡ local oscillator noise power.

Since this is a two-channel receiver, the total allowable LO noise is - 71.9 dBm.

Shurmer[8] suggests the use of Gunn oscillators for local oscillators when the IF is around 30 MHz because of their low noise properties.

The Gunn oscillator is very economical as well because it can be mechanically tuned and requires only a low DC voltage for power.

The local oscillator chosen for the VPI&SU receiver is an RHG G01K131 mechanically tuned Gunn oscillator with the following specifications.

Frequency: 17.62 GHz

Stability: 15 to 35° C

Noise: - 110 dB

Power: 25 mw

The output of the detector is 0.5 VDC when full LO power is allowed to the mixer and no RF power is present at the mixer. This sets a lower limit on the dynamic range of 68 dB. When the attenuators were set for 4/3 of a milliwatt LO power to each channel, the detector output was 0.4 VDC corresponding to a 71.4 dB dynamic range.

The RHG mixers used have an LO to RF isolation of 20 dB. This value is far short of the 42.0 dB polarization isolation needed as predicted in Section 1. A 24 dB isolator was placed in each channel to insure the minimum polarization isolation.

$PI = I_I + T_I + M_I + A_I$

PI = polarization isolation

I_I = isolator isolation = 24 dB

T_I = E plane tee isolation = 3.0 dB

M_I = mixer isolation = 20.0 dB

A_I = attenuator isolation = (0 to 25 dB)

PI = 47 dB (minimum value)

= 72 dB (maximum value)

The 24 dB isolator at the LO output is strictly for VSWR protection for the L.O., because a lossless reciprocal 3-port can never be completely non-reflecting.[9]

The two attenuators are used for adjusting local oscillator power to the mixer. The local oscillator power is 25 mw and each channel requires at least 4/3 mw for proper mixer operation. The amount of attenuation required is given by A_{LO}.

$$A_{LO} = 10 \log \left(\frac{25}{2} \cdot \frac{3}{4}\right) = 10 \log \left(\frac{75}{8}\right)$$

$$A_{LO} = 9.75 \text{ dB}.$$

Commercial uncalibrated attenuators for K_u band are available in 0 to 25 dB varieties or higher, so a 0 to 25 dB uncalibrated attenuator was chosen for each channel. Since LO power to the mixer is the important parameter, the attenuator setting is made by monitoring power from the attenuator. The use of uncalibrated attenuators saved the project $600.00.

The E-plane tee splits the local oscillator power. It is the most economical device available for that purpose, but it does cause the phase of each output leg to be 180° apart. Figure 3.6 represents an E-plane tee and its scattering matrix. Ports 1 & 2 are the mixer legs while port 3 is the local oscillator leg.

$$\begin{bmatrix} b_1 \\ b_2 \\ b_3 \end{bmatrix} = 1/2 \begin{bmatrix} 1 & 1 & \sqrt{2} \\ 1 & 1 & -\sqrt{2} \\ \sqrt{2} & -\sqrt{2} & 0 \end{bmatrix} \begin{bmatrix} a_1 \\ a_2 \\ a_3 \end{bmatrix}$$

If ports 1 and 2 are matched then a_1 and a_2 are both zero.

$$b_1 = \frac{\sqrt{2}}{2} a_3$$

$$b_2 = -\frac{\sqrt{2}}{2} a_3$$

From these calculations it can be seen that the voltage at port 1 is 180° out of phase with the voltage at port 2. After filtering, the mixer outputs are:

$a_2 e_{LO} e_{RF} \cos([\omega_{SIG} - \omega_{LO}]t)$ (port 1)

$a_2 e_{LO} e_{SIG} \cos([\omega_{SIG} - \omega_{LO}]t - \phi)$ (port 2)

$\phi = \pi$ for E-plane tee

Since the detectors respond to input dBm, the phase of the mixer output is of no concern.

7.2.4 Suggested Improvements

The addition of a calibrated phase shifter in one channel would allow the experimentor to set the clear weather phase difference between channels to 0°. This would greatly simplify received signal phase measurements.

7.2.5 Final Receiver Specifications

Figure 2.5 is the transfer function for the VPI&SU 17.65 GHz receiver. Both channels are identically calibrated. Below is a list of the final receiver specifications.

Dynamic Range: 71.4 dB

Channel Isolation: > 60 dB

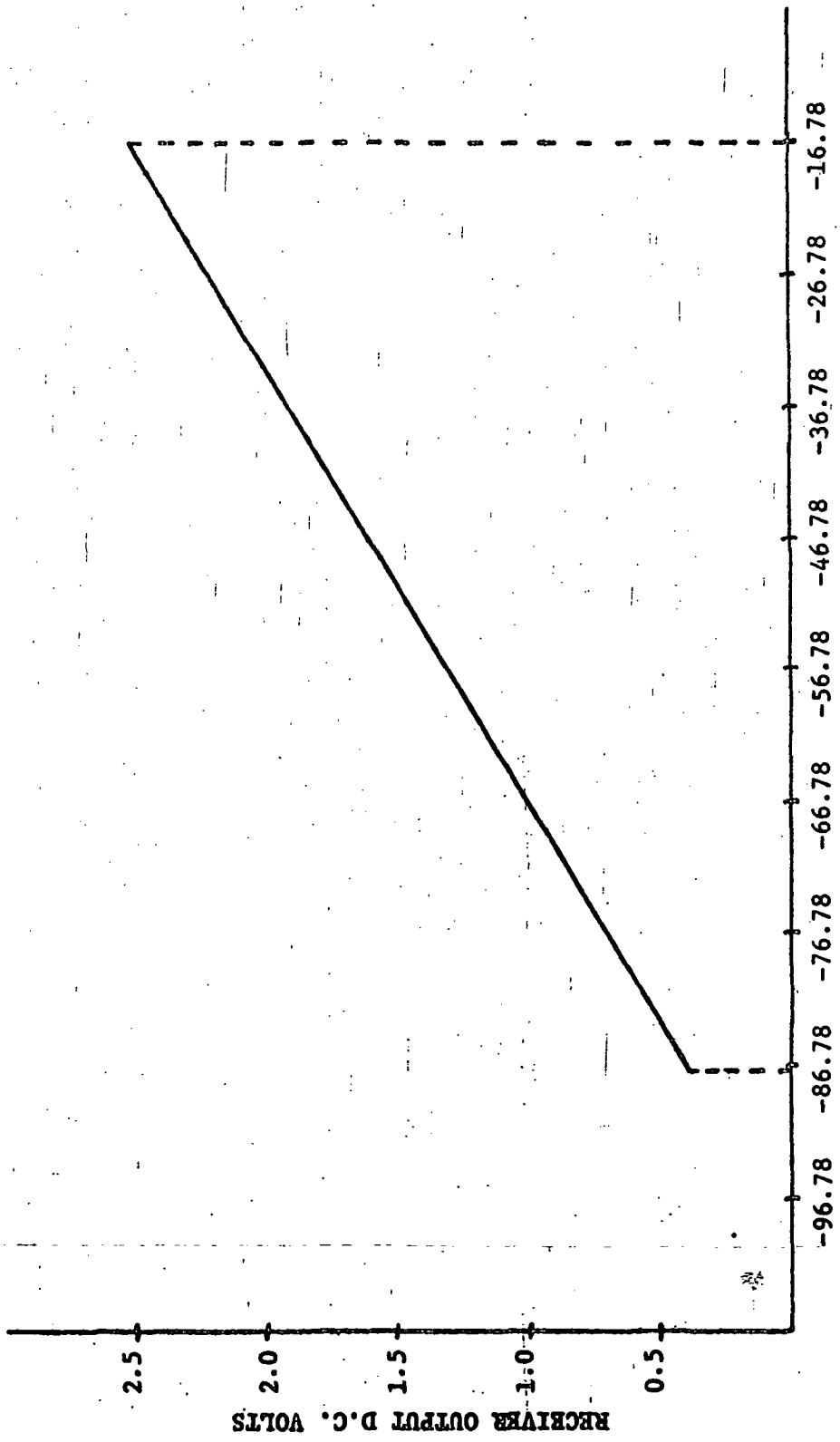

Figure 2.5. VPI & SU Receiver Transfer Function

SECTION 7.3

TRANSMITTER

7.3.1 Scope of Section

Presented in this section are typical transmitters for attenuation and depolarization measurements, design calculations for the VPI&SU 17.65 GHz transmitter, and suggested improvements.

7.3.2 Typical Transmitters

Figure 3.1 is a block diagram of a typical transmitter for attenuation measurements. The source should be stable in both frequency and power. If the source is capable of delivering more than the required power, an uncalibrated attenuator can be used to reduce the transmitter output to the design level and to hold it there as the source ages. An isolator should be used to protect the source from a high VSWR encountered during switching unless one is provided internally with the source. A directional coupler and a power meter will allow continuous monitoring of the output power. It is often convenient during antenna alignment or receiver checks to shut down the transmitter power. A waveguide switch and a matched load will allow the transmitter power to be dissipated safely when so desired.

Figure 3.2 is a block diagram of a typical transmitter for cross-polarization measurements. The components are identical except for the power splitting device. The VPI&SU 17.65 GHz transmitter is identical to this except that a 3 dB coupler is used as the power splitting device and an uncalibrated attenuator is placed in one channel to insure equal

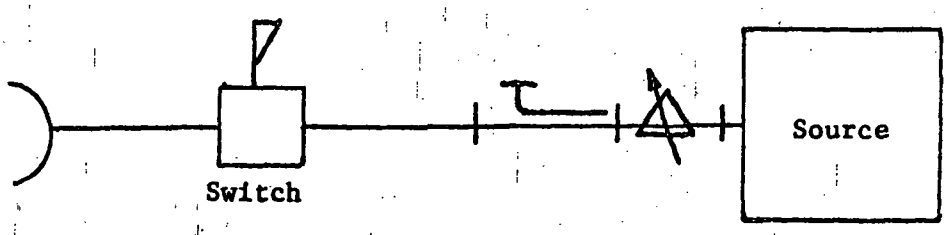

Figure 3.1. Attenuation Transmitter

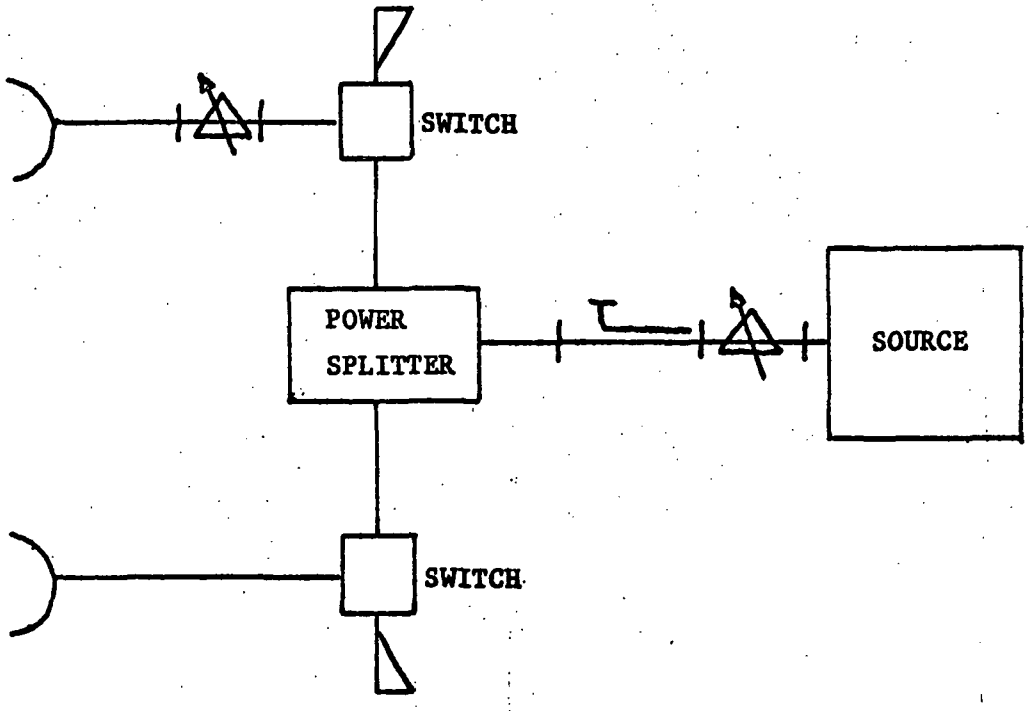

Figure 3.2. Depolarization Transmitter

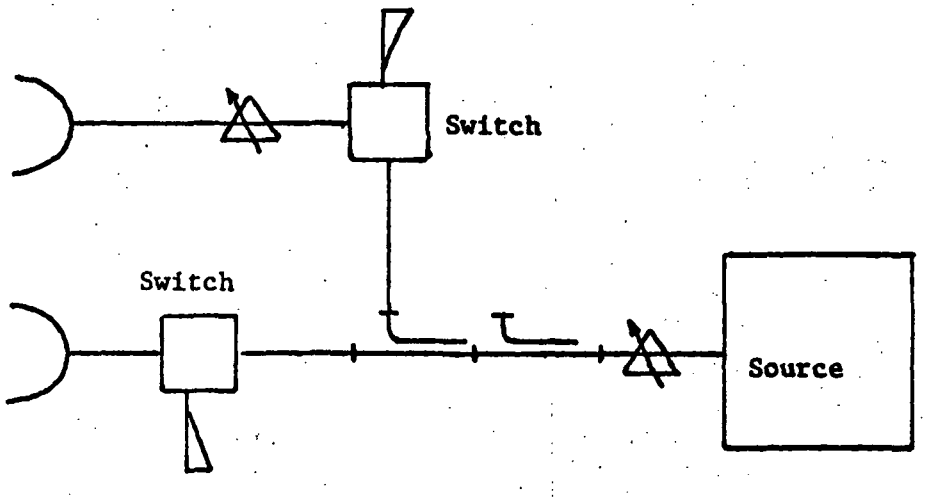

Figure 3.3. VPI&SU Transmitter

outputs.

7.3.3 Necessary Transmitter Power and Stability

The power required depends upon receiver saturation level, path loss, antenna gain, and transmission line loss. Below is a calculation of the required transmitter power for the VPI&SU 17.65 GHz transmitter.

$L \equiv$ path loss $= 21.98 + 20 \log (r/\lambda)$ 10

$r \equiv$ path length

$\lambda \equiv$ wavelength

$\lambda = C/F = 0.017$ m

$L = 120.48$ dB

$P_T \equiv$ power transmitted $= P_R + L - G_{AT}$

$P_R \equiv$ necessary receiver input power $= -16.78$ dBm

$G_{AT} \equiv$ total antenna gain $= 90$ dB

$P_T = 13.7$ dBm or 23.44 mw

For a two channel transmitter, the total output power must be 46.88 mw.

The stability of the source at the required power level is just as important as local oscillator stability. Below is a calculation of required source stability for the VPI&SU 17.65 GHz source.

$S \equiv$ stability $= \pm (BW/2)\ (100/F)$

$BW \equiv$ bandwidth

$F \equiv$ frequency

$S = \pm (.01/2)\ (100/17.65) = \pm 0.028\%$

7.3.4 Component Selection

The source chosen is an RDL POOK(3) crystal oscillator and varactor chain multiplier. The specifications are listed below.

Frequency: 17.65 GHz

Stability: ± 0.005%

Power Output: 70 mw minimum

Temperature: 0 to 50° C

Spurious Noise: < - 40.0 dB

Mechanical waveguide switches were chosen because of their high isolation between ports. The isolation must be as great or greater than the polarization isolation of the receiver or erroneous cross-polarization levels will be observed. The waveguide switches chosen were Waveline 777-E solenoid operated, double pole-double throw, current holding switches.

7.3.5 Transmission Line Components

A major concern in the design of the transmitter was the VSWR introduced by the waveguide switches during switching.

Figure 3.4 is a top view of a Waveline 777-E switch in the rest position. For this explanation port 1 is the source power input, port 4 is matched, and port 2 is the antenna feed. The 90° circular are from part 1 to part 2 is 1.42 inches long. The dimension of the waveguide short wall is 0.311 inches. When the switch is activated, part 1 is fed to part 2 and part 4 is fed to part 3. As the cylinder moves, part 1 is shorted for 1.11 inches of the 1.42 inches of movement. If

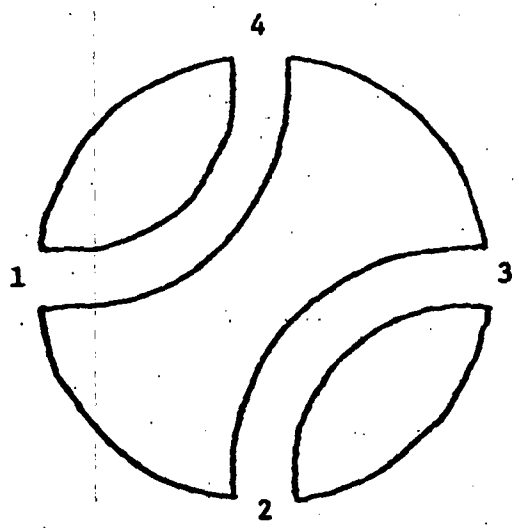

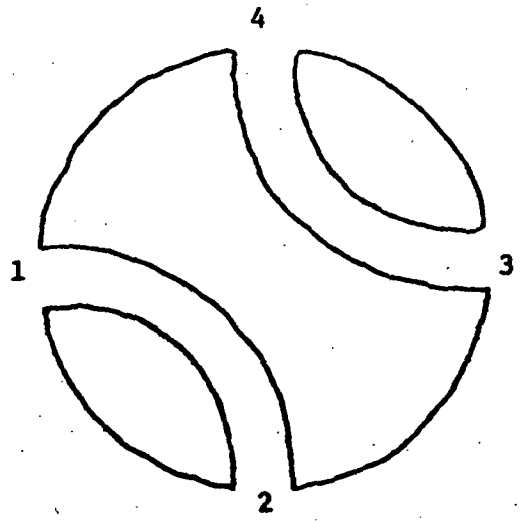

90° Arc = 1.42"
Short Wall = 0.31"
Short = 1.11" or 78% of 90° Arc

Figure 3.4. Waveguide Switches

the cylinder moves at a uniform velocity for the 100 msec switching time, the short will last 78 msec. The short is not perfect however, and a VSWR reading in 78 msec is difficult to obtain. In order to get an estimated value of the VSWR, a shorting plate was placed across part 4 and a slotted line was placed in series with part 1. With the source transmitting and the switch deactivated, the VSWR was 25.0. Under operating conditions, the short will not be this good because of the small clearance between the rotating cylinder and the four ports

$$|\varrho| = \frac{\text{VSWR}-1}{\text{VSWR}+1} = \frac{24}{26} = 0.923$$

$r \equiv$ reflected power coefficient $= |\varrho|^2 = 0.852$

$P_R \equiv$ power reflected $=$ r(source power) $= 25\ r = 21.3$ mw

Not only must the source be protected from this reflected power, but the reflected power should not be coupled into the other channel. Below is an analysis of a 3 dB coupler used as the power splitter. Figure 3.5 represents a 3 dB coupler and its scattering matrix.

$c^2 \equiv$ coupling ratio $= 1/2$ (for a 3 dB coupler)

$a_1 = \sqrt{50}$

$a_2 = 0$ (part 2 terminated with a matched load)

$a_3 = \sqrt{21.3}$ mw (voltage reflected when switch activates)

$$\begin{bmatrix} b_1 \\ b_2 \\ b_3 \end{bmatrix} = \begin{bmatrix} 0 & 1/\sqrt{2} & 1/\sqrt{2} \\ 1/\sqrt{2} & 0 & 0 \\ 1/\sqrt{2} & 0 & 0 \end{bmatrix} \begin{bmatrix} \sqrt{50} \\ 0 \\ \sqrt{21.3} \end{bmatrix}$$

$$b_1 = \frac{\sqrt{21.3}}{\sqrt{2}}$$

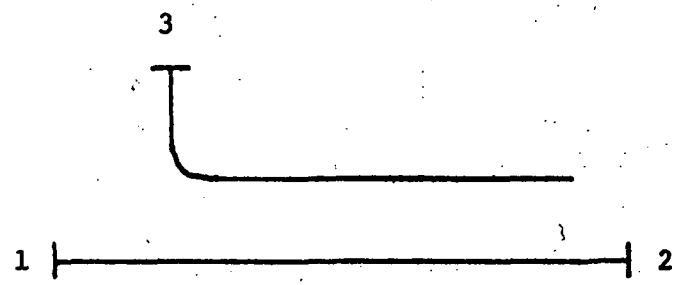

$$\begin{bmatrix} 0 & 1/\sqrt{2} & 1/\sqrt{2} \\ 1/\sqrt{2} & 0 & 0 \\ 1/\sqrt{2} & 0 & 0 \end{bmatrix}$$

Figure 3.5. 3dB Coupler and Scattering Matrix

$P_{RS} \equiv$ power reflected to source = 10.65 mw

When both switches are activated simultaneously, the reflected power will be 21.2 mw.

$$50\ r = 21.3$$

$$r = 0.426 = |\rho|^2$$

$$|\rho| = 0.653$$

$$\text{VSWR} = \frac{1 + |\rho|}{1 - |\rho|} = 4.76$$

Discussions with RDL technicians convinced project personnel that the RDL POOK(3) source would withstand a 4.76 VSWR for 78 msec.

The 3 dB coupler also provides excellent channel isolation for power reflected during switching.

$$\begin{bmatrix} b_1 \\ b_2 \\ b_3 \end{bmatrix} = \begin{bmatrix} 0 & 1/\sqrt{2} & 1/\sqrt{2} \\ 1/\sqrt{2} & 0 & 0 \\ 1/\sqrt{2} & 0 & 0 \end{bmatrix} \begin{bmatrix} a_1 \\ a_2 \\ a_3 \end{bmatrix}$$

$b_2 = \frac{a_1}{\sqrt{2}}$ (contains no reflections from part 3)

$b_3 = \frac{a_1}{\sqrt{2}}$ (contains no reflections from part 2)

The 40.0 dB coupler allows the source power to be continuously monitored. The coupling ratio was carefully checked for accuracy at 17.65 GHz and was found to be 40.0 dB.

The attenuators used are uncalibrated with a range of 0 to 25 dB. The high values of attenuation were never used, but lower value variable attenuators were not available. The VSWR of each attenuator was 1.15 maximum.

7.3.6 Transmitter Performance

The VPI&SU 17.65 GHz transmitter was licensed in the spring of 1972 as a contract developmental station in the experimental radio service. It was assigned the call letters KQ2X0C. In accordance with FCC regulations, the transmitter source was provided with a remote "on-off" circuit located adjacent to the PB-440.

Below are the transmitter specifications measured during the final testing stage.

Frequency: 17.65 GHz ± 800 KHz

Power Output: 26 mw per channel

Isolation between channels: > 60 dB

VSWR: 1.1 (static condition)

The 26 mw value was the transmitter power required to produce a 2.5 volt receiver output. The calculated value was 23.44 mw. One source of error for this calculation is the actual antenna gain. The antenna gain measured by the manufacturer was 44.5 dB as compared to the estimated value used of 45.0 dB.

1.0 dbm is 1.25 mw

Actual required output power = 23.44+1.25 = 24.69 mw

7.3.7 Possible Transmitter Improvements

The addition of a phase shifter in one channel of the transmitter would allow for easier phase measurements between cross-polarized channels at the receiver. The phase shifter should be adjusted so that the received clear weather phase difference is 0 degrees.

In the VPI&SU 17.65 GHz experiment, data is taken 100 msec after a

waveguide switch changes state. The possible VSWR of 25 has disappeared in this time. For this reason, the use of the 3 dB coupler as a splitter may be unwarranted. If the source is properly protected against a high VSWR, an E-plane tee would be more economical to use. Figure 3.6 represents an E-plane tee and the scattering matrix for an ideal E-plane tee. Part 3 is the source feed and parts 1 and 2 are the orthogonal channel feeds.

channel 1 switching:

$a_1 = \sqrt{21.3}$

$a_2 = 0$

$a_3 = \sqrt{50.0}$

$b_2 = -2.68$ or 7.23 mw

$b_2 = 3.26$ or 10.65 mw

channel 2 switching

$a_1 = 0$

$a_2 = -\sqrt{21.3}$

$a_3 = \sqrt{50}$

$b_1 = 2.68$ or 7.23 mw

$b_3 = -3.26$ or 10.65 mw

channel 1 and 2 switching:

$a_1 = \sqrt{21.3}$

$a_2 = -\sqrt{21.3}$

$a_3 = \sqrt{50.0}$

$b_3 = 6.53$ or 42.6 mw

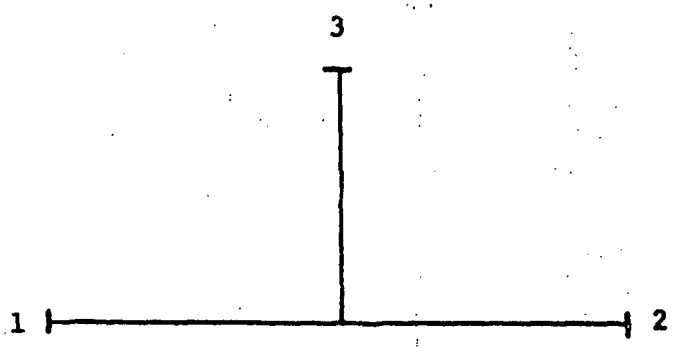

$$1/2 \begin{bmatrix} 1 & 1 & \sqrt{2} \\ 1 & 1 & -\sqrt{2} \\ \sqrt{2} & -\sqrt{2} & 0 \end{bmatrix}$$

Figure 3.6. E-Plane T and Scattering Matrix

$$r = \frac{42.6}{50.0} = 0.853$$

$$r = |p|^2$$

$$|p| = 0.925$$

$$\text{VSWR} = \frac{1 + |p|}{1 - |p|} = \frac{1.925}{.075} = 25.0$$

As can be seen from the calculations above, the E-plane tee works as well as the 3 dB coupler as a protection to the source when only one switch is activated at a time, but the source sees the entire VSWR of 25 when both switches are activated simultaneously. If the source is internally isolated, the E-plane tee would be more economical to use instead of the 3 dB coupler. If the source is not isolated at all, it would be more economical to buy an E-plane tee and an isolator instead of a 3 dB coupler and an isolator.

7.4 LITERATURE CITED

1. Thomas, D. T., "Cross Polarization Distortion in Microwave Radio Transmission Due to Rain," Radio Science, vol. 6, no. 10, October, 1971, pp. 833-840.

2. Watson, P. A., "Measurements of Linear Cross Polarization at 11 GHz," Report to European Space Research Organization, Contract No. 1297/SL, U. of Bradford, Bradford, England, May, 1972.

3. Wiley, P. H., "Depolarization Effects of Rainfall On Millimeter Wave Propagation," Ph.D., dissertation, Virginia Polytechnic Institute and State University, Blacksburg, Virginia, 1973, pp. 1-90.

4. Bostian, C. W., and Stutzman, W. L., "The Influence of Polarization on Millimeter Wave Propagation Through Rain," Semi-Annual Status Report 1 to National Aeronautics and Space Administration, Contract No. NGR-47-004-091, Washington, D. C., July, 1972, p. 77.

5. Saad, T. S., "The Microwave Mixer," Sage Laboratories, Inc., Natick, Massachusetts, 1966, pp. 15-16.

6. Ibid., pp. 17-18.

7. Ibid., p. 7.

8. Shurmer, H. V., Microwave Semiconductor Devices, New York: John Wiley and Sons, Inc., 1972, pp. 177-178.

9. Kerns, D. M., and Beatty, R. W., Basic Theory of Waveguide Junctions and Introductory Microwave Network Analysis, New York: Pergamon Press, 1967, p. 103.

10. Livingston, D. C., The Physics of Microwave Propagation, Englewood Cliffs, New Jersey: Prentice-Hall, 1970, p. 9.

11. Thomas, H. E., Handbook of Microwave Techniques and Equipment, Englewood Cliffs, New Jersey: Prentice-Hall, 1972, pp. 94-99.

12. Bostian, C. W., and Stutzman, W. L., op. cit., pp. 7-8.